

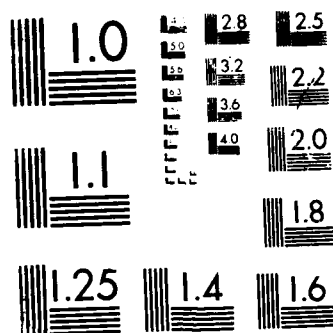
PREDICTABILITY OF ICE CONCENTRATION IN THE  
HIGH-LATITUDE NORTH ATLANTIC F (U) NAVAL POSTGRADUATE  
SCHOOL MONTEREY CA G W FLEMING SEP 87

UNCLASSIFIED

F/G 8/12

NL

Figure 1



MICROCOPY RESOLUTION TEST CHART  
 NATIONAL BUREAU OF STANDARDS-1963-A

AD-A186 621

DTIC FILE CODE

2

# NAVAL POSTGRADUATE SCHOOL

Monterey, California



DTIC  
ELECTE  
DEC 09 1987  
S D

## THESIS

PREDICTABILITY OF ICE CONCENTRATION IN  
THE  
HIGH-LATITUDE NORTH ATLANTIC FROM  
STATISTICAL  
ANALYSIS OF SST AND ICE CONCENTRATION  
DATA

by

Gordon H. Fleming

September 1987

Approved for public release; distribution is unlimited.

## 19. Abstract continued:

enhanced persistence of both SST and ice concentration, allowing them to interact. By contrast, the Davis Strait area, a region of strong confluent currents of different temperatures and limited ice persistence, showed weak cross-correlation values. Statistical analyses of large, homogeneous data sets as conducted in this study appear to be superior to current thermodynamic models in their potential for long-range forecasts of ice concentration.

## 18. Subject terms continued:

ice forecasting

Barents Sea

Iceland Sea

Reception For	
ADIS CRASH	<input checked="" type="checkbox"/>
DIS TAG	<input type="checkbox"/>
Unprocessed	<input type="checkbox"/>
Justification	
By	
On: 01/01/71	
Availability Codes	
Dist	Availability Spec.
A-1	

## 19. Abstract continued:

enhanced persistence of both SST and ice concentration, allowing them to interact. By contrast, the Davis Strait area, a region of strong confluent currents of different temperatures and limited ice persistence, showed weak cross-correlation values. Statistical analyses of large, homogeneous data sets as conducted in this study appear to be superior to current thermodynamic models in their potential for long-range forecasts of ice concentration.

## 18. Subject terms continued:

ice forecasting

Barents Sea

Iceland Sea

Accession For	
NTIS GRA&I	<input checked="" type="checkbox"/>
DTIC TAB	<input type="checkbox"/>
Unannounced	<input type="checkbox"/>
Justification	
By	
Dist. by	
Availability Codes	
Dist	Avail. and/or Special
A-1	

Approved for public release; distribution is unlimited.

Predictability of Ice Concentration in the  
High-Latitude North Atlantic From Statistical  
Analysis of SST and Ice Concentration Data

by

Gordon H. Fleming  
Lieutenant Commander, Canadian Armed Forces  
B.Sc., Royal Roads Military College, Victoria, B.C. 1978

Submitted in partial fulfillment of the  
requirements for the degree of

MASTER OF SCIENCE IN METEOROLOGY AND OCEANOGRAPHY

from the

NAVAL POSTGRADUATE SCHOOL  
September 1987.

Author:

Gordon H. Fleming  
Gordon H. Fleming

Approved by:

John E. Walsh  
John E. Walsh, Co-Advisor

Robert H. Bourke  
Robert H. Bourke, Co-Advisor

C. A. Collins  
C. A. Collins, Chairman,  
Department of Oceanography

Gordon E. Schacher  
Gordon E. Schacher,  
Dean of Science and Engineering

## **ABSTRACT**

A statistical analysis of 27 years of monthly averaged sea surface temperature (SST) and ice concentration data was conducted for 17 locations along the annual mean position of the marginal ice zone spanning the North Atlantic. Anomalies (differences from monthly means) of both variables were observed to have spatial scales of 100s to 1000s of kms, temporal scales of 6 months to several years, and a strong regional dependence. Sea surface temperature autocorrelation values were in general higher than ice concentration autocorrelation values. Cross-correlations between the two variables were found to be highly significant in some regions and poor in others. The various correlation features appeared plausible with respect to understood physical processes in each region. For example, the data for the northern Barents and Iceland Seas showed strong cross-correlations at lags extending to over nine months. The steady-state cold water temperatures and relatively weak currents in these regions enhanced persistence of both SST and ice concentration, allowing them to interact. By contrast, the Davis Strait area, a region of strong confluent currents of different temperatures and limited ice persistence, showed weak cross-correlation values. Statistical analyses of large, homogeneous data sets as conducted in this study appear to be superior to current thermodynamic models in their potential for long-range forecasts of ice concentration.

## TABLE OF CONTENTS

<b>I. INTRODUCTION .....</b>	<b>13</b>
<b>II. ARCTIC OCEAN CHARACTERISTICS .....</b>	<b>22</b>
A. ICE .....	23
B. WATER MASSES .....	25
C. CURRENTS .....	28
D. SEA/ICE FORCING .....	32
<b>III. DATA .....</b>	<b>36</b>
A. COADS .....	36
B. SEIC .....	37
C. DATA SET MANIPULATION .....	39
<b>IV. ASSESSMENT OF SOVIET SKILL .....</b>	<b>46</b>
<b>V. RESULTS .....</b>	<b>56</b>
A. SST/ICE CONCENTRATION ANOMALIES .....	56
B. PERSISTENCE (AUTOCORRELATION) CONTOURS .....	57
C. CROSS-CORRELATION CONTOURS .....	60
D. CORRELATION FEATURES .....	63
E. STRONG ANOMALY YEARS .....	65

<b>VI. DISCUSSION .....</b>	<b>106</b>
A. PERSISTENCE .....	106
B. TEMPORAL SCALES OF VARIABILITY .....	111
C. CROSS-CORRELATIONS .....	114
D. ICE FORECAST POTENTIAL .....	118
E. THRESHOLD VALUES .....	122
F. DATA LIMITATIONS .....	123
<b>VII. CONCLUSIONS AND FUTURE WORK.....</b>	<b>130</b>
A. CONCLUSIONS.....	130
B. FUTURE WORK .....	131
LIST OF REFERENCES .....	133
INITIAL DISTRIBUTION LIST .....	138

## LIST OF TABLES

Table I	Data sources for COADS [from Slutz et al. (1985)].....	42
Table II	Data sources for SEIC [from Walsh and Johnson (1979)]...	43
Table III	The 25 anomaly pairs used to calculate the high cross-correlation value for POI 15 at lag +2 for October (see Figure 5.18). The products of the two anomalies and the percentages of the final negative cross-covariance which each pair contributes are also listed .....	68
Table IV	The 25 anomaly pairs used to calculate the high cross-correlation value for POI 10 at lag -6 for July (see Figure 5.17). The products of the two anomalies and the percentages of the final negative cross-covariance which each pair contributes are also listed .....	69
Table V	The 25 anomaly pairs used to calculate the high cross-correlation value for POI 10 at lag -4 for October (see Figure 5.22). The products of the two anomalies and the percentages of the final negative cross-covariance which each pair contributes are also listed .....	70
Table VI	The POIs, their grid and geographic positions, and the respective oceanic areas with which they are associated .....	125

## LIST OF FIGURES

1.1	Compilation of autocorrelations of SST, sea ice, snow and 700 mb pressure anomalies from various authors. Autocorrelations were obtained over large areas of the north Pacific (SST and 700 mb), North American continent (snow) and north Atlantic (ice). Data were averaged over several months. [from Davis (1976), Lemke et al, (1980), Walsh (1982) and Namias and Born (1970)].....	20
1.2	Schematic representation of the coupling mechanisms between sea surface temperature (SST) and sea ice extent [from Walsh and Sater (1981)]. .....	21
2.1	Ice extremes for the period 1953-1977 [from Walsh and Johnson (1979)].....	33
2.2	Vertical profiles of temperature and salinity from various northern high-latitude basins. [from Coachman and Aagaard (1974)]. .....	34
2.3	Schematic picture of the North Atlantic circulation as derived from drift experiments. Vertical shading indicates flow associated with the North Atlantic Current and horizontal shading indicates association with the subtropical gyre. Area between A and A' is the shifting boundary between the two. Warm currents are marked by solid arrows and cold currents by dashed arrows. [from Krauss (1986)].....	35
3.1	Chart depicting the 1° latitude spaced Cartesian grid. The 17 points of interest (POIs) used in this study are highlighted. ....	44
3.2	Data manipulation flow diagram. ....	45
4.1	Region of study for the Soviet ice cover prediction method. Ocean stations are labelled by letter. Solid arrows are average warm currents and dashed arrows are average cold currents. The numbered positions are meteorological stations: 1-Cape Tobin; 2-Iceland Sea; 3-Angagssalik; 4-Reykjavik [from Nikol'skaya et al. (1977)].....	51
4.2	Comparison of Soviet correlations (USSR) with correlations calculated using our data and Soviet regression constants (USSR coef.) and our data with recalculated regression	

	constants (rev. coef.). The same variables are used in all three cases. This figure shows values for the Greenland Sea.....	52
4.3	As for 4.2 except using values for the latitude band 73°-78° N.....	53
4.4	As for 4.2 except using values for the latitude band 68°-73° N.....	54
4.5	Correlations between ice cover and the three individual predictors (ice, surface air temperature, and SST) for the three regions. The 25-year (1955-1979) data set is used.....	55
5.1	SST anomaly (difference from monthly mean) contours for POIs 1 through 17 and months 1 through 108. Solid lines are positive anomalies, dashed lines are negative anomalies. The heavy line is 0 anomaly. Contour increments are 0.5 degrees centigrade.....	71
5.2	As for 5.1 except covering months 109 through 216.....	72
5.3	As for 5.1 except covering months 217 through 324.....	73
5.4	Ice anomaly (difference from monthly mean) contours for POIs 1 through 17 and months 1 through 108. Solid lines are positive anomalies, dashed lines are negative anomalies. The heavy line is 0 anomaly. Contour increments are 0.5 tenths of ice concentration.....	74
5.5	As for 5.4 except covering months 109 through 216.....	75
5.6	As for 5.4 except covering months 217 through 324.....	76
5.7	Ice concentration autocorrelation (persistence) contours for the 17 POIs. Solid lines are positive correlation values and dashed lines are negative correlation values. Values are contoured in increments of 0.1 for lags of -12 months to +12 months. The base month is January.....	77
5.8	Same as 5.7 except using base month of April.....	78
5.9	Same as 5.7 except using base month of July.....	79
5.10	Same as 5.7 except using base month of October.....	80
5.11	SST autocorrelation (persistence) contours for the 17 POIs. Solid lines are positive correlation values and dashed lines	

are negative correlation values. Values are contoured in increments of 0.1 for lags of -12 months to +12 months. The base month is January.....	81
5.12 Same as 5.11 except using base month of April.....	82
5.13 Same as 5.11 except using base month of July.....	83
5.14 Same as 5.11 except using base month of October.....	84
5.15 SST/ice concentration cross-correlation contours for the 17 POIs. Solid lines are positive correlation values and dashed lines are negative correlation values. Values are contoured in increments of 0.1 for lags of -12 months to +12 months. Base month is January.....	85
5.16 Same as 5.15 except using base month of April.....	86
5.17 Same as 5.15 except using base month of July.....	87
5.18 Same as 5.15 except using base month of October.....	88
5.19 Ice concentration/SST cross-correlation contours for the 17 POIs. Solid lines are positive correlation values and dashed lines are negative correlation values. Values are contoured in increments of 0.1 for lags of -12 months to +12 months. Base month is January. ....	89
5.20 Same as 5.19 except using base month of April.....	90
5.21 Same as 5.19 except using base month of July.....	91
5.22 Same as 5.19 except using base month of October.....	92
5.23 Graph of temperature anomalies for the most influential years for cross-correlation feature A. Anomaly values are for the month of August.....	93
5.24 As for 5.23 except anomaly values are for the month of October.....	94
5.25 As for 5.23 except anomaly values are for the month of November.....	95
5.26 As for 5.23 except anomaly values are for the month of December.....	96

5.27	Graph of temperature anomalies for the most influential years for cross-correlation feature B. Anomaly values are for the month of January.....	97
5.28	As for 5.27 except anomaly values are for the month of March.....	98
5.29	As for 5.27 except anomaly values are for the month of May.....	99
5.30	As for 5.27 except anomaly values are for the month of July..	100
5.31	As for 5.27 except anomaly values are for the month of September. ....	101
5.32	Graph of temperature anomalies for the most influential years for cross-correlation feature C. Anomaly values are for the month of April. ....	102
5.33	As for 5.32 except anomaly values are for the month of June.	103
5.34	As for 5.32 except anomaly values are for the month of August. ....	104
5.35	As for 5.32 except anomaly values are for the month of October.....	105
6.1	Average current and an example of winter temperature distribution in the Iceland Sea. [from Swift and Aagaard (1981)]. ....	126
6.2	SST and ice concentration anomaly values for cross-correlation feature A. SST is plotted in negative scale to emphasize the correlation.....	127
6.3	Same as 6.2 except for cross-correlation feature B.....	128
6.4	Same as 6.2 except for cross-correlation feature C.....	129

## **ACKNOWLEDGMENTS**

I would like to thank Professor John E. Walsh for his guidance and enlightenment throughout this thesis project. Thanks also to Professor R. W. Bourke for his critical support and encouragement. And finally, a special note of appreciation to my wife, Maria, for making the time, despite many other demands, to assist me in the completion of this thesis.

## **I. INTRODUCTION**

The ability to forecast sea ice cover in Arctic waters is of prime concern to many agencies. The oil industry must know the extent of ice to plan drilling operations and design appropriate rigs. Fishing fleets may be prevented from utilizing choice fishing grounds due to ice cover. Surface shipping must be routed to avoid the dangers of ice collision but retain the economy of shorter distances over great circle northern routes. In some regions of the Arctic, resupply by sea can only be conducted during minimal ice seasons. Significant volumes of merchant vessel traffic that operate in the northern European and USSR waters can only operate in relatively ice free seas.

Sea ice introduces many complications to military operations. Naval vessels used in northern waters must be properly designed if they are to function effectively in the unique and extreme conditions encountered in the region.

The highly variable temperatures, surfaces, and material composition of water and ice in the polar regions have a dramatic effect on both the air and ocean boundary layers. This in turn affects electromagnetic, electro-optical and acoustic transmission and reception. Sea ice is a strong source of ambient acoustic noise and radar scatter. Detection of underwater targets by passive or active means is difficult. Detection of low level or surface targets by radar also becomes more of a problem in the ice.

Obviously, a reasonably precise knowledge of where the ice is and where it is expected to be in the future can be very useful. One method to approach this problem, and indeed the focus of this work, is to closely examine the so-called "interannual variability" of sea ice. In the meteorological/oceanographic context, interannual variability will refer to departures from monthly and seasonal means defined from data for periods of 10 to 30 years. Longer base periods are generally not used because climatic trends may induce changes in the means or "normals." Interannual variations are the focal points of long-range forecasts. Long-range forecasts can be considered as predictions of monthly or seasonally averaged departures from the climatological mean.

In the case of atmospheric forecasts, deterministic prediction of daily weather fluctuations is presently limited to 5 to 10 days. Theoretical arguments indicate that the ultimate range of such predictions is several weeks. Evaluations of prediction skill at longer ranges is based on averages of forecast and observed fields over periods of 30 to 90 days. Forecasts of 30- or 90-day average fields may well show significant and useful skill even though day-to-day variability is not forecast with skill. The same time scales apply to sea-ice forecasts.

Previous studies (Lemke et al., 1980; Lebedev and Uralov, 1982; Walsh and Johnson, 1979) have indicated that the persistence of ice anomalies (departures from normal) is considerably greater than the persistence of atmospheric anomalies (Figure 1.1). Stated differently,

daily fluctuations contribute considerably more to the variance of atmospheric anomalies than to the variance of sea ice anomalies.

Several other implications of Figure 1.1 deserve mention. First, the relatively large autocorrelations of sea ice anomalies imply that persistence will be a competitive control forecast. While the autocorrelations in Figure 1.1 are not region-specific, they imply that persistence alone can predict approximately 0.46 and 0.20 of the variance (autocorrelation squared) of departures from normal ice cover at lead times of one and three months, respectively. Persistence statistics will therefore be evaluated in the present work as a benchmark for comparison with skill statistics derived from other forecasts. Second, the sea ice autocorrelations in Figure 1.1 are comparable to those of sea surface temperature (SST), which has long been used as an input to long-range weather forecasts for mid-latitudes. The similarity of time scales suggests that SSTs are associated with ice concentration anomalies. If the two variables are coupled, then the skill of prediction of one variable may be enhanced by considering the distribution of the other.

Variable sea surface temperatures and ocean currents have been cited as likely sources of the "unexplained" ice variance in studies of atmospheric forcing of sea ice (Haupt and Kant, 1976). Schell (1970) and Rogers and van Loon (1979) have compared large-scale SST and sea ice variations in selected regions and selected years. Considerable effort has also been expended in evaluating the coupling between

large-scale SST and atmospheric anomalies over the North Pacific (e.g., Namias, 1976; Elsberry and Raney, 1978; Broccoli and Harnack, 1981) and the North Atlantic (e.g., Ratcliffe and Murray, 1970; Rowntree, 1976; Haworth, 1978). Because these studies have indicated the existence of statistically significant associations between SST anomalies and the atmospheric circulation, the link between SST anomalies and the high-latitude sea ice distribution must be viewed in the context of Figure 1.2. The "direct association," in which high SSTs enhance melting and/or retard freezing, is to be distinguished from the "indirect association," in which the sea ice distribution is influenced by SST through an SST-induced effect on the atmospheric circulation. The interpretation of the SST-ice coupling in observational data analysis is complicated by the possibility that both mechanisms may act concurrently. Indeed, while the present study will focus on the predictive applications of the "direct" association between SST and sea ice in the North Atlantic, the "indirect" association is the basis of Soviet claims concerning seasonal predictability of North Atlantic sea ice (Chapter IV).

The present work is a data-based investigation of SST-derived predictability of sea ice in the North Atlantic. The study is motivated by three major considerations:

1. SST represents potentially valuable but as yet largely unexploited input to long-range sea ice prediction
2. Previous studies addressing the high-latitude portions of the Pacific and Atlantic Oceans have achieved considerably less

diagnostic success in the Atlantic than in the Pacific (e.g., Walsh and Sater, 1981); and

3. The recent release of the Comprehensive Ocean Atmosphere Data Set (COADS) provides the most solid foundation to date for an analysis of SST/ice concentration associations. However, the potential for high latitude forecasting is still unclear as COADS has yet to be utilized for this purpose.

The following points will serve as objectives for this study:

1. Autocorrelations of sea ice and SST anomalies will be systematically evaluated in order to place the SST-derived ice predictability into a framework of practical utility
2. Lag relationships between SST and sea ice concentration anomalies will be evaluated in order to determine which variable (SST or ice concentration) may serve as a useful predictor for the other in high-latitude regions.
3. Soviet studies (e.g., Lebedev and Uralov, 1982) contain claims of high levels of skill in seasonal forecasts of summer ice coverage in the Greenland Sea. Since an SST input contributes to this skill, the Soviet scheme will be tested and used as one benchmark for the evaluation of the sea ice concentration-SST associations obtained here.
4. In view of (3), particular attention will be given to the spatial and seasonal generality of the SST/ice concentration relationships obtained for regions such as the Greenland Sea. Specifically, the temporal and spatial scales of North Atlantic sea ice concentration and SST fluctuations will be evaluated. This should allow assessment of regional and seasonal dependencies of SST-derived forecast skill.

The statistical correlations describing the SST/ice coupling will be diagnosed by isolating the contribution of individual years to the correlations, and by then examining the seasonal evolution of the anomalies within these years.

The methodology chosen for use in this study is primarily statistical rather than model-oriented. The choice of this strategy was made

because numerical models have not yet proven effective for long-range ice forecasting, even when run uncoupled to variable SSTs. The use of numerical models for operational forecasting of ice conditions by the United States Navy is presently limited to the 0-6 day range, and this model (see Preller, 1985) uses prescribed ocean currents and heat fluxes. State-of-the-art coupled ice-ocean models of the North Atlantic are constrained by either the use of prescribed North Atlantic fluxes into the Arctic (Semtner, 1987) or by a damping of the ocean variables to a prescribed climatology (Hibler and Bryan, 1987). Even when these constraints are eventually eliminated, the ice/ocean models will require prognostic forcing fields (at least from the atmosphere) for applications to monthly or seasonal ice forecasting. The relatively low levels of skill shown by atmospheric forecasts at monthly or seasonal ranges implies that numerical ice model forecasts for these ranges will be severely limited by atmospheric input. It is therefore likely that the present reliance on statistical techniques in monthly and seasonal ice forecasting (e.g., Stringer et al., 1984) will continue through the foreseeable future. This was the main consideration in the decision to use statistical techniques for this work.

Chapter II contains a description of the ocean characteristics of North Atlantic high latitudes, with an emphasis on the variables relevant to seasonal forecasts of the ice cover. A description of the data sets used and manipulations applied to them follows in Chapter III. Chapter IV contains an evaluation of a Soviet study of Greenland Sea

Chapter IV contains an evaluation of a Soviet study of Greenland Sea ice predictability. The results provide one of the benchmarks for comparison to the results obtained in the present work. Chapter V presents the results of this thesis and is followed by a discussion in Chapter VI. Finally, the conclusion and recommendations for future work are included in Chapter VII.

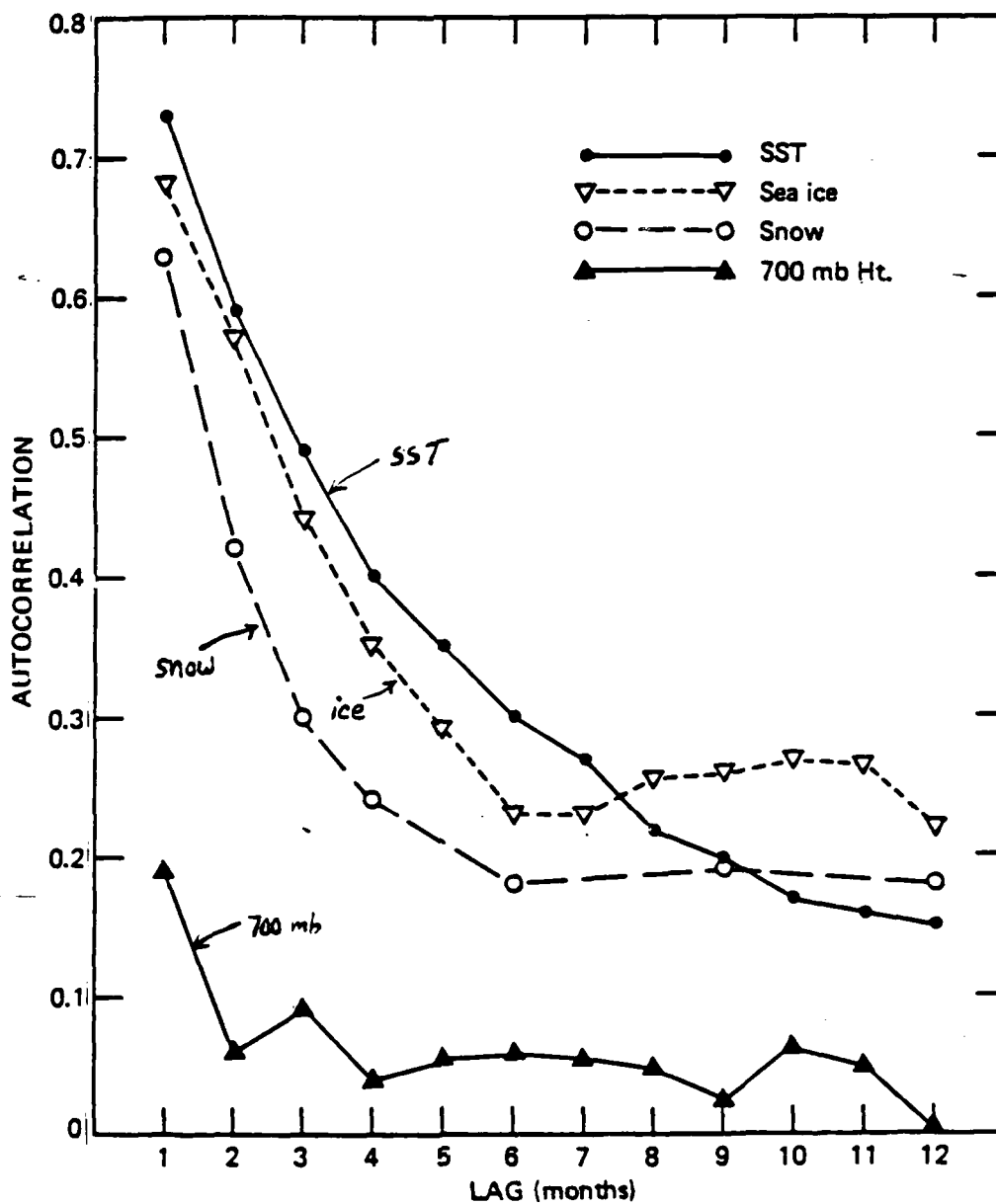


Figure 1.1 Compilation of autocorrelations of SST, sea ice, snow and 700 mb pressure anomalies from various authors. Autocorrelations were obtained over large areas of the north Pacific (SST and 700 mb) North American continent (snow) and north Atlantic (ice). Data were averaged over several months. [from Davis (1976), Lemke et al, (1980), Walsh (1982) and Namias and Born (1970)].

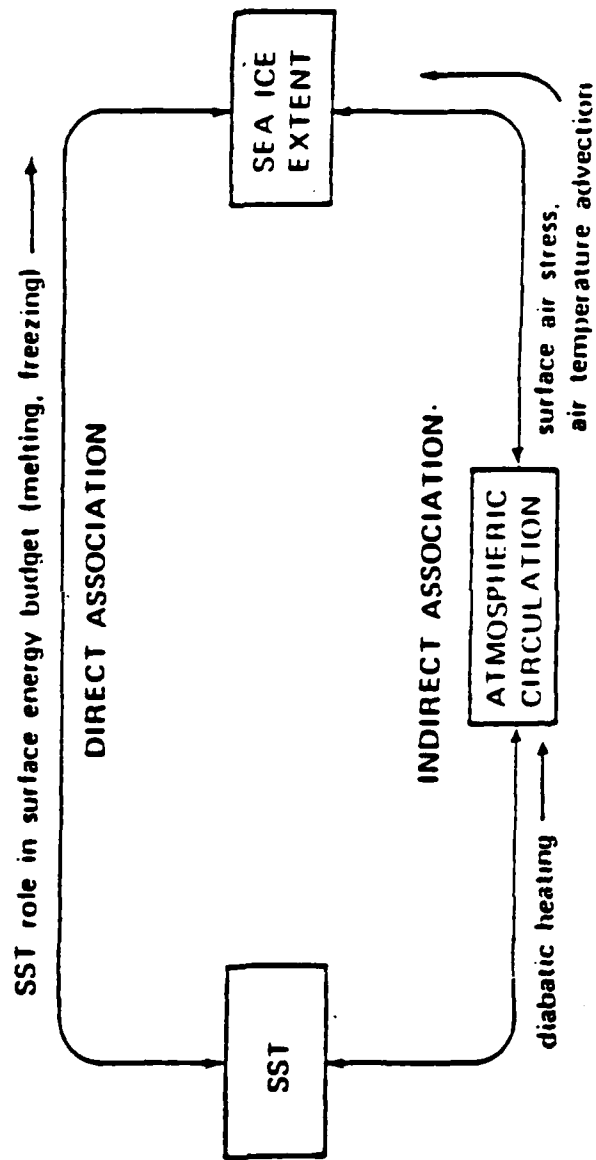


Figure 1.2 Schematic representation of the coupling mechanisms between sea surface temperature (SST) and sea ice extent [from Walsh and Sater (1981)].

## II. ARCTIC OCEAN CHARACTERISTICS

A feature which contributes to the uniqueness of the oceanography of the Arctic region is sea ice. Coachman and Aagaard (1974) state:

The general oceanographic consequences of a perennial or seasonal ice cover are:

1. The water temperature of the near-surface layer in the presence of ice is always maintained close to the freezing point for its salinity by the change of phase process.
2. Salt is excluded from the ice to a varying extent, but the water under the ice is always enriched in salt by any ice growth. The dependence of water density on temperature and salinity is such that close to the freezing point density is almost solely a function of salinity. Therefore, ice formation can increase the density locally and some vertical convection may result.
3. In the transfer of momentum from the atmosphere to the ocean, the wind must act on the sea through the intermediary of the ice.

The focus of this work is on the relationship between SST and ice concentration. Points 1 and 2 listed above indicate two mechanisms which serve to make the relationship an important one. The third point, especially in the resultant form of ocean currents, is also relevant.

A closer look at these three factors (ice, water and currents) is considered useful to put this study in perspective. Much of the information contained in the following sections A through C was extracted from Coachman and Aagaard (1974); Sater et al. (1971); and CIA (1978).

## A. ICE

The Arctic Ocean ice pack is confined by a nearly continuous boundary of land. The associated constraint on equatorward transport is a major reason why ice which forms here survives longer and develops into more complex forms than ice found in southern polar regions. An annual net heat loss and stratification of the underlying water also contribute to Arctic ice longevity.

Ice formation in open water starts in the autumn. As days grow shorter and nights longer, the amount of solar insolation decreases. Since radiation from the earth remains approximately constant, the energy budget changes from a net gain in summer through equilibrium to a net loss in the fall. The relatively warm mixed ocean surface layer of summer is cooled until reaching its freezing point and ice crystal formation commences.

Ice initially forms around the boundaries of the polar ice pack and over the shallow protected waters of high-latitude coastlines. The ice-covered areas continue to expand until they merge, forming an ice-locked Arctic Ocean from October to June. The ice cover starts from a summer minimum of approximately 5.2 million square km, then more than doubles in areal extent to a maximum of 11.7 million square km by the end of the ice season (CIA, 1978, p. 12).

The ice cover grows continuously until spring. Once the days start to lengthen, the amount of solar radiation increases until the surface energy budget is again positive. Snow cover will reflect up to 90 percent of the sun's incident radiation, which slows the initial

heating stages. However, once the air temperature reaches the snow's melting point, the albedo rapidly drops to approximately 40 percent. This results in a period of rapid snow melting.

Continued heating initiates melting of the underlying ice, causing cracks and flaws to develop. The surface melt water drains through the cracks, further eroding them until the ice breaks up into floes. Eventually, the ocean surface layer heats up, the floes gradually dissolve, and the cycle is complete.

The extremes of ice cover in the period 1953-1977 are shown in Figure 2.1. Minima and maxima for both summer and winter are presented. Obviously, sea ice cover has a large degree of variability both inter-seasonally and inter-annually. Ice cover is something of a misnomer as the sea surface is rarely covered by an unbroken expanse of ice. Even in the very thick ice regions of the winter polar pack, infrared measurements indicate that up to 10 percent of the area of the ocean is either open water or thin ice from recently refrozen leads (Sater et al., 1971, p. 41).

Multi-year ice (ice which has survived a summer's melting) comprises the majority of the polar pack, which averages 3 m in depth (Bourke and Garret, 1987). First-year ice rarely grows to a thickness greater than 2 m. However, the depth of the ice in any location is largely dependent on the external forces of wind and currents. These cause the ice to converge and diverge. When a region of ice converges, it buckles, folds, and overlaps, forming a rugged terrain and areas of considerably thick ice. For example, the Beaufort Gyre's

anticyclonic flow causes ice to converge along the north coast of Ellesmere Island and Greenland. The number of ridges in this region is well above the average for the Arctic pack (Weeks, 1978). The mean ice thickness here is of the order of 6 to 8 m (Bourke and Garrett, 1987). In contrast, the ice pack east of Spitzbergen (Svalbard) is not confined by land and is free to diverge. Here, the average ice thickness is significantly less, averaging approximately 2 m.

## **B. WATER MASSES**

The waters of the Arctic Seas are often described on the basis of temperature and salinity. As such, they are comprised of three main water masses: Arctic Surface Water, Intermediate or Atlantic Water, and Deep or Bottom Water (Coachman and Aagaard, 1974). Arctic surface water is generally limited in depth to 200 m. It has the most variable characteristics and can be modified by the weather, the season, and/or the physical environment. Temperatures in this layer vary from  $-1^{\circ}\text{C}$  to over  $2^{\circ}\text{C}$ . The salinity may be uniform to approximately 50 m, below which a sharp halocline increases the salinity to about 34.5 ‰ at the bottom of the layer. The variety of conditions in the surface water is evident in Figure 2.2, where vertical profiles of temperature and salinity from a variety of Arctic basins are plotted. Coachman and Aagaard (1974, p. 9) state that

The most important processes conditioning and modifying the surface layer are:

1. Addition of mass (fresh water) from the land, primarily from the large Siberian rivers;
2. Additions of fresh water locally through melting of ice;
3. Heat gain through absorption of solar radiation in non-ice-covered areas during summer;
4. Concentration of salt and hence increase of density of surface water, through freezing of ice;
5. Heat loss to the atmosphere through any open water surface, including leads in the central Arctic pack ice; and
6. Inflow and subsequent mixing of Atlantic and Pacific waters.

Processes 1, 2, and 3 occur only from June to September and lead to a decrease in water density. These buoyant waters form a surface cap which absorbs radiation and warms. Therefore, in summer, ice-free regions tend to have warmer and less saline surface layers. In areas where the ice does not recede, surface temperatures remain near freezing as incoming energy is used to melt the ice but surface layer salinities are reduced due to ice melting.

Processes 4 and 5 have the greatest impact in winter. In some areas, such as the shelf waters, conditions are such that the water becomes dense enough to penetrate into the intermediate Atlantic layer (Aagaard et al., 1985). However, in general, the strong pycnocline at the base of the surface layer prevents mixing due to surface density changes from penetrating below 200 m (Coachman and Aagaard, 1974).

As a consequence of the halocline-derived mixing barrier, process 6 does not have a great influence on the surface water variability. However, regions of high surface salinities (33 to 34.5 ‰) are found in

the Greenland and Labrador Seas and East Baffin Bay. These high salinities are due to the advection of North Atlantic surface water into the Arctic via warm surface currents from the south. One further consequence of the halocline barrier is that, in winter, when the surface layer cools below freezing, the relatively warm Atlantic layer is insulated from the ice cover. This severely limits any vertical heat flux. However, cases have been observed along the continental slopes where the Atlantic layer is forced to shallower-than-normal depths. Vigorous surface mixing can then break through the halocline, and vertical heat flux can occur (Coachman and Aagaard, 1974). This results in the ice melting from the bottom or not forming at all, forming open polynas in the ice cover.

The second water mass is called the Atlantic Layer. It is the result of the influx of warm and salty (35.0 to 35.1 ‰) North Atlantic water flowing into the Arctic basin through Fram Strait and the Barents Sea (Weigel, 1987). It extends from 200 m to 900 m with temperatures above 0° C. A temperature maximum of approximately 0.45° C, observed throughout the Arctic Basin, occurs between 300 m and 500 m, dependent on location. The salinity gradually decreases to approximately 34.9 ‰ in the Arctic Ocean and Greenland Sea and approximately 34.6 ‰ in Baffin Bay.

The final water mass, the bottom water, has temperatures below 0° C. The salinity is nearly constant from the bottom of the Atlantic layer to the ocean floor. The intermediate Atlantic water and deep water are advected into and out of the Arctic seas from adjacent areas.

principally through Fram Strait in the North Atlantic. The difference between intermediate and deep water is simply defined as where the temperature is above  $0^{\circ}\text{C}$  and below  $0^{\circ}\text{C}$ , respectively. Both water masses are nearly isohaline and therefore of nearly uniform potential density.

A temperature difference does exist between deep waters of the Canadian and Eurasian basins. The deep Canadian basin averages approximately  $-0.45^{\circ}\text{C}$  while the Eurasian basin temperature is approximately  $-0.79^{\circ}\text{C}$  (Aagaard et al., 1985). The two temperatures are kept separate by the Lomonosov Ridge, which acts as a sill between the two disparate water masses.

Observations of the vertical structure at various stations have been taken over long time periods and in many different locations. A remarkable similarity in the profiles has led to the conclusion that the Arctic basins are in a long-term dynamic steady-state condition (Coachman and Barnes, 1961). It is further noted that observed distributions of Arctic water properties are a result of continuing processes within the basins. Therefore, surface water T-S profiles indicate the local modifying processes, while T-S profiles for depths below 200 m indicate the common origin of the water.

### **C. CURRENTS**

The surface circulation of the Arctic basin has been derived from satellite observations and the plotting of ice island, buoy and floe station movement, as well as ship's tracks. The circulation of the Arctic waters is due both to water density differences and wind forcing.

Although large anomalies in the flow (compared to the long-term mean currents) are often observed, the long-term mean currents have been reasonably well documented in the north Atlantic seas (Krauss, 1986). A chart covering the majority of the area of interest in this study is included in Figure 2.3 which indicates the primary ocean currents.

Circulation and ice movement patterns in the peripheral Atlantic seas of the Arctic Ocean are dominated by two major currents systems, one warm, the other cold (Krauss, 1986). The warm North Atlantic Drift (NAD) Current splits off the Gulf Stream extension south of Newfoundland and heads northeast. It divides at the Mid-Atlantic ridge at approximately  $51^{\circ}$  N. One portion flows north to Iceland, where it becomes the Irminger Current. The Irminger Current itself then splits, with one branch taking water eastward around the north coast of Iceland, where it becomes the North Icelandic Current (NIC) and then the East Icelandic Current (EIC). The other branch flows westward, then to the south along the east Greenland slope, eventually rounding Kap Farvel and heading into the Davis Strait. The main portion of the NAD passes through the Scotland-Faroes gap and up along the Norwegian coast, where it is known as the Norwegian Atlantic Current. At the northern tip of Norway, the current splits again. One portion continues along the north shore of the USSR to Novaya Zemlya as the North Cape Current, while the other portion, called the West Spitsbergen Current (WSC), heads north into the Arctic Ocean just west of Svalbard.

The Transpolar Drift Stream is a major cold current originating under the polar ice cap and exiting the Arctic Ocean through Fram Strait, between Svalbard and Greenland. It passes down the east coast of Greenland as the East Greenland Current (EGC) and splits just north of Iceland (Aagaard and Coachman, 1968). One portion continues down the Greenland coast, rounds its southern tip, and heads north up the western coast of Greenland as the West Greenland Current. This portion merges with water flowing through the various passages of the Canadian Archipelago to form the cold Labrador Current. The Labrador Current follows the east coast of Canada from Baffin Island to Newfoundland. The second of portion of the split north of Iceland, known as the Jan Mayen Current, flows southeastward until it merges with the EIC and then finally with the northeastward-flowing Norwegian Atlantic Current. The southward EGC, eastward Jan Mayen Current, and north and westward flowing WSC combine to form a cyclonic gyre in the Greenland Sea. Filaments of cold water from the Transpolar Drift Stream also flow south from the Arctic Ocean in a broad, slow pattern from Svalbard to Svernaya Zemlya. This flow essentially limits the northward warming influences of the Norwegian Atlantic Current.

Figure 2.1 clearly shows the impact of the major current patterns on the mean ice coverage. The cold currents support ice growth and enhance the spatial extent of sea ice, while the warm currents melt the ice or preclude its formation. The southerly extent of the ice edge between regions of dissimilar temperatures can vary as much as 30

degrees of latitude. For example, the cold Labrador Current can often support ice cover as far south as Newfoundland. However, the North Cape of Norway, which is under the influence of the warm Norwegian Atlantic Current, rarely experiences sea ice. An extreme example is a region northwest of Svalbard, where open water can normally be found in winter as far north as  $80^{\circ}$  N. This is over 800 km farther north than any other open water in this season (Sater et al., 1971).

The currents also explain many other features of ice coverage and movement. Sea ice off the east coast of Greenland is found to originate primarily in the Arctic basin and as a result can be quite thick. The East Greenland Current continually carries a wide belt of Arctic pack ice southward through Fram Strait. As the ice season develops, the ice edge migrates farther and farther south down the east Greenland coast. Extreme years will have the ice edge as far south as Kap Farvel or as far north as  $70^{\circ}$  N. Although sea ice exists north of  $70^{\circ}$  at all times of the year, the belt narrows and has more open water in the late summer (Sater et al., 1971).

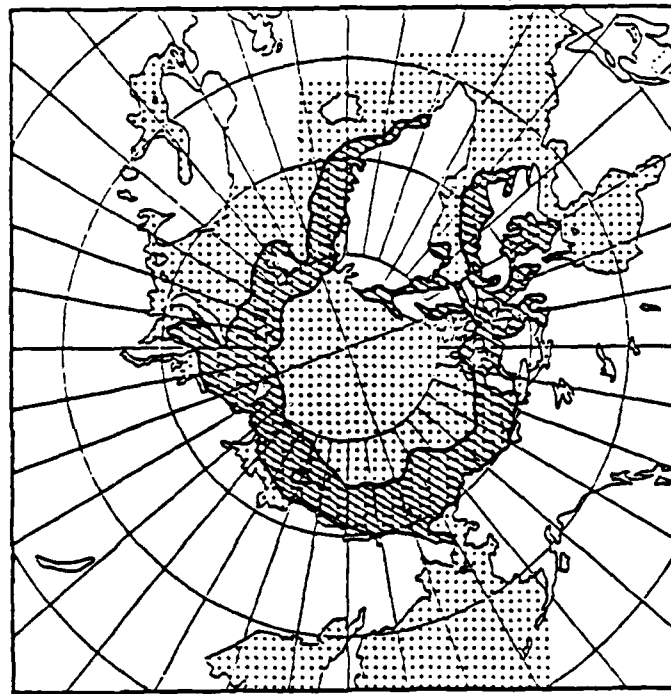
Strong contrasts in ice coverage are also observed within the Baffin Bay-Davis Strait region. The warm WGC follows the bathymetric contours of the southern and western Greenland continental shelf, keeping the southwest coast of Greenland ice free during most winters. However, the cold Labrador Current, as noted before, contributes to the large concentrations of ice found along Canada's east coast well south of Baffin Island. This current also carries the majority of

icebergs southward through the Grand Banks fishing zones and the Hibernia oil fields, and into the north Atlantic sea lanes (CIA, 1978).

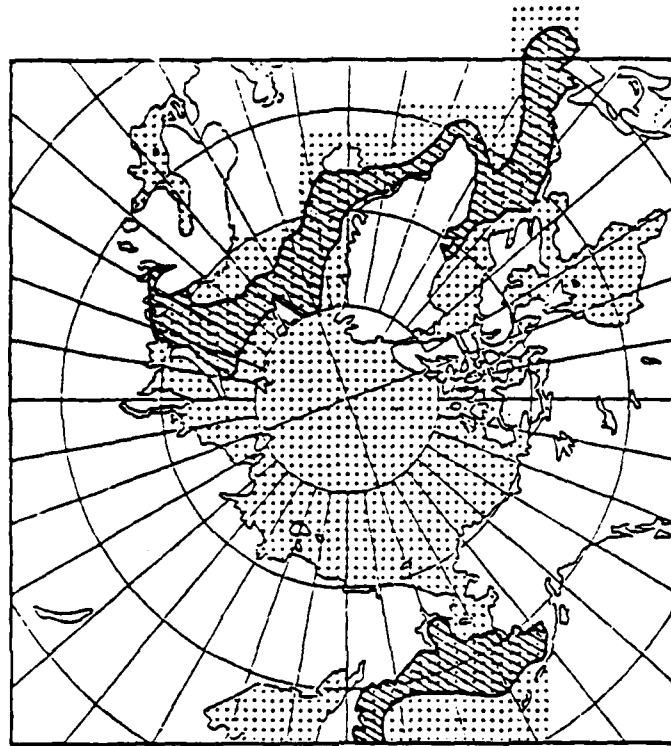
#### **D. SEA/ICE FORCING**

The primary driving forces for sea ice growth and movement are the air stress resulting from wind-induced surface drag and the water stress resulting from ocean currents. Variations in wind forcing are determined by the passage of synoptic scale weather systems having spatial scales of 100 to 1000 km and a duration of several days. Responses of the sea ice to mesoscale features of the atmospheric and oceanic forcing produce eddies and other fluctuations with length scales of 10 km and time scales of hours to days. Inertial oscillations of the drift of sea ice have similar periods. Longer term fluctuations, with time scales of weeks to seasons, represent responses to atmospheric and ocean forcing integrated over equivalent time scales.

When examining fluctuations varying on time scales of a season to several decades, the dominant signal in sea ice variability is clearly the annual cycle (Parkinson et al., 1987). Figure 2.1 contains 25-year envelopes of the positions of the Arctic ice edge at the end of February and August, the approximate times of maximum and minimum ice extent. At most longitudes, the seasonal change from summer to winter ice edge positions is considerably greater than the 25-year range of extremes for a particular month. The annual cycle is primarily a response to the seasonally varying insolation and may therefore be attributed to thermodynamic rather than dynamic forcing.



**(a) August**



**(b) February**

Figure 2.1 Ice extremes for the period 1953-1977 [from Walsh and Johnson (1979)].

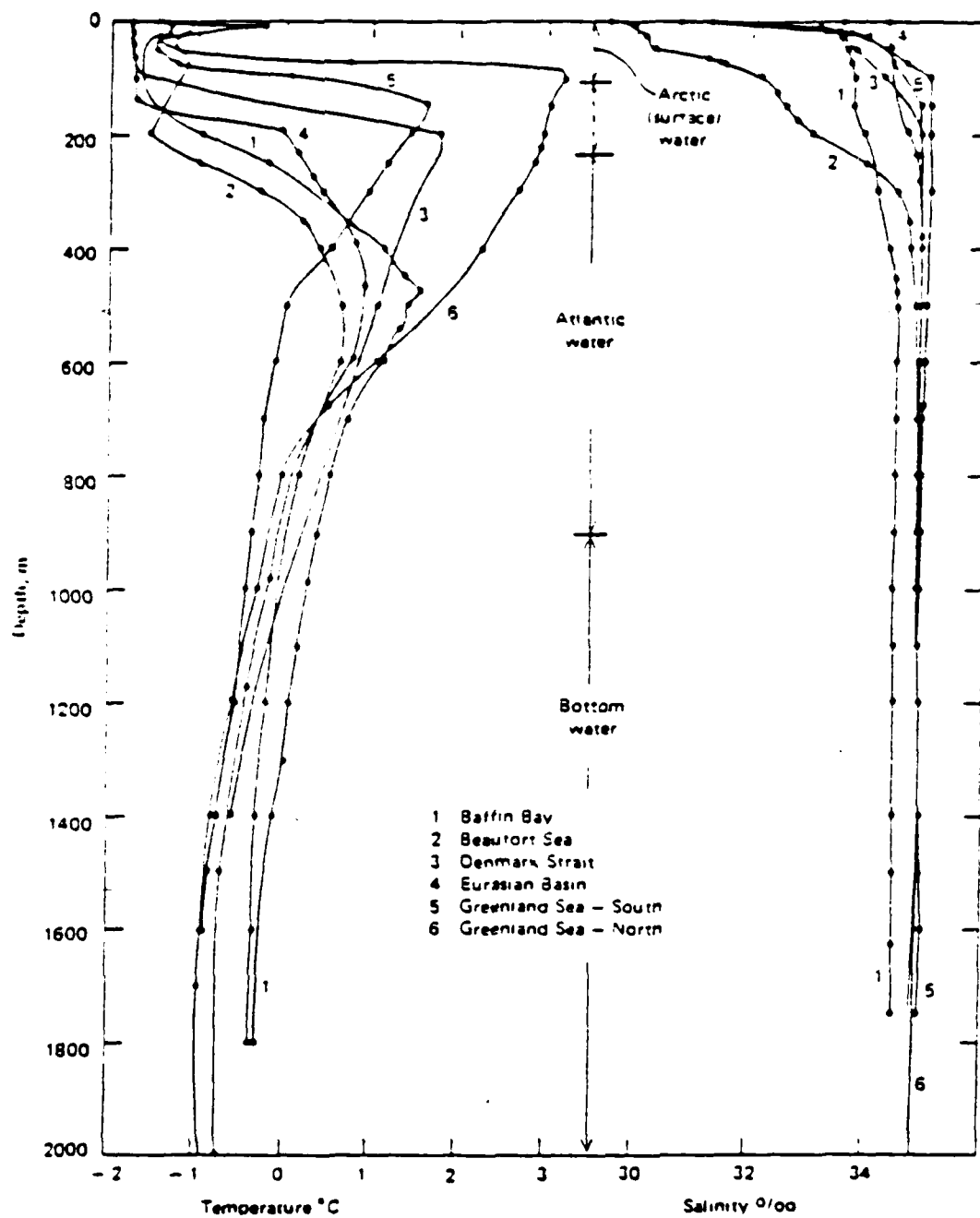


Figure 2.2 Vertical profiles of temperature and salinity from various northern high-latitude basins. [from Coachman and Aagaard (1974)].

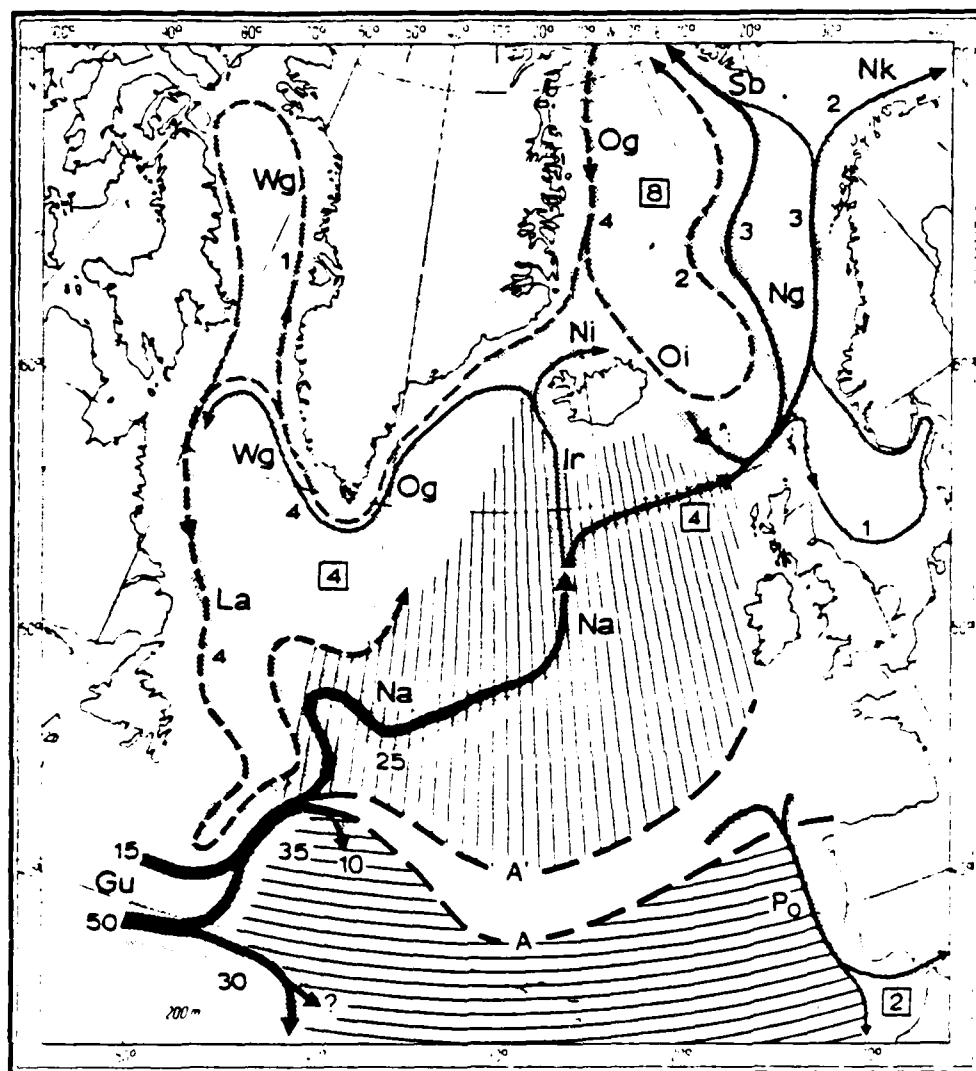


Figure 2.3 Schematic picture of the North Atlantic circulation as derived from drift experiments. Vertical shading indicates flow associated with the North Atlantic Current and horizontal shading indicates association with the subtropical gyre. Area between A and A' is the shifting boundary between the two. Warm currents are marked by solid arrows and cold currents by dashed arrows. [from Krauss (1986)].

### **III. DATA**

The statistical analysis in this study were based on two data sets. A modified COADS (Comprehensive Ocean-Atmosphere Data Set) data base provided monthly averaged sea surface temperatures, and the SEIC (sea ice concentration) data base provided sea ice concentrations (in tenths) determined for the end of each month.

#### **A. COADS**

COADS contains approximately 70 million reports from ships of opportunity, ocean weather ships, buoys, and bathythermographs. The data have been assimilated, sorted, edited, and summarized statistically for each month during the years 1854 to 1979 in 2° latitude X 2° longitude boxes over the entire world's oceans (Slutz et al., 1985). Data sources are noted in Table I.

COADS is considered to be the most complete data set of environmental parameters now available for the ocean/atmosphere boundary. However, as described below, Slutz et al. (1985) suggested that careful attention must be paid to the sometimes serious, and usually poorly understood, limitations inherent in any data set of this type.

Potential error sources for the COADS data set include:

1. Instruments, observation and coding methods, navigation accuracy, ship construction, and data density have all undergone historical changes. Many of these changes were unrecorded in the data sets from which COADS was derived.
2. SST measurement. Temperatures measured by engine intake have been shown by Ramage (1984) to be approximately 0.5° C

warmer than temperatures measured by bucket, but Slutz et al. (1985) indicate that, in a data set in which both bucket and intake temperatures are used indiscriminately, there is currently no way to effectively differentiate between the two and make appropriate corrections. Fortunately, inhomogeneities attributable to this problem were not severe during the time period examined by this study.

3. Diurnal effects. The data sets identify how much daylight had occurred prior to each observations. However, effects discussed by Ramage (1984), such as insolation, heating from the ship, and cloud cover biases, are not taken into account.
4. Significant errors can occur at every stage of observation, recording, transmission, and processing. Outlier filters were applied, but these can only remove the most obvious mistakes.
5. Duplication. Data files often contain numerous duplicate entries of one observation. This obviously biases the data. Over 25 percent of the original data were rejected because of duplication. However, other duplications undoubtedly still remain.

The region of interest for this thesis was contained in latitudes 28° North to 88° North. Preliminary review indicated that the compression of the longitude lines as they converge at the pole reduces the area of the 2° X 2° boxes to the point where the number of data reports per box become too sparse for reasonable analysis. As a result, the COADS data were averaged into 4° longitude X 4° latitude boxes. The average sea surface temperature in each box was then assigned to a grid point at the center of the 4° box. This resulted in a monthly grid of  $90 \times 15 = 1350$  points.

## **B. SEIC**

The SEIC data set containing monthly ice concentration was compiled by Walsh and Johnson (1979) from existing sea ice distribution observations. The original data sources are noted in Table II. The

data set was recently updated with the digitized ice data for 1972-1984 from the United States Navy/NOAA Joint Ice Center (Gross, 1986).

These data sets were compiled by applying observations to the 1648 data points contained in a 58 x 80-point grid. The spacing was 1° latitude (approximately 110 km). The grid covered those portions of the Arctic seas where ice was observed during any month. The 110 km spacing was chosen to permit resolution of year-to-year fluctuation. Grid point values contain the fraction (tenths) of area covered by ice within each box.

The data set contains values for each month from 1953 to 1984. 1953 was chosen as the first year since data records for several regions of the Arctic seas became essentially continuous from that period on.

Walsh and Johnson (1979) noted that SEIC, like the COADS, had limitations. Briefly, these included:

1. The data set covers a time period both before and after satellite coverage. Different observational methods cause nonuniformity in the data interpretation.
2. Imprecise concentration classifications. Ice conditions can vary considerably over relatively small areas. Ice-observing agencies such as the British Meteorological Office and the United States Naval Oceanographic Office tend to group the concentrations into categories such as "very open" (1/10 to 3/10) and "open" (4/10 to 6/10). When the source charts were digitized, the center value of these classification groups was used.
3. Overlapping data. When more than one source covered the same area, discrepancies were sometimes observed. In these cases, the mean was the value digitized and applied to the grid point.

4. Missing data. Some points in the early years had no data, particularly the Siberian Sector during the 1950s. In such cases, grid values were either linearly interpolated between prior and following months or a 25-year (1953-1977) monthly mean was used. These estimated values were flagged in the digital storage mode.

### C. DATA SET MANIPULATION

Correlations between SST and ice concentration required data covering the same years. The time period of January 1953 to December 1979, a total of 27 years or 324 months, was selected for both variables as each was available over this time frame.

The 58 x 80 ice concentration grid was considered the simplest to work with. Because the SST data field was reasonably dense, a simple bi-linear objective analysis was used to shift the SST values to the 58 x 80 grid. The four adjacent SST values were weighted as a linear function of distance. Data points on land were compensated by applying a zero weighting factor to land values but maintaining the total "correct" weightings at 1.0.

Statistical analysis of every grid point was both impractical and unnecessary. The prime concern was making predictions in areas of the marginal ice zone (MIZ). Therefore, a procedure was designed to select designated points of interest (POI) in that region.

Correlations of SST with regions of near ice absence (0/10) or total ice coverage (10/10) generally do not produce good results as the ice concentration does not vary much at these extreme conditions. The most useful correlations are obtained where large changes in ice concentration occur. The entire 324 months of ice concentration values

were averaged in order to form a mean grid for the entire sample period. Since the annual cycle contained the largest ice concentration variance, the 5/10 average concentration contour on this mean grid was considered the most probable location for these large variance values. A total of 17 well-spaced POIs were chosen along the 5/10 contour from Hudson's Bay to the northern tip of Norway. The points were selected to cover a wide variety of current, latitude, water mass type, and data density regimes. Subsequent analysis revised these POIs to permit better usage of available data and more consistent spacing north of Norway. The final POIs, plotted on the ice concentration grid, are shown in Figure 3.1. Ice concentration values at each POI were then averaged with values from 24 surrounding points. The 24 points were those which had positions two or less grid steps in both directions from the POI. This 25-point average provided some smoothing to the data.

Monthly averages for each POI over the 27 years were calculated for both ice concentration and SST. These monthly means were then subtracted from each mean monthly POI value to produce a monthly anomaly field. This process removed the annual cycle leaving monthly anomalies of SST (STDMA) and ice concentration (ICDMA). The removal of the annual cycle severely reduces the ice/SST correlations which, in "raw" form, are dominated by the annual cycle. The use of departures from the monthly mean focused concentration on the interannual fluctuations of the two variables.

Initial correlation runs were conducted using no time averaging, three-month centered averaging, and five-month centered averaging. Increasing the time averaging reduced the noise, allowing better determination of the correlation signal. Consequently, a five-month centered averaging was chosen as the final smoothing routine. A precedent for the use of five-month smoothing was established by Climate Analysis Center (NOAA/NWS/NMC). Its monthly climate diagnostics bulletin (NOAA, 1987) contains a number of products (e.g., the Southern Oscillation Index) where five-month averaging has been used to good effect for reducing contamination of signals by short-term noise. A summary of the data set manipulations is included in Figure 3.2.

TABLE I  
DATA SOURCES FOR COADS  
(Slutz et al., 1985)

	Million Reports (approx.)	Source
Atlas	38.6	NCDC
HSST (Historical Sea Surface Temperature Data Project)	25.20	NCDC, Germany
Old TDF-11 Supplements B and C	7.00	NCDC
Monterey Telecommunications	4.00	NCDC
Ocean Station Vessels, and Supplement	0.90	NCDC
Marsden Square 486 Pre-1940	0.07	NCDC
Marsden Square 105 Post-1928	0.10	NCDC
National Oceanographic Data Center (NODC) Surface, and Supplement	2.00	NCDC
Australian Ship Data (file 1)	0.20	Australia
Japanese Ship Data	0.13	M.I.T.
IMMPC (International Exchange)	3.00	NCDC
South African Whaling	0.10	NCAR
<u>Eltanin</u>	0.001	NCDC
'70s Decade	18.00	NCDC
IMMPC (International Exchange)*	0.90	NCDC
Ocean Station Vessel Z*	0.004	NCDC
Australian Ship Data (file 2)*	0.20	Australia
Buoy Data*	0.30	NCDC
'70s Decade Mislocated Data*	0.003	NCDC
<hr/>		
	100.00**	

\* Additions solely to 1970-1979 decade

\*\* The approximate total includes 26.58 million relatively certain duplicates, and some seriously defective or mis-sorted reports, which were removed by initial processing steps.

TABLE II

**DATA SOURCES FOR SEIC**

(Walsh and Johnson, 1979)

- U.S. Navy Fleet Weather Facility, 1976-1977: Arctic Sea Ice Analyses, Eastern and Western (weekly charts), Suitland, MD.
- \_\_\_\_\_, 1976a: Eastern Arctic Sea Ice Analyses, 1972-75. ADA 033344, Suitland, MD.
- \_\_\_\_\_, 1976b: Western Arctic Sea Ice Analyses, 1972-75. ADA 033345, Suitland, MD.
- British Meteorological Office, 1959-77: Monthly Ice Charts, HMSO, London (1959 charts in Mariners Weather Log, vols. 3-4).
- U.S. Naval Oceanographic Office, 1953-71: Report(s) of the Arctic Ice Observing and Forecasting Program, Tech. Reps. TR-49 through TR-52, TR-66, TR-69: Spec. Pubs. SP-70 through SP-81, Washington, DC.
- Canadian Meteorological Service, 1966-71: Ice Summary and Analysis, 1964-69 (Yearbooks), Toronto, Ontario.
- Arbok Norsk Polarinstitut, Oslo, 1963-71: Sea ice and drift speed observations (Annual reports). Also, T. Lunde, 1965: Ice conditions at Svalbard, 1946-1963. Arbok Norsk Polarinstitut (1963).
- Danish Meteorological Institute, 1957-1968: The Ice Conditions in the Greenland Waters (Yearbooks), Charlottenlund, Copenhagen.
- U.S. Navy Hydrographic Office, 1958: Oceanographic Atlas of the Polar Seas. Part II. Arctic, H. O. Publ. No. 705, Washington, DC.
- Danish Meteorological Institute. 1953-56: The state of the ice in the Arctic Seas. Appendices to Nautical-Meteorological Annuals (Yearbooks), Charlottenlund, Copenhagen.
- Jokill, 1953-67: Reports of sea ice off the Icelandic coasts (Annual reports). Icelandic Glaciological Society, Reykjavik.

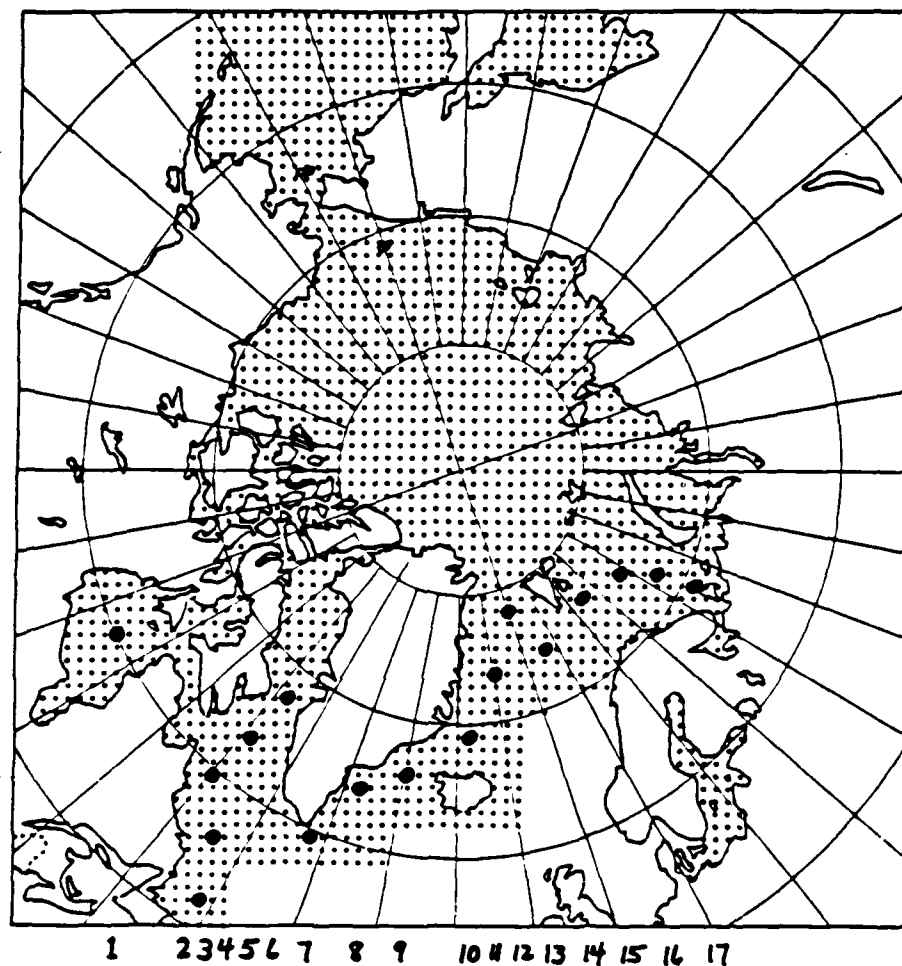


Figure 3.1 Chart depicting the 1° latitude spaced Cartesian grid. The 17 points of interest (POIs) used in this study are highlighted.

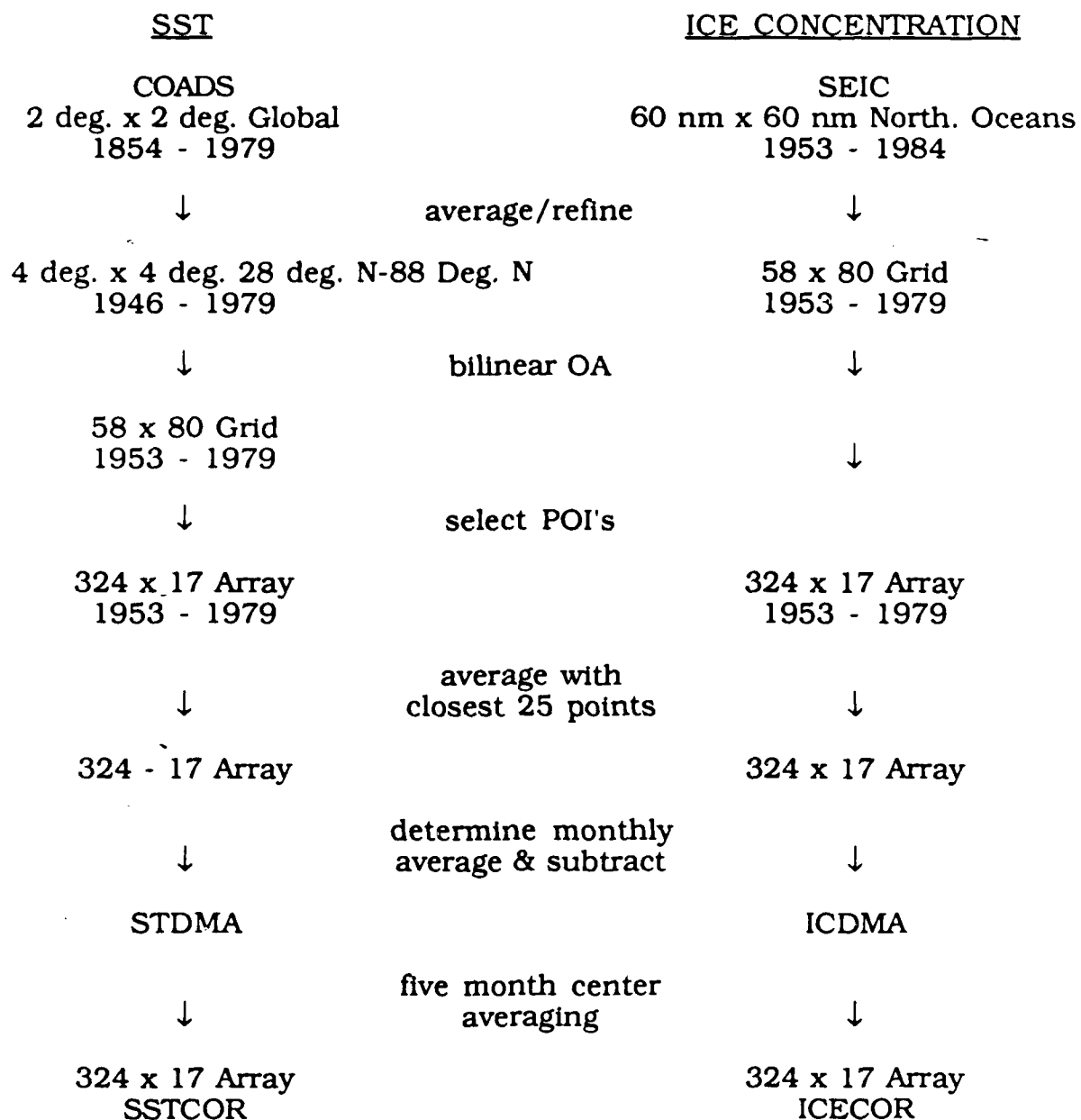


Figure 3.2 Data manipulation flow diagram.

#### IV. ASSESSMENT OF SOVIET SKILL

Soviet efforts at forecasting North Atlantic sea ice conditions appear to have increased substantially during the 1970s. The translated unclassified literature contains methodologies and results for the Labrador Sea and the Danish Strait produced from various studies done at the Murmansk branch of the Arctic and Antarctic Institute (e.g., Nikol'skaya et al., 1977; Orlov, 1977). Results for the Danish Strait and Greenland Sea have been reported by Kirillov and Khromtsova (1971), Kogan and Orlov (1981) and Lebedev and Uralov (1982). Although the studies cited above are based exclusively on empirical techniques, thermodynamic budget computations have also been used in other studies (e.g., Moskal', 1977) as the basis for long-range predictions of freeze-up dates in the Barents Sea.

With respect to ice forecasting efforts by the Western nations, the Soviets appear to have explored more thoroughly the use of statistical techniques for long-range ice forecasting, especially as regards the use of SST data. Kirillov (1977) states that the empirical procedures used by the Soviets have been more successful for the Atlantic seas than for the Pacific seas. The more limited studies of ice forecasting skill by western scientists (Kelly, 1979; Walsh and Sater, 1981) do not indicate a similar regional dependence.

Because the Soviets claim considerable skill in seasonal sea ice forecasts that use SST data as a predictor input, it was felt that tests of

their forecast procedures would provide a useful benchmark for the results obtained in this analysis. Accordingly, the Greenland Sea ice forecast procedures of Lebedev and Uralov (1982) were tested using the data sets described in Chapter III. These procedures permit predictions of Greenland Sea ice coverage for April, May, ..., August in terms of land station air temperatures and SST gradients from the previous winter (October to February) and the ice cover of the previous August. Separate equations for seven latitude zones and for each of the five months were derived by the Soviets using multilinear regression. The use of 7 x 5 sets of regression parameters increases the likelihood of sampling error, as the data base used by the Soviets was only 15 years long (1958 to 1972) for two of the regions and 25 years long for the other regions (years unspecified). The 25-year period used in this study for testing the results was 1955 to 1979, inclusive. This period was chosen in order to mesh with the SST/ice analysis of the present work.

The air temperatures used by the Soviets were for land surface stations in the general vicinity of the Greenland Sea: Fjord Radio, Jan Mayen Island, Cape Tobin, Medvezhil Island, and Reykjavik. Temperatures averaged over different combinations of these stations were used for different latitude zones. The SST index, which is similar to that used in earlier studies of the North Atlantic (e.g., Lebedev and Uralov, 1976), is the gradient or difference of SST between two pairs of Ocean Weather Ships. Specifically, the average of the SSTs for Ships A and C is subtracted from the average for Ships I and J (Figure

4.1). The physical basis of the index, as presented by Lebedev and Uralov (1982), is an apparent "indirect association" between SST and sea ice (see Chapter I). The authors argue that a stronger-than-normal SST gradient in the region shown in Figure 4.1 favors cyclone trajectories from the Danish Strait northeastward towards Spitsbergen, favoring easterly winds and reduced ice cover in the Greenland Sea. Weaker-than-normal SST gradients favor more eastward cyclone trajectories across southern Iceland to northern Norway, favoring northerly winds and increased ice cover over the Greenland Sea. The authors further state that, in the latter case, the SSTs close to the MIZ are likely to be warmer than normal, despite the postulated dynamical tendency for above-normal ice coverage.

Because the SST and air temperature predictors are averaged over the October-February period preceding the spring/summer being forecast, the "lead time" of the forecasts is 2 to 6 months. The procedure does not require forecasts of atmospheric variables. (Lebedev and Uralov claim that the SST/cyclone association is largely absent during the spring/summer months.)

The 35 Soviet regression equations (5 months x 7 latitudinal sectors) were tested in several ways:

1. Forecasts were computed using the regression equations exactly as listed by the Soviets, but using SEIC and COADS data as the Soviet data was not available;
2. Forecasts were computed using the Soviet predictors but with the regression constants re-derived from the COADS and SEIC data; and

3. Forecast skill was evaluated separately for the 1955-79 and 1958-72 periods.

The results for three of the seven regions are shown in Figures 4.2 to 4.4 in terms of overall correlation coefficients (predicted vs. observed) for the two periods. The following general conclusions are apparent from these figures:

1. Considerable skill is present in nearly all cases, both in forecasts based on the Soviet regression constants and in forecasts based on the re-derived constants;
2. In most cases the recomputation of the regression constants produced modest enhancements of skill over the values obtained directly from the Soviet equations; and
3. The skill obtained using SEIC and COADS data and Soviet predictors, even with the re-derived constants, is generally five percent or more lower for nearly all cases than that listed by the Soviets.

The average correlations for all plotted data points in Figure 4.2 are 0.73 for the published Soviet claims, 0.59 for the forecasts based on the re-derived regression constants, and 0.43 for the forecasts based on the Soviet regression constants.

The partial correlations between the observed ice coverage and the individual predictors are shown in Figure 4.5. While there is some scatter among the various regions and months, several conclusions can again be drawn:

1. The persistence predictor (ice cover of the previous August) is generally the weakest of the three correlators. In no case does the correlation based on this predictor exceed the 95-percent significance level;
2. The surface air temperature is the highest individual correlator in the early portion of the predicted season (April and sometimes May); and

3. The SST predictor is generally the highest correlator in the latter half of the ice season (June-August).

Of the results gleaned from the Soviet skill assessment, the most pertinent to the present work are that SST input does enhance the seasonal predictability of the Greenland Sea ice coverage, and that the correlation between winter SST and summer ice coverage is statistically significant. Findings such as these have not been reported in the Western literature. The additional observation that the skill levels reported by the Soviets are significantly better than those achieved by other techniques suggests that predictor selection, whether the result of explicit or implicit screening, has introduced some sampling bias. This cannot be tested quantitatively without additional information concerning the data used by the Soviets, especially the source of their ice data. Differences in the ice data may have contributed to the discrepancies between the two sets of forecast statistics. Nevertheless, the confirmation of the SST/ice association in the Soviet results provides perspective for the more general SST/ice analyses described in the following chapters.

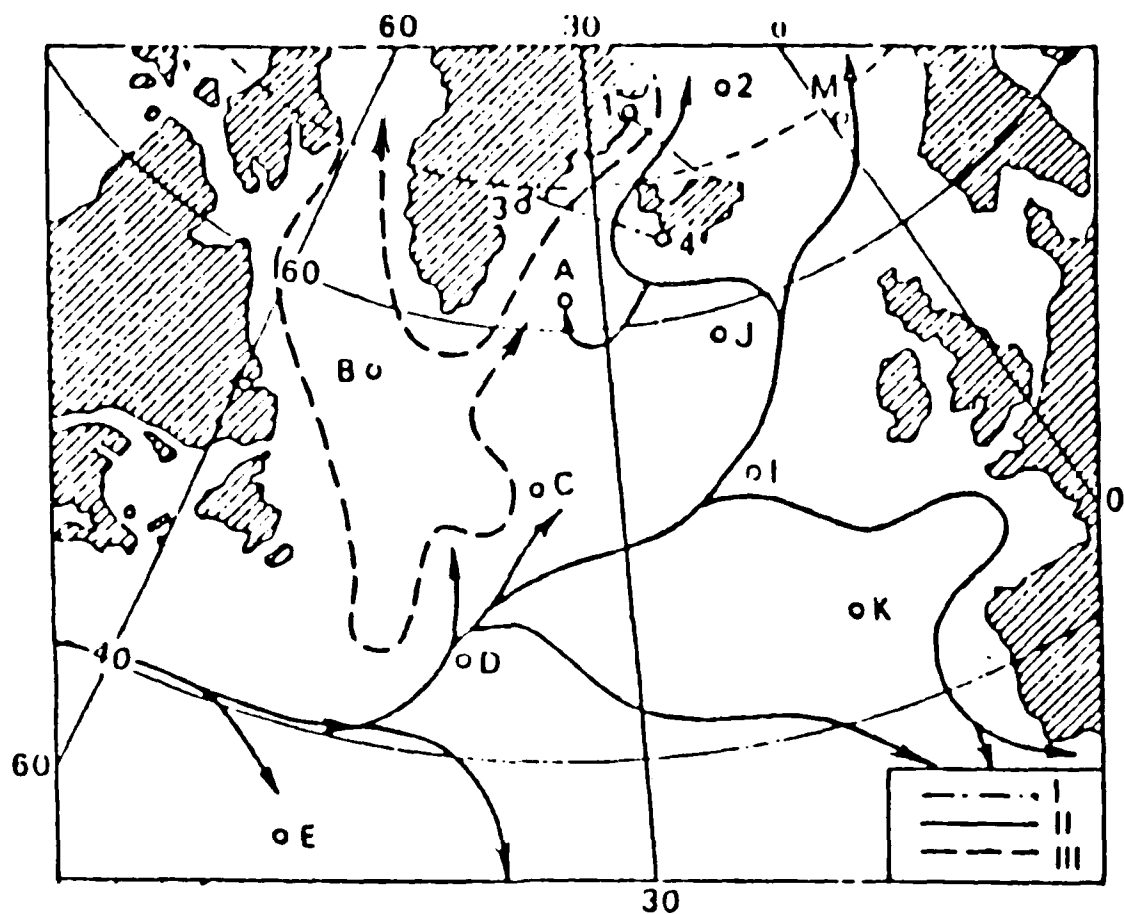


Figure 4.1 Region of study for the Soviet ice cover prediction method. Ocean stations are labelled by letter. Solid arrows are average warm currents and dashed arrows are average cold currents. The numbered positions are meteorological stations: 1-Cape Tobin; 2-Iceland Sea; 3-Angagssalik; 4-Reykjavik [from Nikol'skaya et al. (1977)].

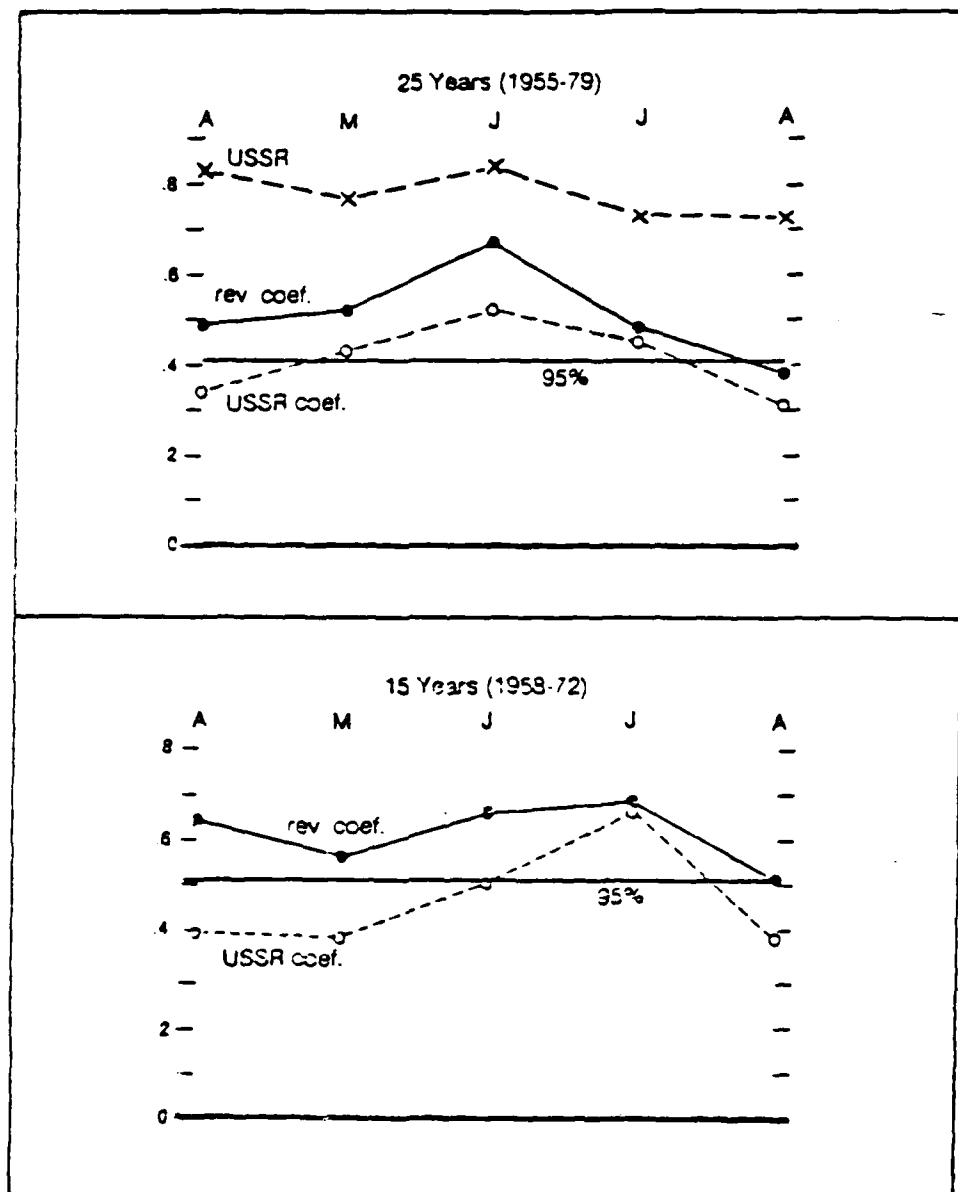


Figure 4.2 Comparison of Soviet correlations (USSR) with correlations calculated using our data and Soviet regression constants (USSR coef.) and our data with recalculated regression constants (rev. coef.). The same variables are used in all three cases. This figure shows values for the Greenland Sea.

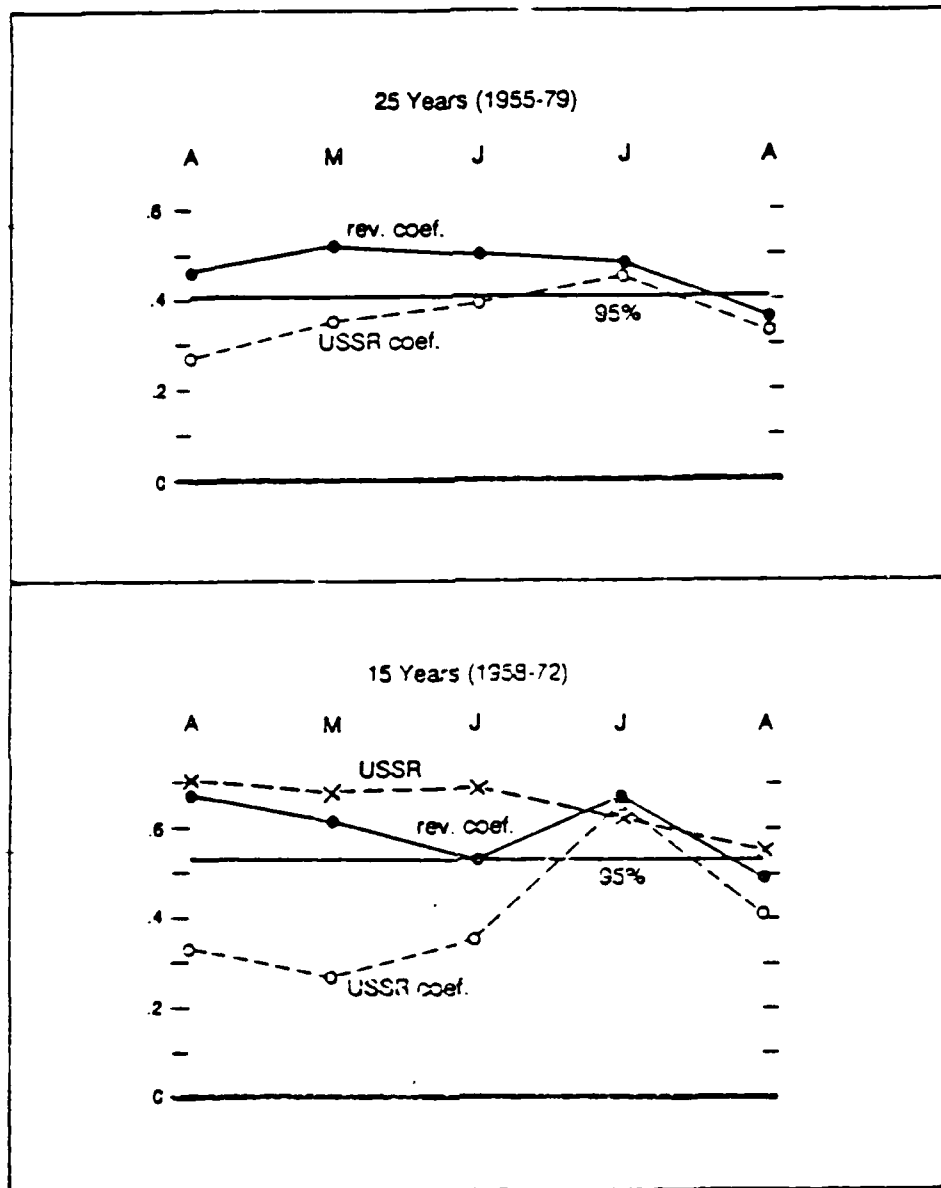


Figure 4.3 As for 4.2 except using values for the latitude band 73°-78° N.

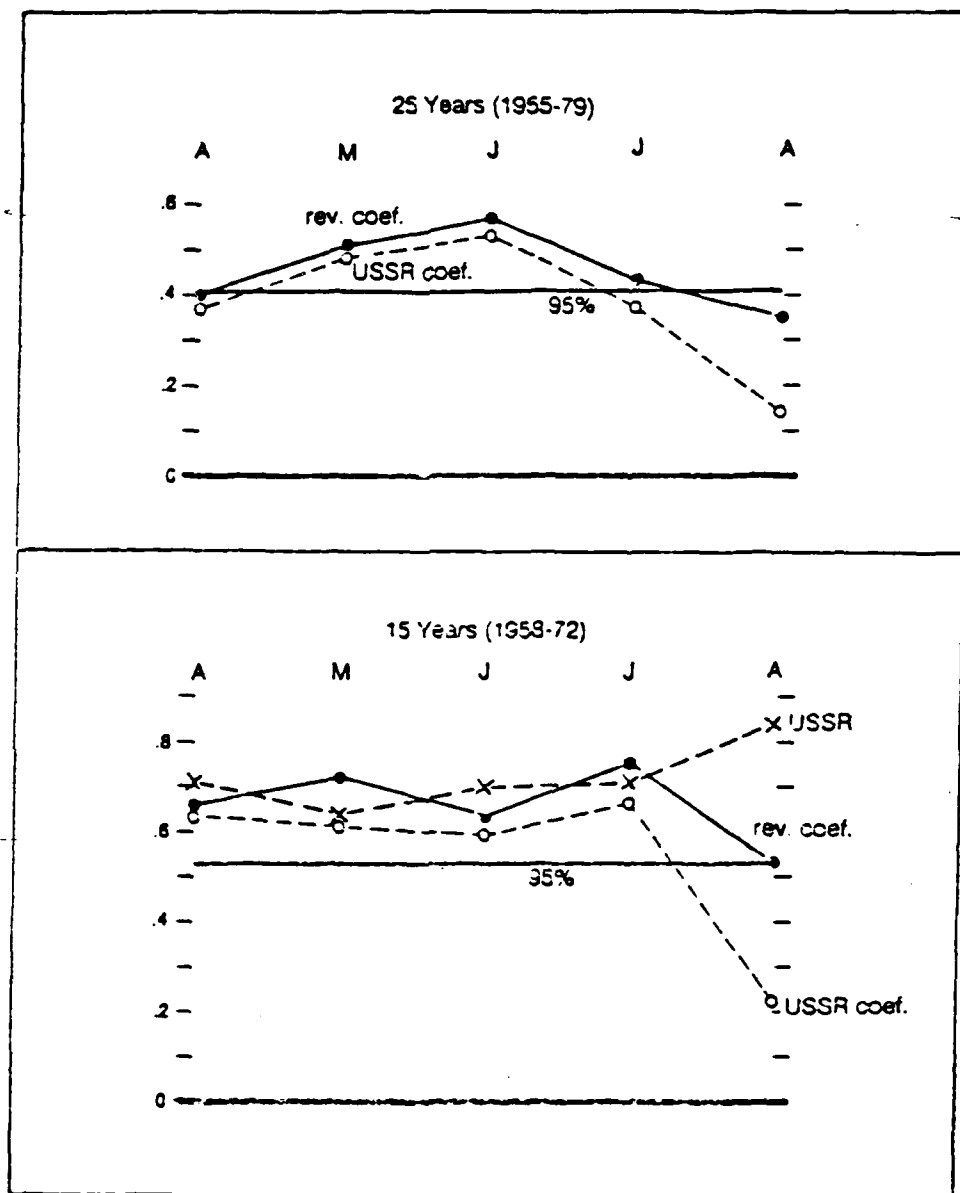


Figure 4.4 As for 4.2 except using values for the latitude band 68°-73° N.

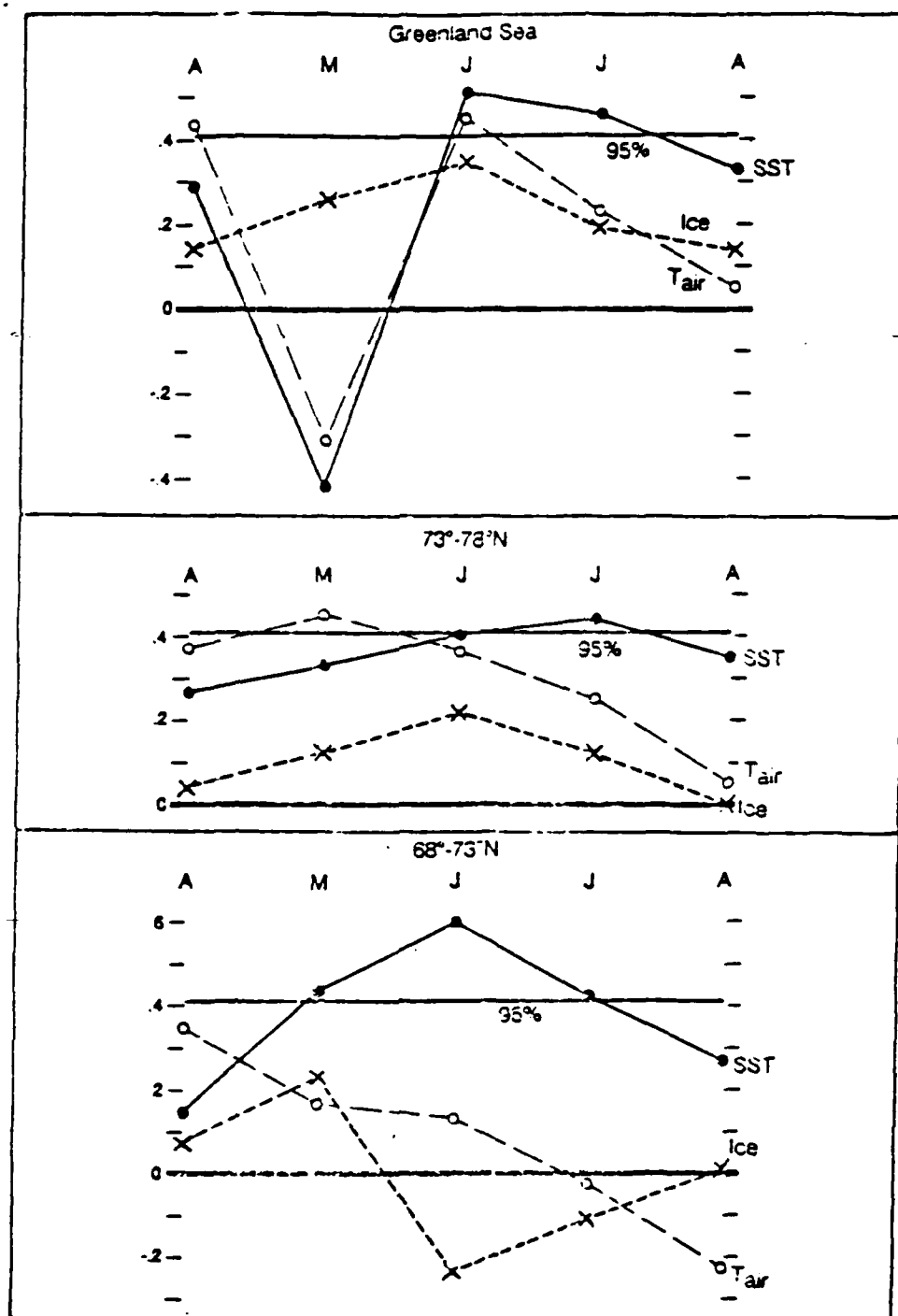


Figure 4.5 Correlations between ice cover and the three individual predictors (ice, surface air temperature, and SST) for the three regions. The 25-year (1955-1979) data set is used.

## **V. RESULTS**

Statistical analyses of the COADS and SEIC data sets resulted in a large volume of information. The most effective means of displaying and presenting this data was in the form of time-longitude contour plots. The time scale was displayed in the vertical and labeled in months. The horizontal scale identified the POIs. Although the seventeen selected points were approximately evenly spaced, the bottom scale is not a linear function of longitude. It ranges from approximately 90° W to 60° E.

### **A. SST/ICE CONCENTRATION ANOMALIES**

The SST and ice concentration anomalies (difference from monthly means) are shown in Figures 5.1 to 5.6. Both variables have typical time scales ranging from a season to a year and spatial scales covering several POIs. Although five-month time averaging was used to smooth the time scales, no distance averaging between POIs was conducted. Therefore, distances covered by the anomalies on the contour plots are representative of their true extent.

Anomalies lasting over a year and covering the entire POI range are observed in both fields. Months 82 to 122 for Figures 5.1 and 5.2 and Figures 5.4 and 5.5 show positive SST and negative ice concentration anomalies, respectively. Figures 5.2 and 5.3 and 5.5 and 5.6 show opposite anomalies for months 200 to 230. These two anomaly

periods correspond to the relatively ice free years of 1960-1963 and heavy ice years of 1970-1972.

There does not appear to be any tendency for advection of the anomalies along the MIZ as evidenced by a lack of anomaly movement between POIs over time.

## **B. PERSISTENCE (AUTOCORRELATION) CONTOURS**

Persistence (autocorrelation) in this report is similar to, but has some important differences from, the purely mathematical definition of autocorrelation. To address whether or not some degree of "seasonality" existed in the correlations, four base months (January, April, July, and October) were chosen to represent the four seasons (Winter, Spring, Summer, and Fall). For each correlation calculation, the base month remained fixed for each successive year, while the lag determined the second month of the correlation pair. Since lags were calculated up to  $\pm 12$  months, the number of correlation pairs was reduced from 27 to 25. For example, if July were chosen as the base month and the autocorrelation value were calculated for lag +4, data from July for the years 1954-1978 would be correlated with data from the following November for the same 25 years. However, if the autocorrelation value was calculated for lag -4, data from the Julys would be correlated with data from the previous Marches. Note that the correlation pairs at lag +4 are not the same as at lag -4, therefore, the normal property of an autocorrelation that  $AC(L) = AC(-L)$  does not hold. Similarly, the autocorrelation calculated in this work can not be transformed to determine spectra.

The formula used to calculate autocorrelation values was as follows:

$$AC(L) = \frac{\sum_{y=2}^{26} Ay(T) Ay(T+L)}{\sqrt{\sum_{y=2}^{26} Ay(T)^2 \sum_{y=2}^{26} Ay(T+L)^2}}$$

where

AC(L) = persistence (autocorrelation) at lag L

Y = the data year (1 to 27 corresponds with 1953 to 1979)

Ay(T) = variable value for designated month T and year Y

Ay(T+L) = variable value at designated month T plus lag L for year Y

The nomenclature has been changed from the normal representation to emphasize the unique character of the autocorrelation. Assuming a normal distribution, the 95-percent significance level for a sample size of 25 lies within approximately two standard deviations of the mean. Therefore:

$$r_{.95} \doteq \frac{2.00}{\sqrt{25-1}} = \frac{2}{\sqrt{24}} \doteq 0.4$$

Thus, for a null hypothesis of zero correlation, all correlations exceeding 0.4 have less than a 5-percent likelihood of having occurred by chance.

Persistence contours are presented for both ice concentration and sea surface temperature in Figures 5.7 to 5.14. Since the four designated base months were three months apart, and lags of  $\pm 12$

designated base months were three months apart, and lags of  $\pm 12$  months were used for each of them, considerable time overlap exists between contour plots. This overlap allows cross-checks to be made to confirm that calculations are consistent.

To demonstrate this cross-check ability, examine Figure 5.7. This figure shows a negative correlation of  $-0.1$  to  $-0.3$  for position 6 at-lags of  $+5$  to  $+9$  months. Although not statistically significant, this indicates that January ice concentration is negatively correlated with ice concentration the following summer and fall. The feature is repeated in Figure 5.9 at lags of  $-4$  to  $-7$  months. Here, the summer ice concentration is negatively correlated with the ice concentration values of the previous winter and spring. This feature can also be confirmed in Figure 5.10 at lags of  $-5$  to  $-9$  months where ice concentration in fall correlates negatively with ice the previous winter and spring.

For ice persistence, the average 0.7 correlation (50 percent of variance) contour is at  $\pm 2$  months lag. However, the contours show marked differences between POIs. For example, Figure 5.10 shows very low correlation for region 2 even at  $\pm 2$  month lag, yet a 0.7 correlation is observed at a lag greater than  $+4$  months for region 14. Similarly in Figure 5.8, correlations at region 6 decrease rapidly with time, especially at positive lags, yet the 0.7 contour extends to lags longer than  $-6$  months for regions 8 and 14.

Ice persistence is in general at a minimum starting in summer and at a maximum starting in winter. Averaged over the year, POIs 1, 5-7, 11-13, and 15-17 appear to have the lowest persistence values.

while 7-10 and 13-15 appear to have the highest values. It should be noted that, with five-month centered averaging, lags must be greater than four months in order for the data pairs to be totally independent.

SST persistence is generally stronger than the ice persistence. The average 0.7 correlation contour for SST extends to almost  $\pm 3$  months. The SST persistence contours also display marked differences between POIs. Strong SST persistence gradients are particularly noticeable at position 1 and so are low persistence lobes at position 11 and 12. Subsequent analysis indicated that these low persistence values are due primarily to the lack of data at these points.

The summer season SST values have the highest persistence values while the spring and winter values have the lowest. Aside from the low data regions, position 4 has the lowest yearly average SST persistence. Positions 7-10 and 14-16 indicate the highest average. Two notable features in Figure 5.14 are the 0.7 contour at -6 months lag for position 8 and at +8 months lag for position 6. Figure 5.12 also shows two high persistence features. Position 8 has the 0.7 contour at a lag of +7 and position 10 has the contour at a lag of -5 months.

### **C. CROSS-CORRELATION CONTOURS**

Cross-correlation coefficients were calculated for each POI in a similar manner as the persistence plots, with similar differences from the true mathematical definition of cross-correlation. The cross-correlation formula used was:

$$XC(L) = \frac{\sum_{y=2}^{26} Ay(T) By(T+L)}{\sqrt{\sum_{y=2}^{26} Ay(T)^2 By(T+L)^2}}$$

where

$XC(L)$  = cross-correlation at lag  $L$

$Ay(T)$  = first variable value for designated month  $T$  and year  $Y$

$By(T+L)$  = second variable value for designated month  $T$  plus lag  $L$  for year  $Y$

$Y$  = data year (1 to 27 corresponds with 1953 to 1979)

As for the autocorrelations, lags from -12 to +12 months were calculated, thereby reducing the number of pairs of correlated values to 25 for each POI. The same four designated months were chosen as the basis for the correlation calculations and the large time overlap between seasons again permitted cross-checking of notable correlation features.

Negative correlations were expected, especially at short lags because cold temperatures are associated with more ice and warm temperatures with less ice. Lead and lag relationships were expected to provide some information regarding cause and effect. That is, does a cold temperature anomaly precede a more concentrated ice field or is the reverse true?

The cross-correlation contours are contained in Figures 5.15 to 5.22. Cross-correlation values for POIs 1 to 4 and 11 to 12 are positive for most seasons. These are not physically meaningful values, but an

artifact resulting from insufficient data density in the applicable regions as mentioned previously. These regional values should be ignored.

Regions of high negative cross-correlations were observed. Cross-correlation coefficient values of 0.4 or greater were statistically significant and 0.5 or greater were considered noteworthy. The high negative correlation regions in general cover two to three POIs and two to eight months in lag. The same correlation features can be observed on different plots due to the large time overlap. The four most prominent correlation features are located as follows:

1. Feature A

This feature is observed in Figure 5.18 between points 13 and 16 (E. Norwegian Sea, Bear Island, and N. Barents Seas) from lag -1 to +10. It shows the largest extent of continuous negative correlation greater than -0.6. Confirmation is observed in Figure 5.19, where the same feature appears at lags +1 to -8. This feature also shows strongly in Figure 5.17 at 0 to 12 months lag, with additional confirmation in Figure 5.22 at lags of +3 to -8 months. The cross-correlation suggests that summer and autumn SSTs might be useful for points 13 to 16 in predicting ice cover 1 to 10 months later.

2. Feature B

This feature is observed in Figure 5.19 at point 10 (Iceland Sea) for lags of +2 to +11 months. It is confirmed in Figure 5.17 at lags of 0 to -9 months. The spatial extent of this feature is probably larger than depicted, but the poor data density at points 11 and 12 has

reduced its spatial scale. The correlation suggests that winter ice concentration values at point 10 might be a good predictor for SSTs up to nearly a year later.

### 3. Feature C

Figure 5.17 also shows a second high correlation lobe for region 10 at lags of 0 to +7 months. It is confirmed in Figure 5.22 at lags of -2 to -8. This feature suggests that summer SSTs might be useful predictors for ice cover the following autumn and winter in the Iceland Sea.

### 4. Feature D

This feature is observed in Figure 5.18 at point 7 (Kap Farvel) for lags of -8 to -12 months. The correlation is confirmed in Figure 5.19 for lags of +7 to +10 months. The correlation suggests that, for point 7, winter ice might be used to predict SSTs the following autumn. Although this feature is notable for its large lag, it is small in spatial scale and will not be examined in detail.

## **D. CORRELATION FEATURES**

Once it was determined that significant cross-correlation features existed, they were compared to determine if any similarities or notable differences could be observed.

Large negative correlations may result from a few extremely anomalous years (1-2 years with large ice or temperature anomalies of opposite sign) or from a systematic opposition of the signs of the ice and temperature anomalies during the 25 years. The following decomposition is included to address the questions of which and how

many years contributed to the notable ice concentration/temperature correlations of the previous section. Assessment of contributions to the correlation may provide information on thresholds of anomaly magnitudes which must be reached in order to use the anomalies in operational long-range ice forecasting.

Table III lists the 25 anomalies of SST and ice concentration used to calculate the cross-correlation value at lag +2 months for Feature A. This particular region was chosen from Figure 5.18. Also listed is the product of the anomalies and the percentage of the final negative cross-covariance which each year combination provided from 1954 to 1978. Positive cross-covariance values were disregarded as they were generally small. Similar tables were compiled for Feature B at lag -6 months and Feature C at lag -4 months. These are included as Table IV and Table V and were chosen from Figures 5.17 and 5.22, respectively.

The most noticeable feature indicated in the tables is that the negative correlation coefficients are heavily dominated by anomalies in only 3 or 4 years. Table III indicates 19 of the 25 SST/ice concentration anomaly pairs provide a negative correlation. However, the years 1961, 1964, 1968, and 1978 contribute over 69 percent of the total negative cross-covariance. Table IV indicates that 20 of 25 correlations are negative with 1960, 1961, 1962, and 1968, providing over 44 percent of the total negative cross-covariance value. Similarly, Table V shows that 21 of 25 correlations are negative with 1960.

1961, 1967, and 1968, providing over 55 percent of the total negative cross-covariance.

The signs of the anomalies of SST and ice concentration appear evenly distributed over the 25 year data period. Each variable has approximately half of its anomaly values positive and half negative. Neither negative nor positive anomalies for either variable appear to dominate for any of the correlation values examined. The absence of any trend is also apparent from these tables.

#### **E. STRONG ANOMALY YEARS**

The final analysis step of this project was to examine the SST anomalies in the four dominant years for each of the three most notable regions of high negative cross-correlation. The purpose of this analysis was to determine whether the spatial and temporal characteristics of the anomalies of the key years were sufficiently similar to permit generalizations about the evolution of the feature producing the larger lag-correlations.

Graphs of SST anomalies for the four dominant years were constructed. The series of graphs for Feature A are contained in Figures 5.23 to 5.26. Feature B graphs are included as Figures 5.27 to 5.31, and Feature C graphs as Figures 5.32 to 5.35. The sequence of graphs for each feature contains anomaly plots for the months preceding and following the highest cross-correlation value month. The intent was to determine the degree of consistency in the anomaly development. The following general observations were made.

1. The largest SST anomalies, both positive and negative, occurred at POIs 10, 13, and 14;
2. The east-west extent of anomalies was typically two to three points. However, the consistently low anomaly values at POIs 11 and 12 can probably be attributed to the "data void" noted previously for these points. If the low values at these points are ignored, the east-west extent of a very large anomalous region is observed from POIs 9 to 16 (almost the entire water mass from Greenland to the USSR);
3. The largest anomalies do not occur specifically in the months of highest negative cross-correlation, but instead are generally observed in the summer season. The anomalies grow in spring and decay in the fall and winter. They appear to decay at a slower rate than they grow;
4. The four high correlation years for Features A and C contain two years of mainly positive and two years of mainly negative SST anomalies. Feature B contains three years of positive and 1 year of primarily negative SST anomaly;
5. After examining the results from several high correlation regions, it was noted that the most influential years are not randomly distributed through the data set. The years which most often provided high correlations and the signs of their respective SST anomalies were:
 

1960	positive
1961	positive
1964	negative/positive
1967	negative
1968	negative
1972	negative/positive
1978	negative/positive
6. Consecutive prominent years show similar anomaly profiles for certain months (for example, the years 1960-1962 in Figure 5.32). However, in general, the anomaly graphs display a wide variety of profiles with no apparent links. This is further support for the observation that SST anomalies appear to be regionally dependent (differ widely between POIs). Additionally, no evidence could be found to indicate that thermal advection was a factor in SST anomaly persistence. This finding also supported earlier conclusions about the lack of influence by advection.

While the results summarized above indicated that there was some spatial and temporal coherence in the anomaly fields, the differences were sufficiently large that generalizations about evolutionary characteristics of the anomalies could not be made. It is therefore likely that predictive applications will need to rely more heavily on threshold values of local or regional anomalies rather than on broad-scale patterns in space and time. Predictive applications are discussed further in the following chapter.

TABLE III

**THE 25 ANOMALY PAIRS USED TO CALCULATE  
THE HIGH CROSS-CORRELATION VALUE  
FOR POI 15 AT LAG +2 FOR OCTOBER**

Year	SST Anomaly	Ice Conc. Anomaly	Product	% of Negative Cross- Covariance
1954	0.420	-0.370	-0.155	0.690
1955	0.070	-0.620	-0.043	0.193
1956	-0.260	0.020	-0.005	0.023
1957	-0.030	0.760	-0.023	0.101
1958	-0.120	0.530	-0.064	0.283
1959	0.760	0.480	0.365	0.000
1960	0.860	-1.370	-1.178	5.234
1961	1.850	-3.300	-6.105	27.122
1962	-0.090	-1.330	0.120	0.000
1963	0.410	-1.980	-0.812	3.606
1964	1.570	-2.420	-3.799	16.879
1965	-0.110	0.540	-0.059	0.264
1966	-1.770	0.600	-1.062	4.718
1967	-0.420	1.510	-0.634	2.817
1968	-1.370	2.770	-3.795	16.859
1969	1.060	-0.160	-0.170	0.753
1970	-0.540	0.950	-0.513	2.279
1971	-0.580	1.340	-0.777	3.453
1972	1.600	-0.190	-0.304	1.351
1973	-0.270	-0.370	0.100	0.000
1974	0.560	0.350	0.196	0.000
1975	0.340	0.060	0.020	0.000
1976	0.140	0.810	0.113	0.000
1977	-1.030	1.100	-1.133	5.033
1978	-1.490	1.260	-1.877	8.341

TABLE IV

THE 25 ANOMALY PAIRS USED TO CALCULATE  
THE HIGH CROSS-CORRELATION VALUE FOR  
POI 10 AT LAG -6 FOR JULY (SEE FIGURE 5.17)

Year	SST Anomaly	Ice Conc. Anomaly	Product	% of Negative Cross- Covariance
1954	0.780	-0.590	-0.460	3.649
1955	0.160	-0.630	-0.101	0.799
1956	0.460	-0.920	-0.423	3.356
1957	0.760	-1.160	-0.882	6.991
1958	0.760	-1.000	-0.760	6.027
1959	0.720	0.030	0.022	0.000
1960	1.500	-1.010	-1.515	12.014
1961	1.140	-1.340	-1.528	12.113
1962	0.790	-1.260	-0.995	7.893
1963	-1.300	0.440	-0.572	4.536
1964	0.020	0.240	0.005	0.000
1965	-0.850	0.450	-0.382	3.033
1966	-0.290	0.770	-0.223	1.771
1967	-0.950	0.940	-0.893	7.081
1968	-1.240	1.310	-1.624	12.881
1969	-0.240	1.830	-0.439	3.483
1970	-0.800	0.970	-0.776	6.153
1971	-0.360	0.650	-0.234	1.856
1972	0.220	0.270	0.059	0.000
1973	-0.420	-0.210	0.088	0.000
1974	0.340	0.080	0.027	0.000
1975	-1.060	0.240	-0.254	2.017
1976	-1.040	0.290	-0.302	2.392
1977	-0.870	0.180	-0.157	1.242
1978	0.360	-0.250	-0.090	0.714

TABLE V

THE 25 ANOMALY PAIRS USED TO CALCULATE  
THE HIGH CROSS-CORRELATION VALUE  
FOR POI 10 AT LAG -4 FOR OCTOBER

Year	SST Anomaly	Ice Conc. Anomaly	Product	% of Negative Cross- Covariance
1954	0.800	0.110	0.088	0.000
1955	0.580	-1.050	-0.609	5.243
1956	0.640	-0.720	-0.461	3.967
1957	0.520	-0.200	-0.104	0.895
1958	0.600	-0.500	-0.300	2.583
1959	0.700	-0.530	-0.371	3.194
1960	1.510	-1.200	-1.812	15.599
1961	1.190	-1.120	-1.333	11.474
1962	0.370	-0.080	-0.030	0.255
1963	-1.120	0.300	-0.336	2.893
1964	0.230	-0.090	-0.021	0.178
1965	-0.690	0.710	-0.490	4.218
1966	-0.070	0.690	-0.048	0.416
1967	-1.170	1.140	-1.334	11.483
1968	-1.220	1.600	-1.952	16.805
1969	-0.160	1.030	-0.165	1.419
1970	-0.680	0.630	-0.428	3.688
1971	-0.310	0.910	-0.282	2.429
1972	0.200	-0.840	-0.168	1.446
1973	-0.200	0.580	-0.116	0.999
1974	0.180	0.310	0.056	0.000
1975	-1.070	0.500	-0.535	4.606
1976	-0.870	-0.750	0.652	0.000
1977	-0.880	0.820	-0.722	6.212
1978	0.420	0.080	0.034	0.000

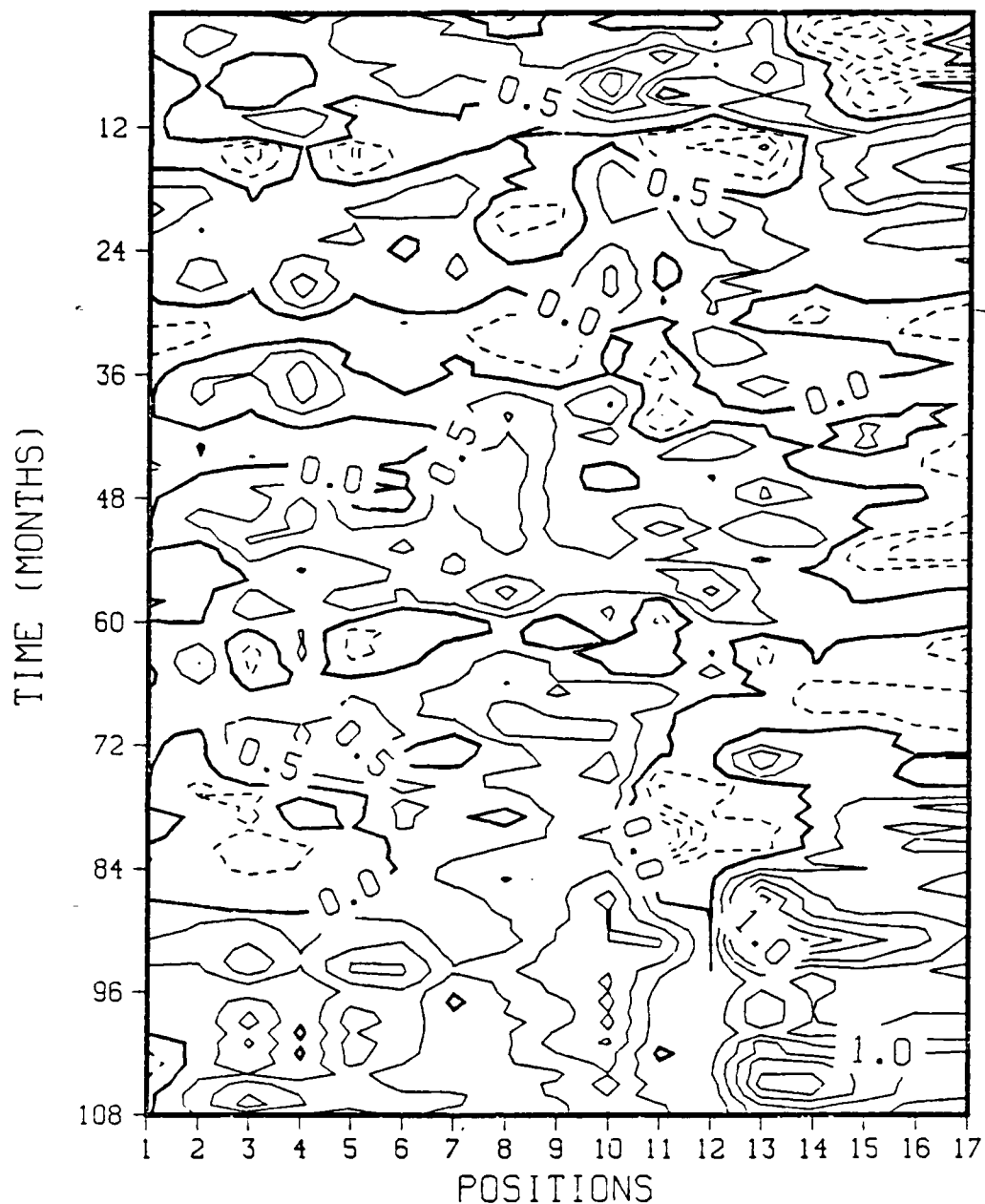


Figure 5.1 SST anomaly (difference from monthly mean) contours for POIs 1 through 17 and months 1 through 108. Solid lines are positive anomalies, dashed lines are negative anomalies. The heavy line is 0 anomaly. Contour increments are 0.5 degrees centigrade.

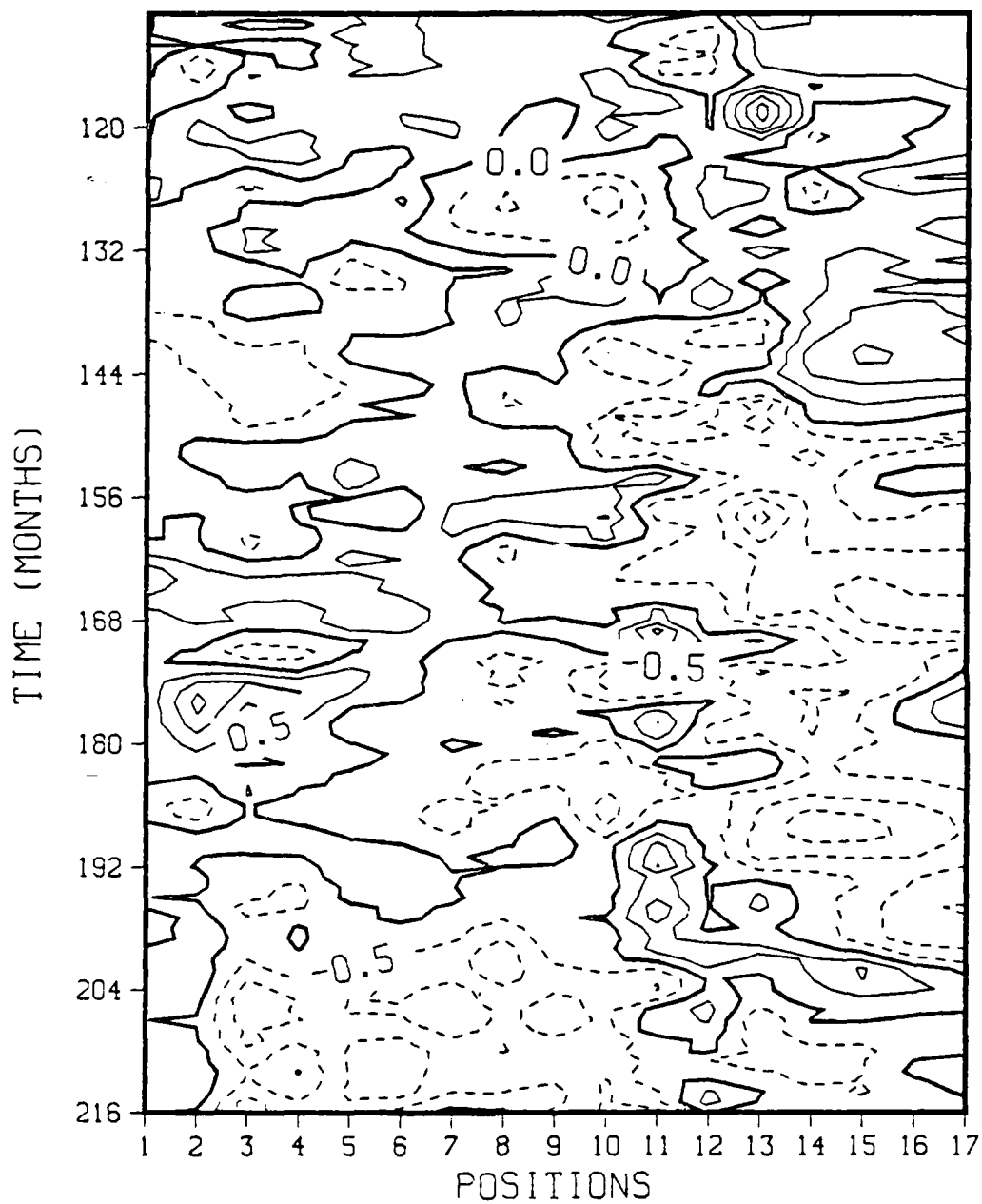


Figure 5.2 As for 5.1 except covering months 109 through 216.

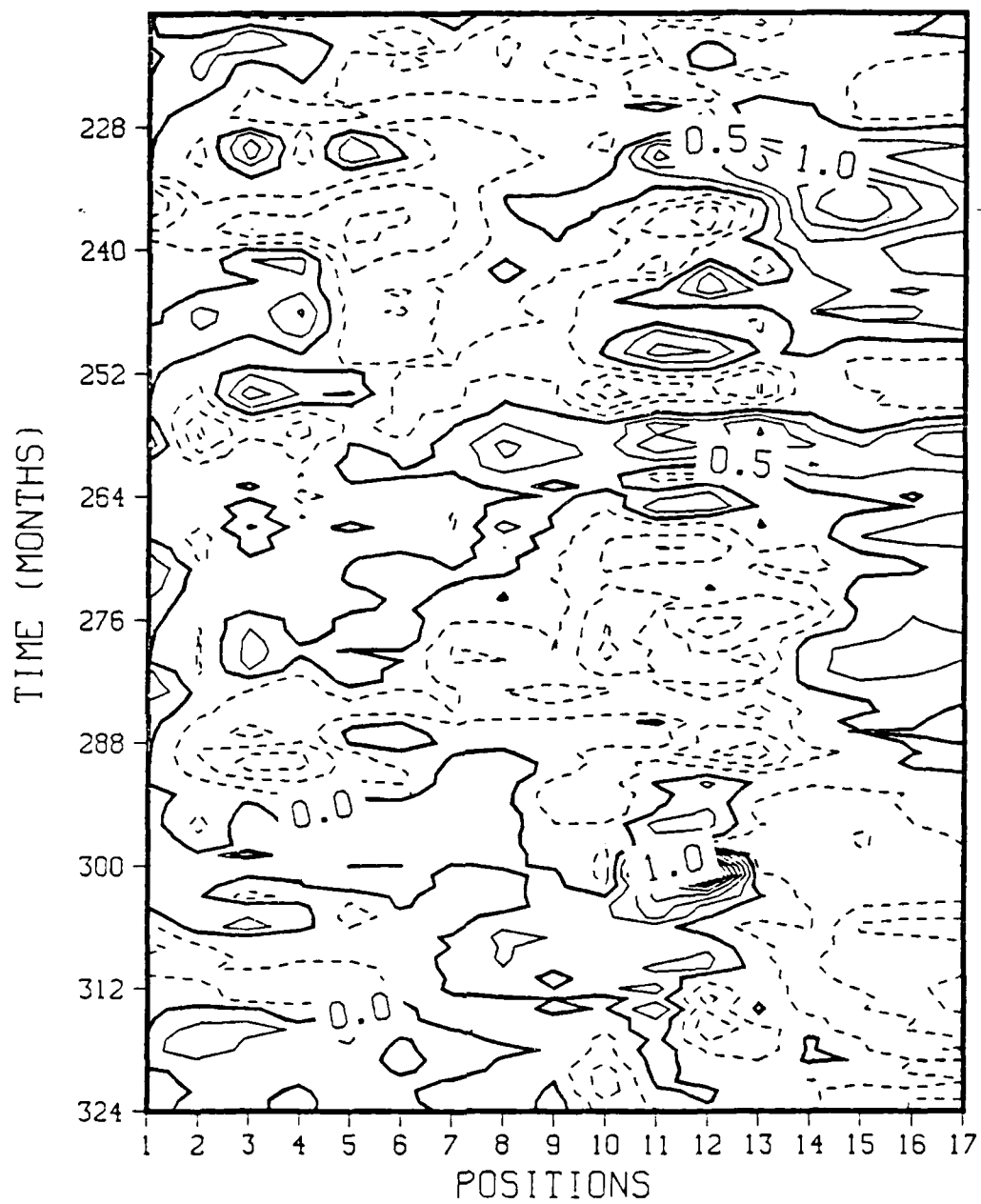


Figure 5.3 As for 5.1 except covering months 217 through 324.

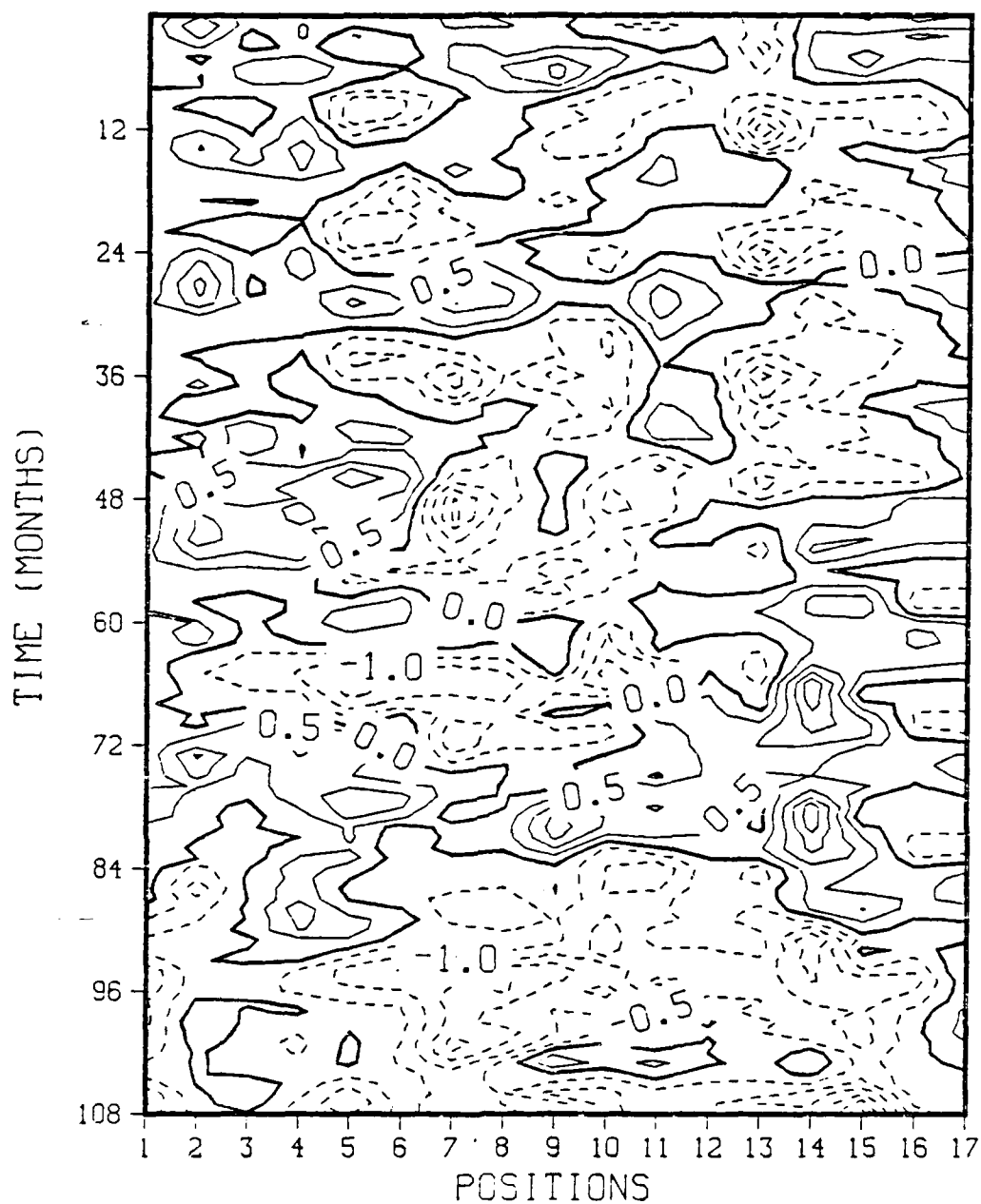


Figure 5.4 Ice anomaly (difference from monthly mean) contours for POIs 1 through 17 and months 1 through 108. Solid lines are positive anomalies, dashed lines are negative anomalies. The heavy line is 0 anomaly. Contour increments are 0.5 tenths of ice concentration.

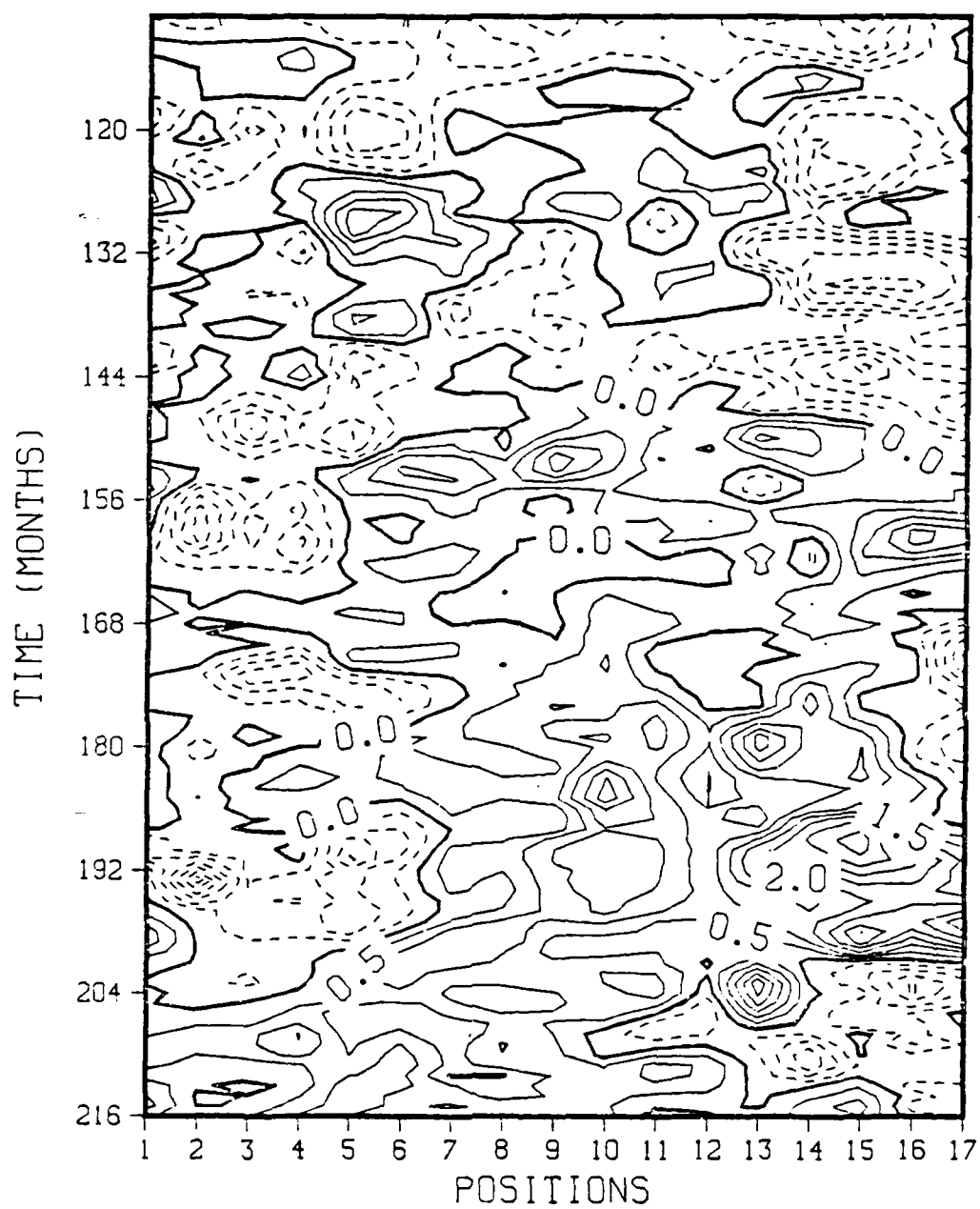


Figure 5.5 As for 5.4 except covering months 109 through 216.

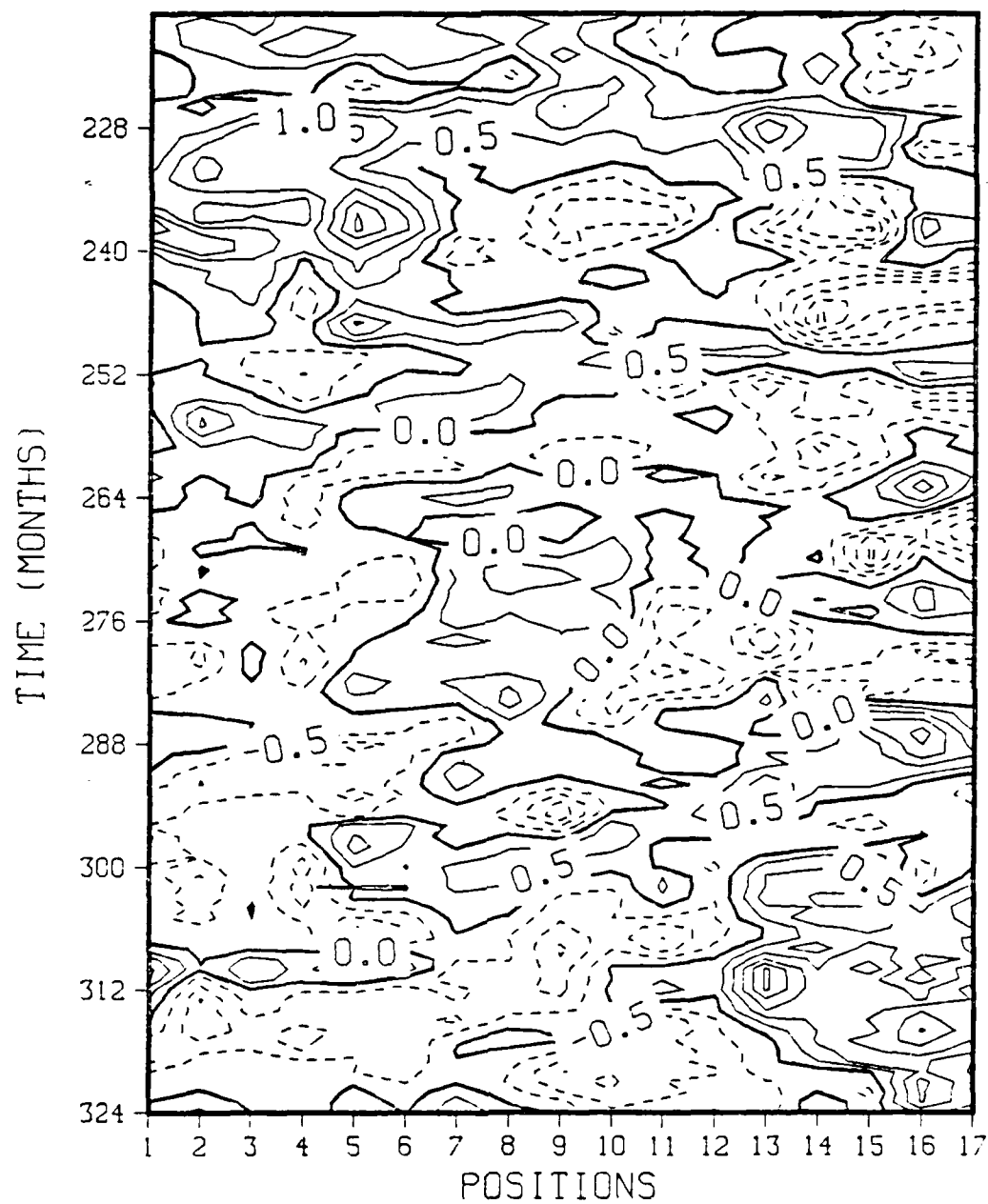


Figure 5.6 As for 5.4 except covering months 217 through 324.

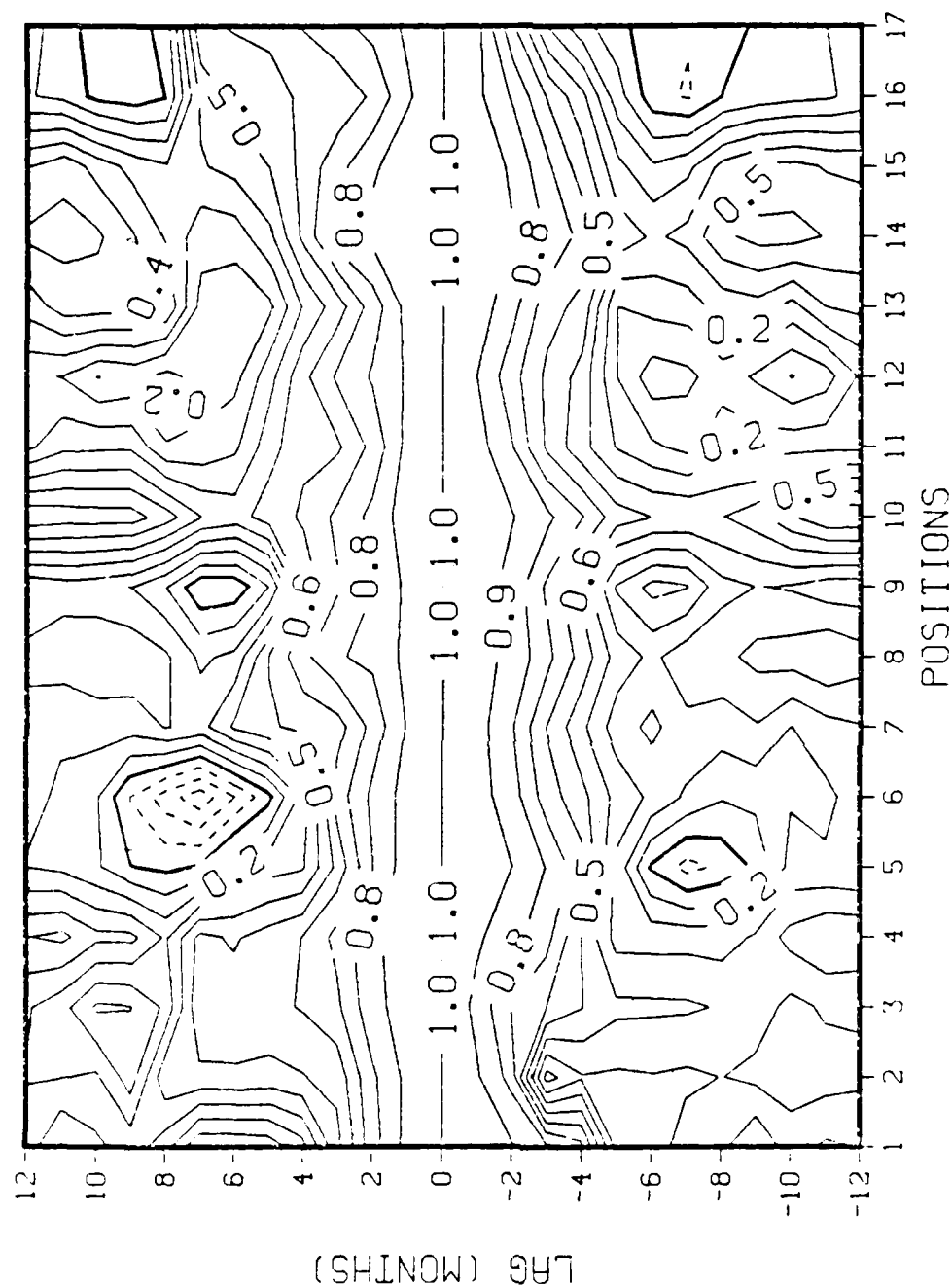


Figure 5.7 Ice concentration autocorrelation (persistence) contours for the 17 POIs. Solid lines are positive correlation values and dashed lines are negative correlation values. Values are contoured in increments of 0.1 for lags of -12 months to +12 months. The base month is January.

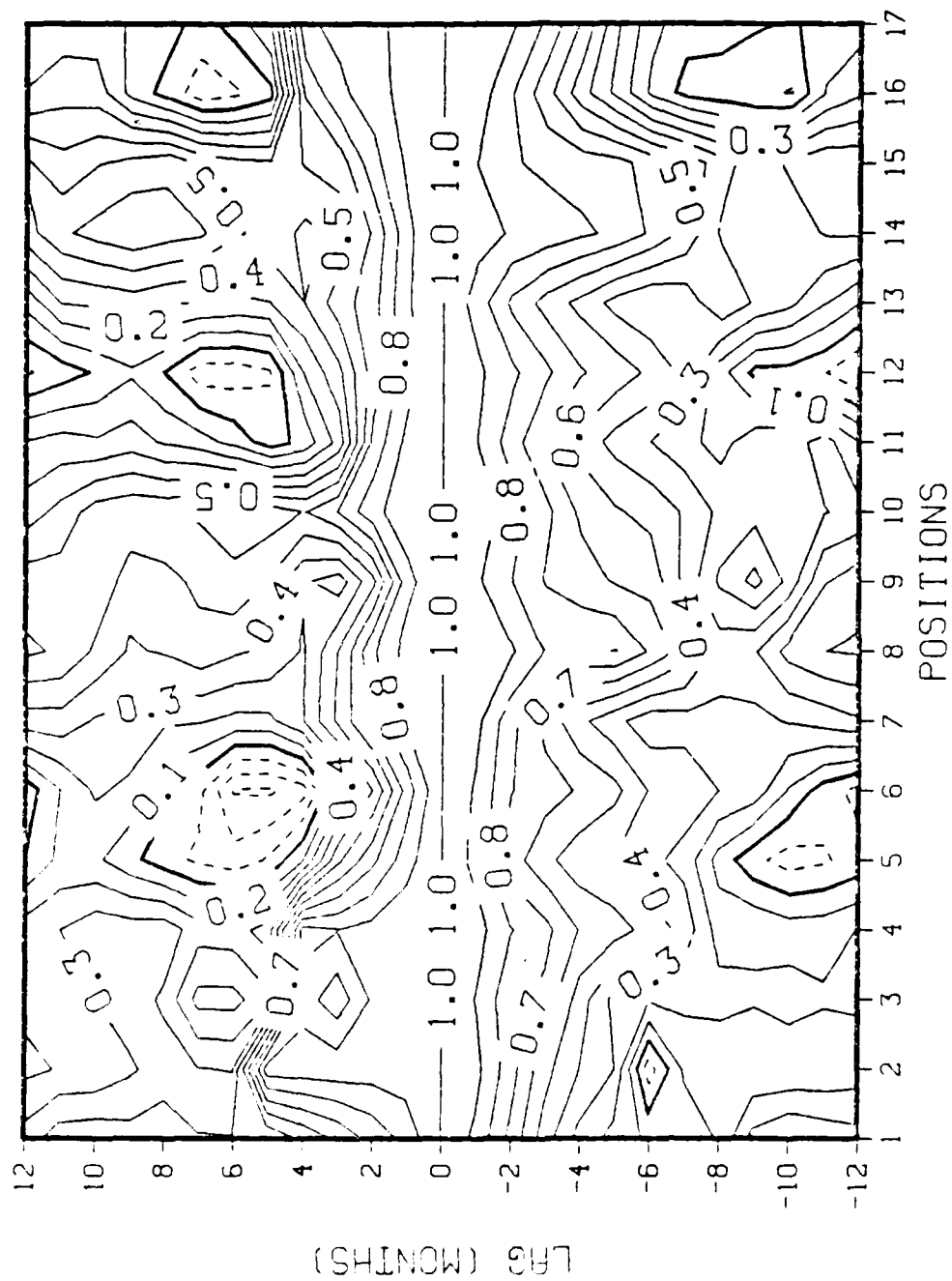


Figure 5.8 Same as 5.7 except using base month of April.

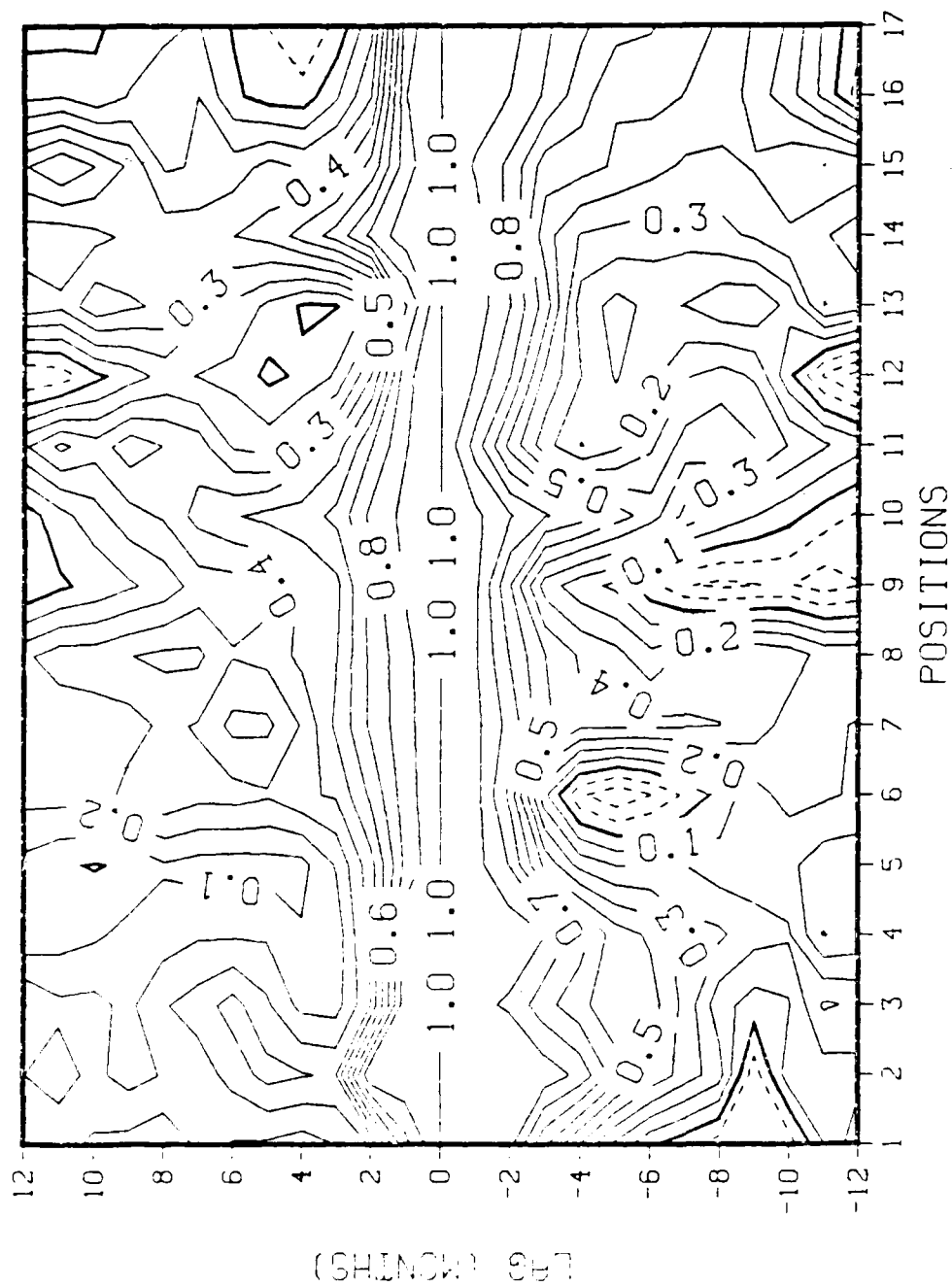


Figure 5.9 Same as 5.7 except using base month of July.

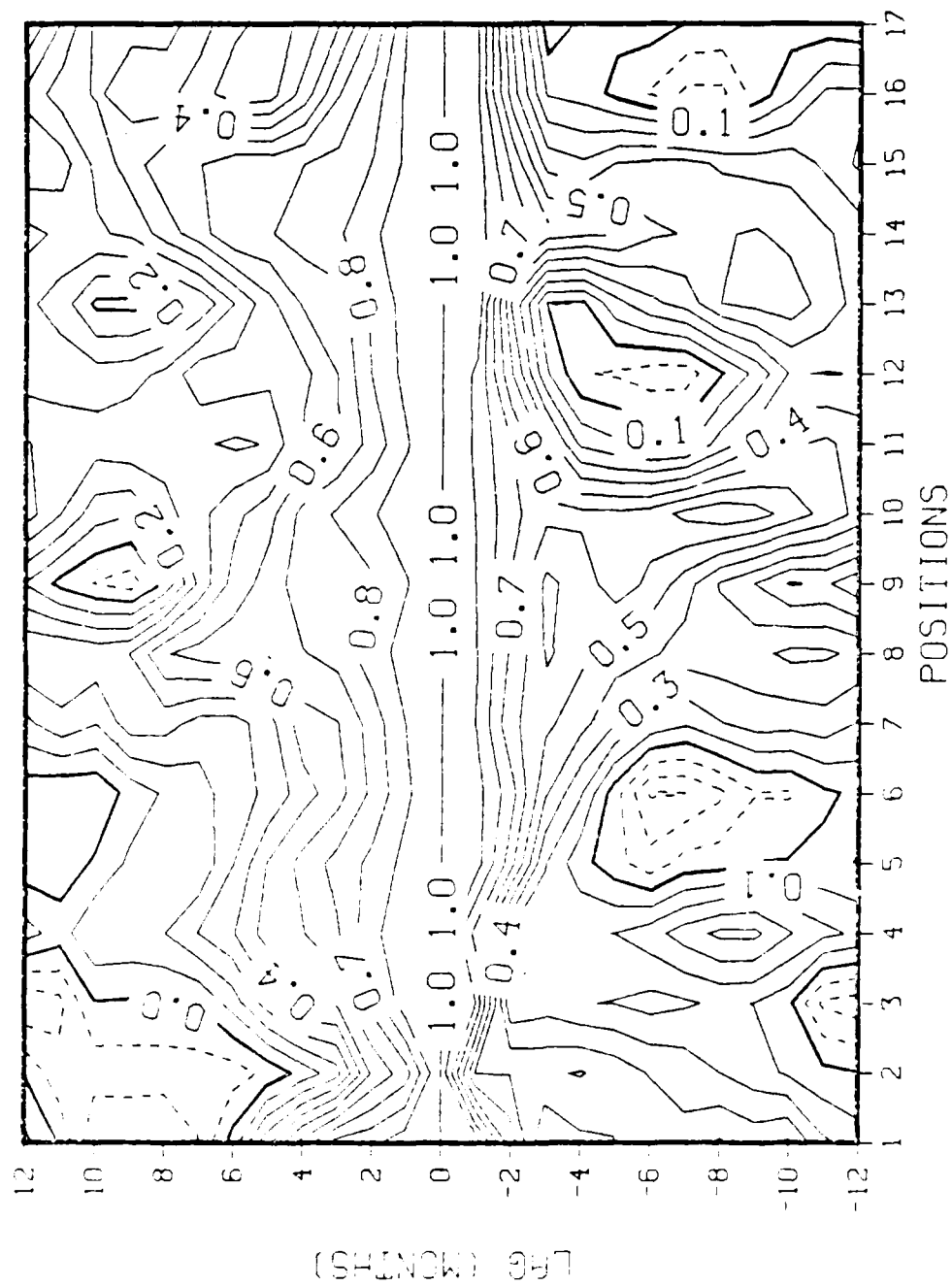


Figure 5.10 Same as 5.7 except using base month of October.

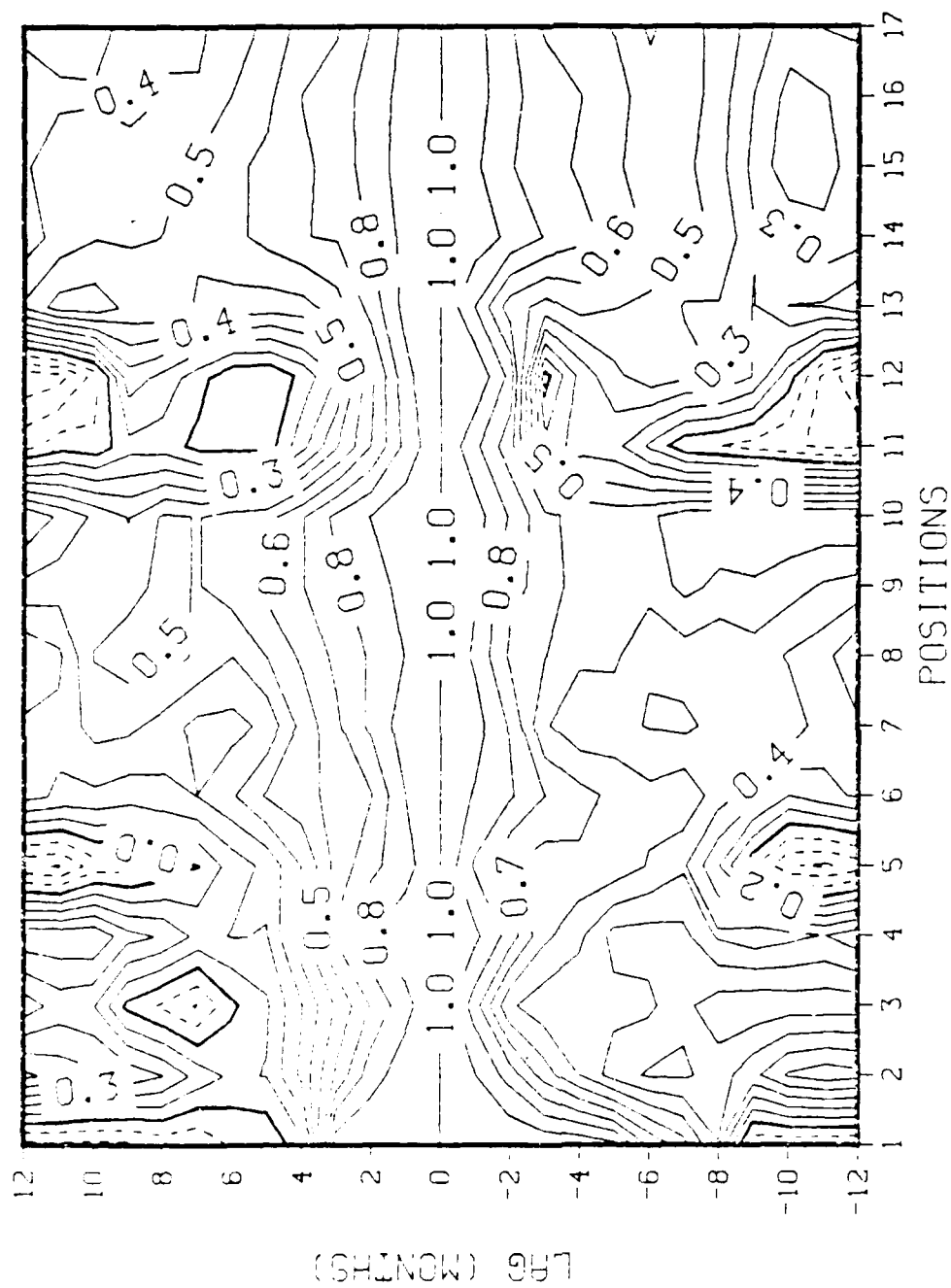


Figure 5.11 SST autocorrelation (persistence) contours for the 17 POIs. Solid lines are positive correlation values and dashed lines are negative correlation values. Values are contoured in increments of 0.1 for lags of -12 months to +12 months. The base month is January.

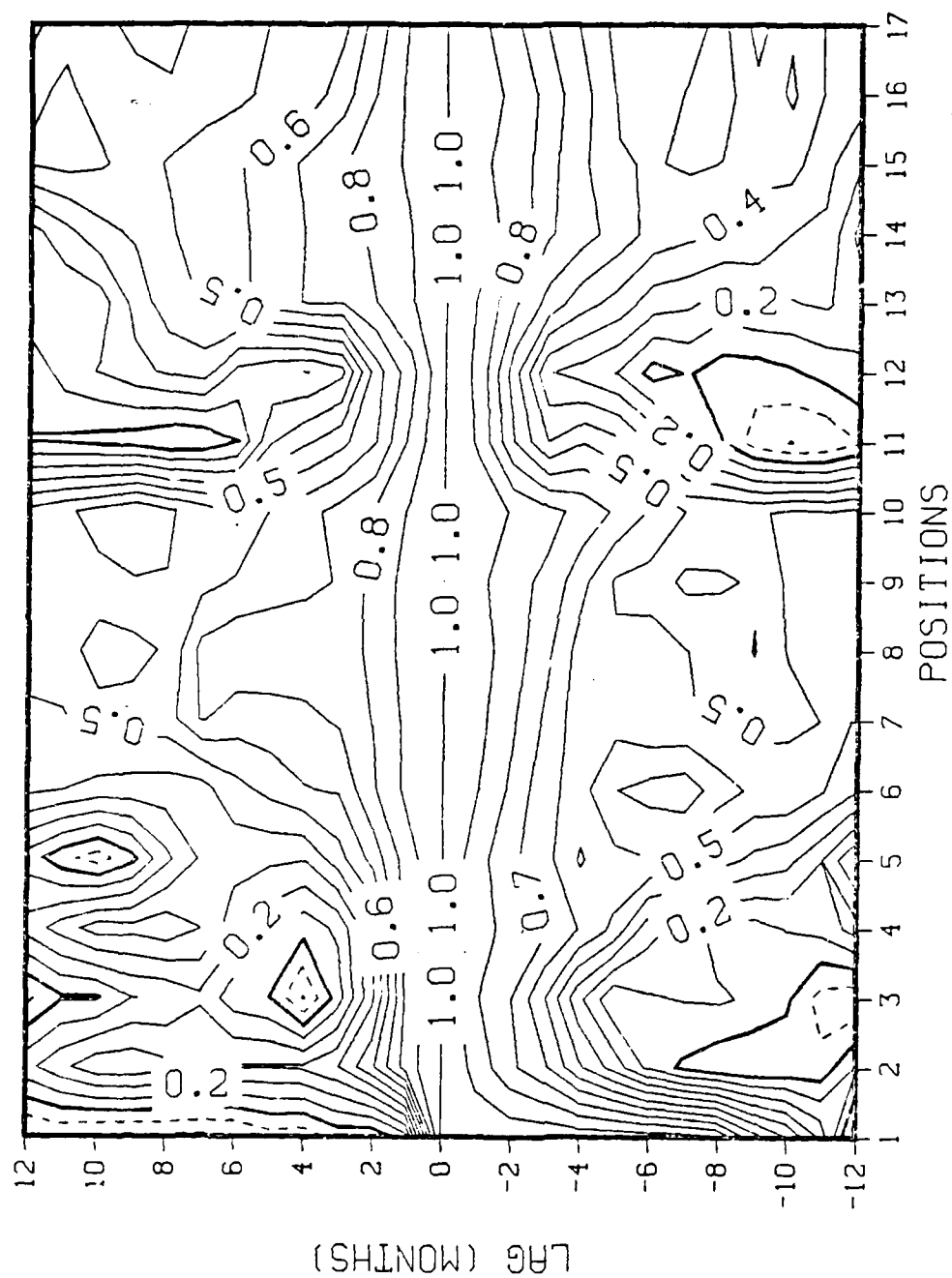


Figure 5.12 Same as 5.11 except using base month of April.

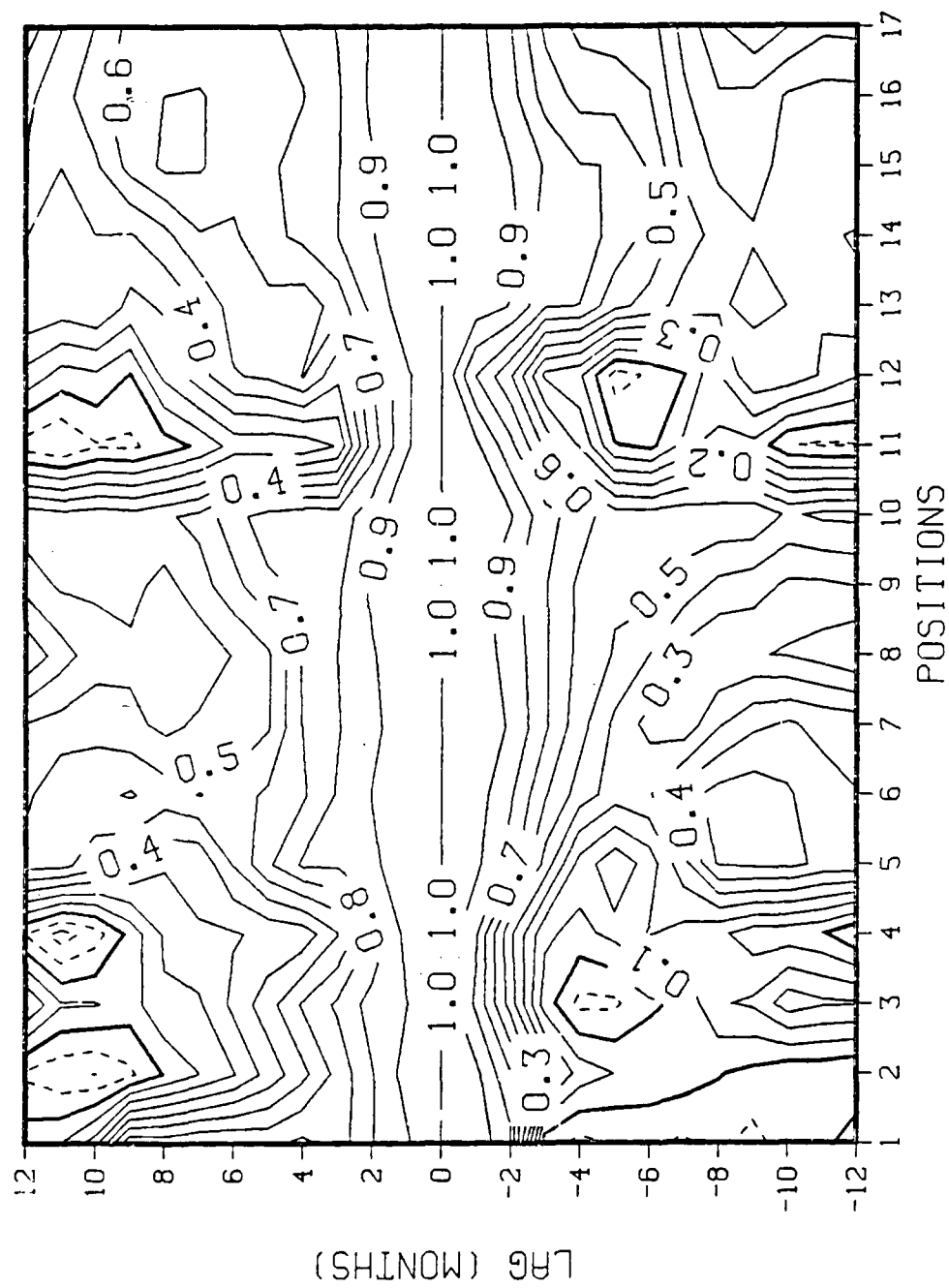


Figure 5.13 Same as 5.11 except using base month of July.

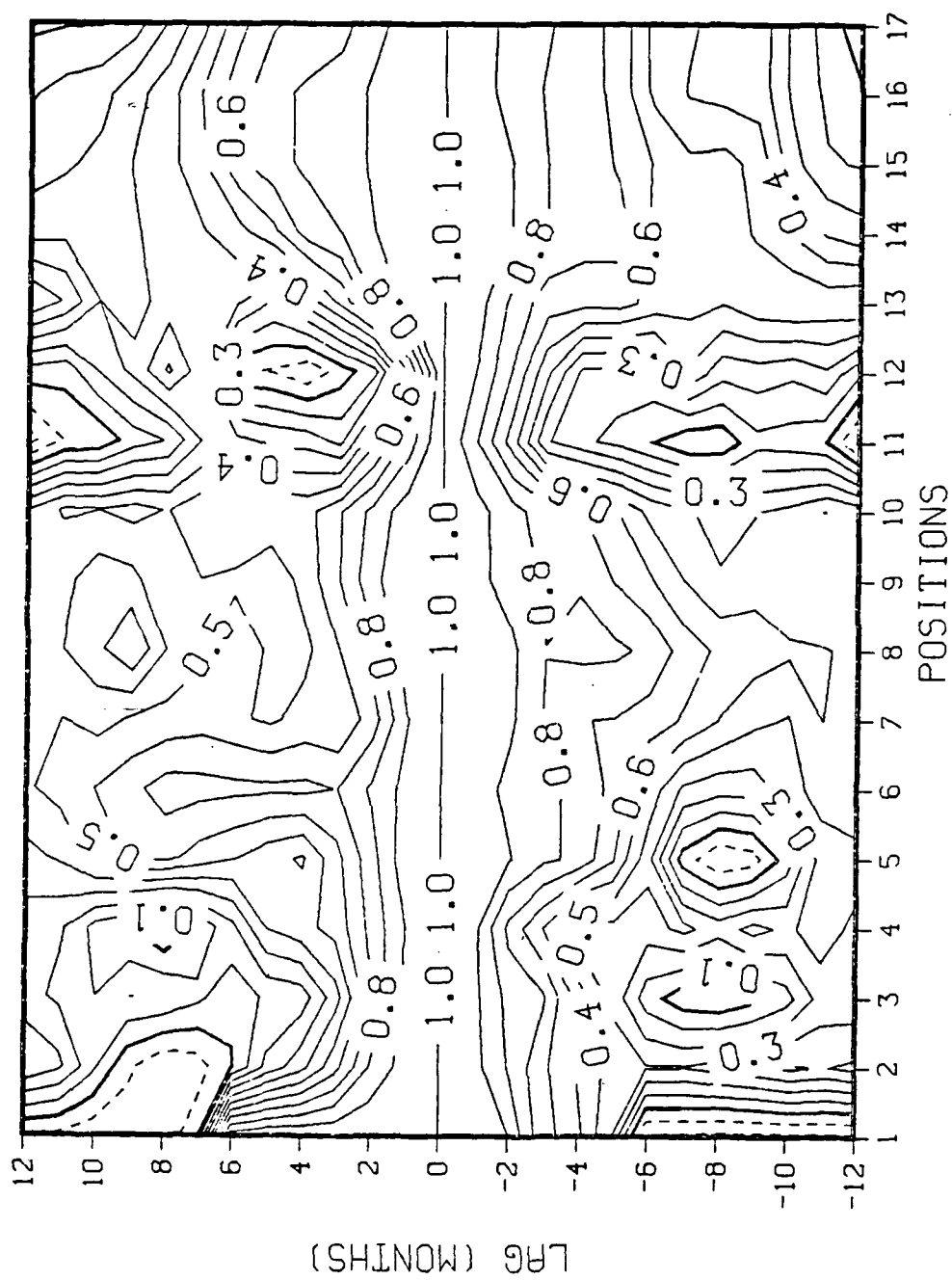


Figure 5.14 Same as 5.11 except using base month of October.

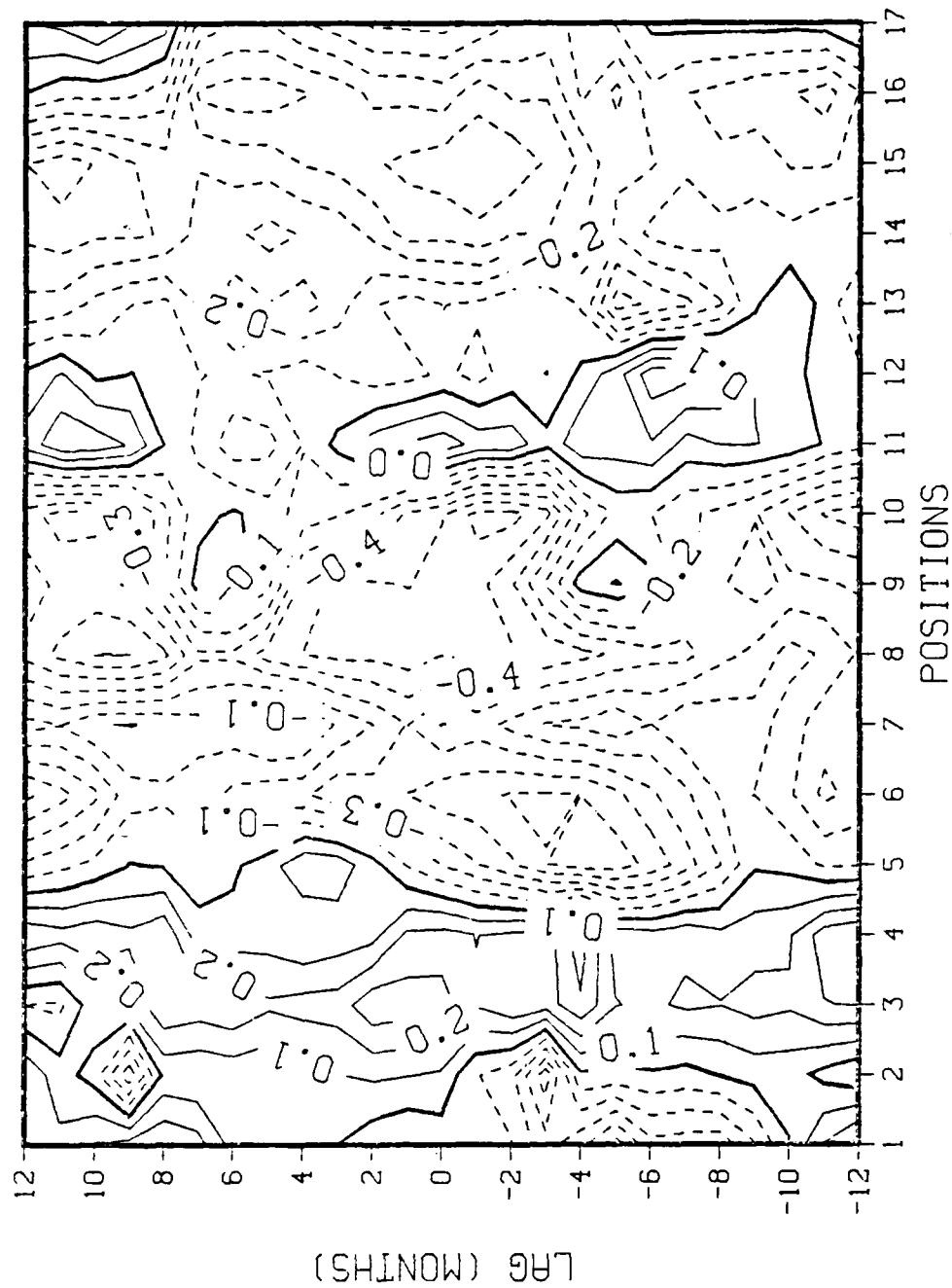


Figure 5.15 SST/ice concentration cross-correlation contours for the 17 POIs. Solid lines are positive correlation values and dashed lines are negative correlation values. Values are contoured in increments of 0.1 for lags of -12 months to +12 months. Base month is January.

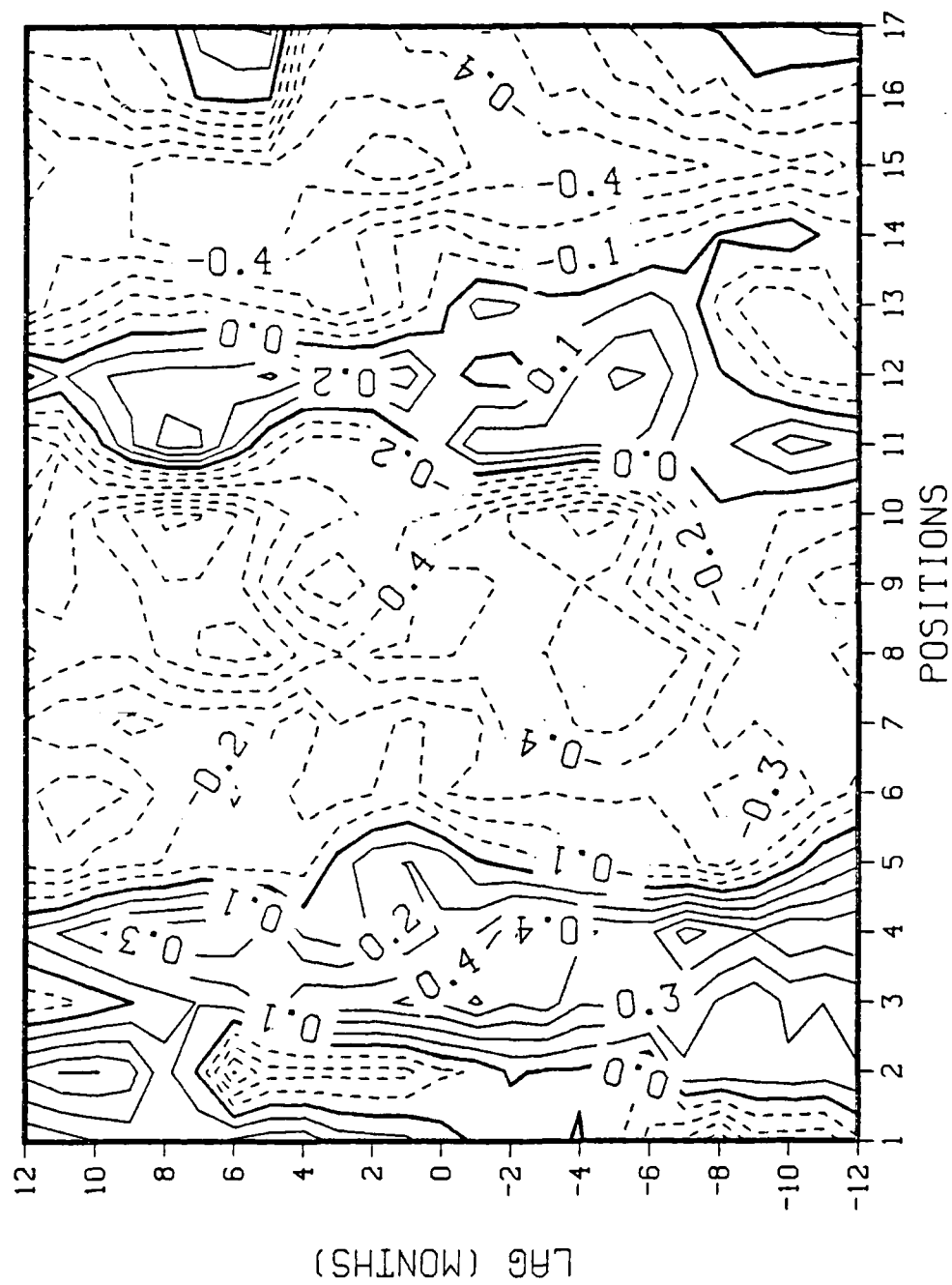


Figure 5.16 Same as 5.15 except using base month of April.



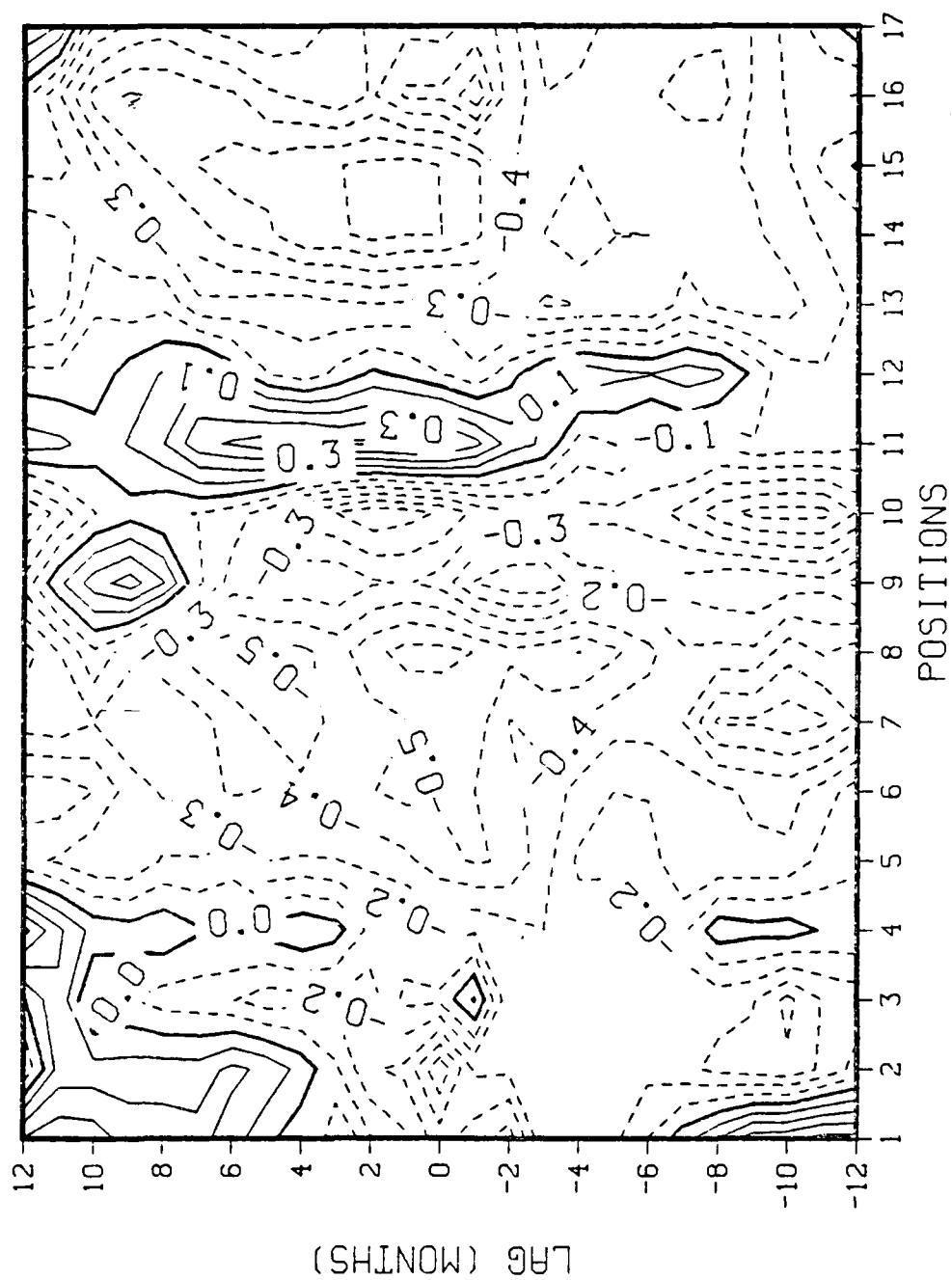


Figure 5.18 Same as 5.15 except using base month of October.

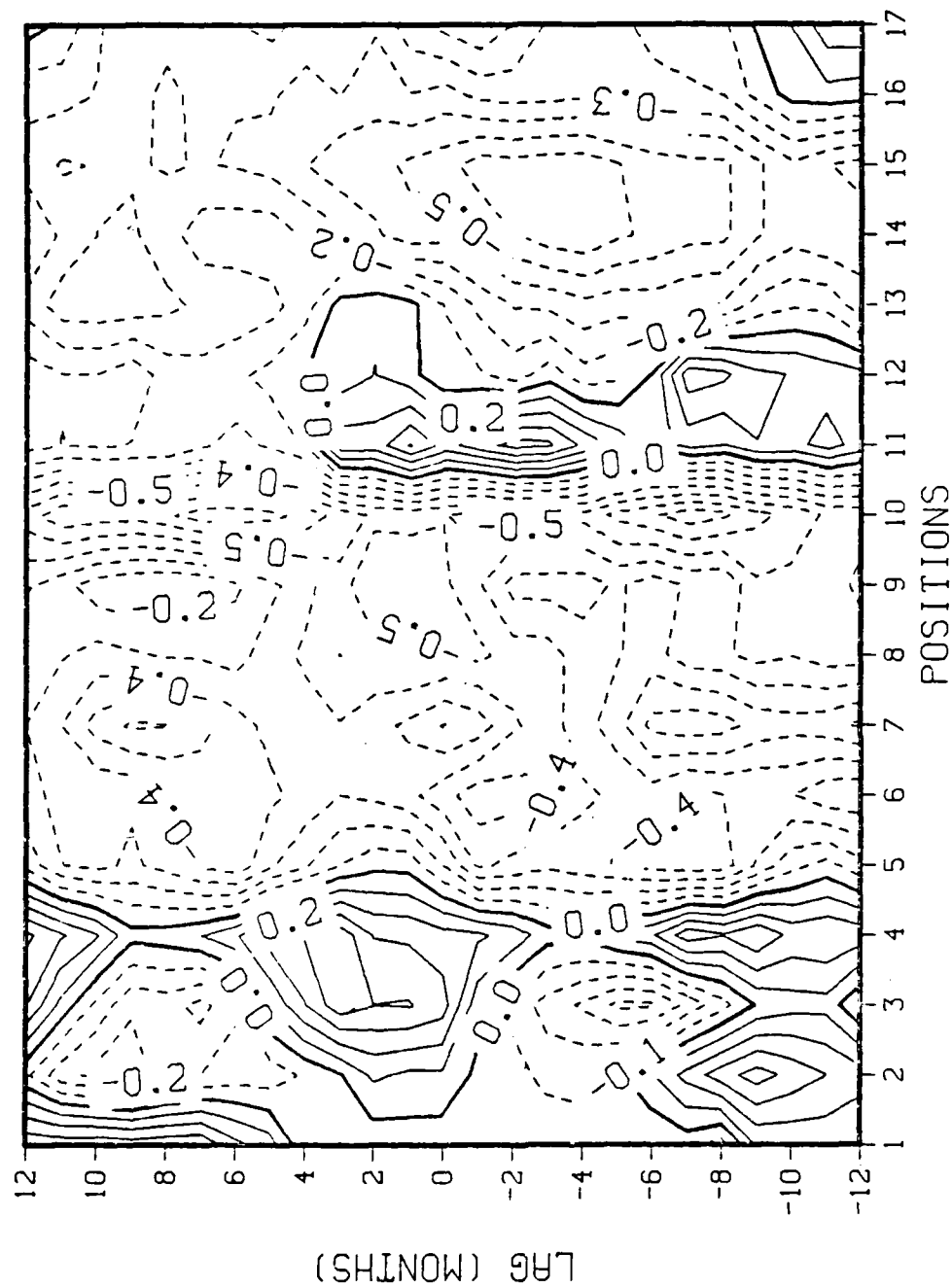


Figure 5.19 Ice concentration/SST cross-correlation contours for the 17 POIs. Solid lines are positive correlation values and dashed lines are negative correlation values. Values are contoured in increments of 0.1 for lags of -12 months to +12 months. Base month is January.

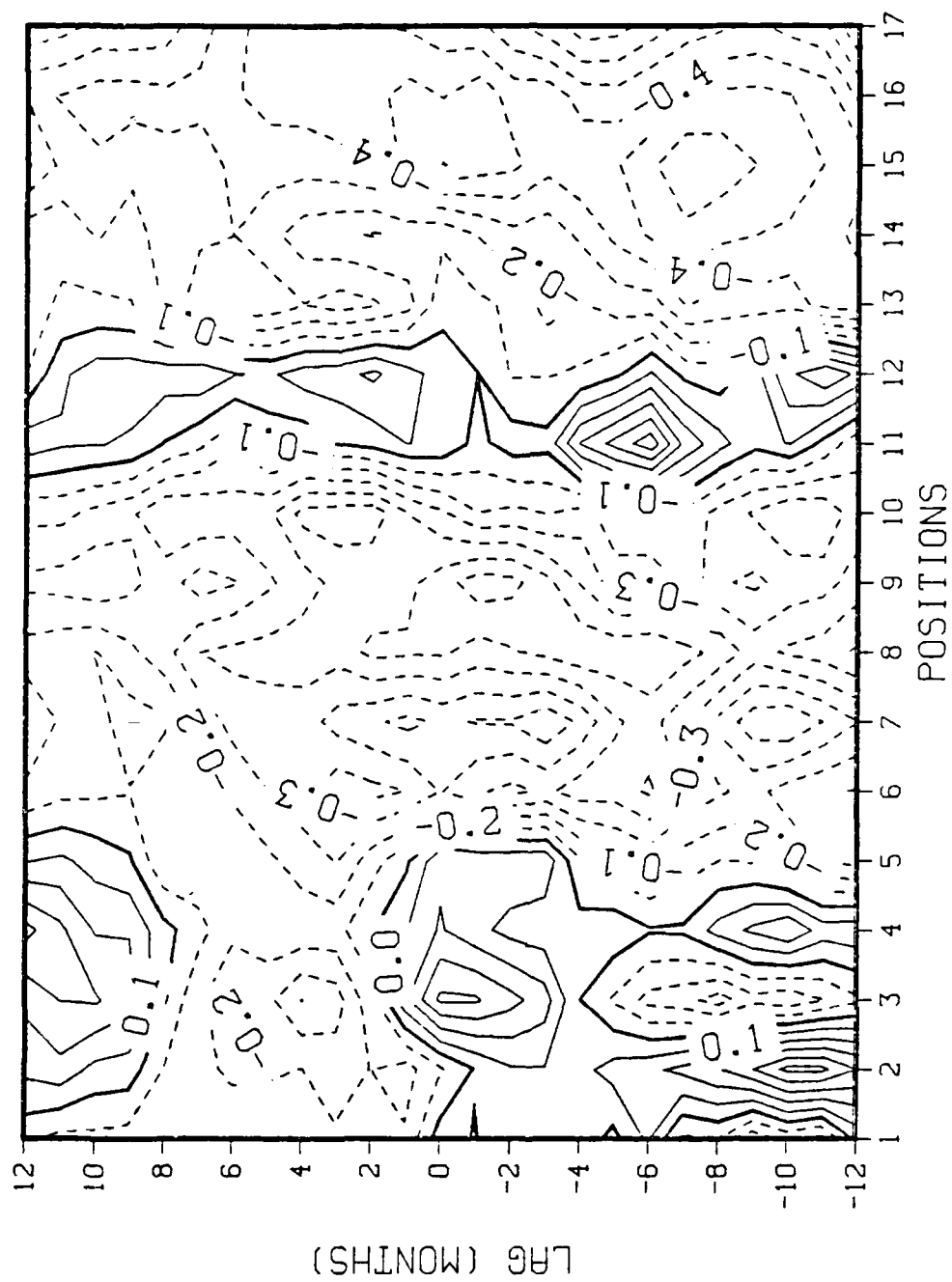


Figure 520 Same as 5.19 except using base month of April.



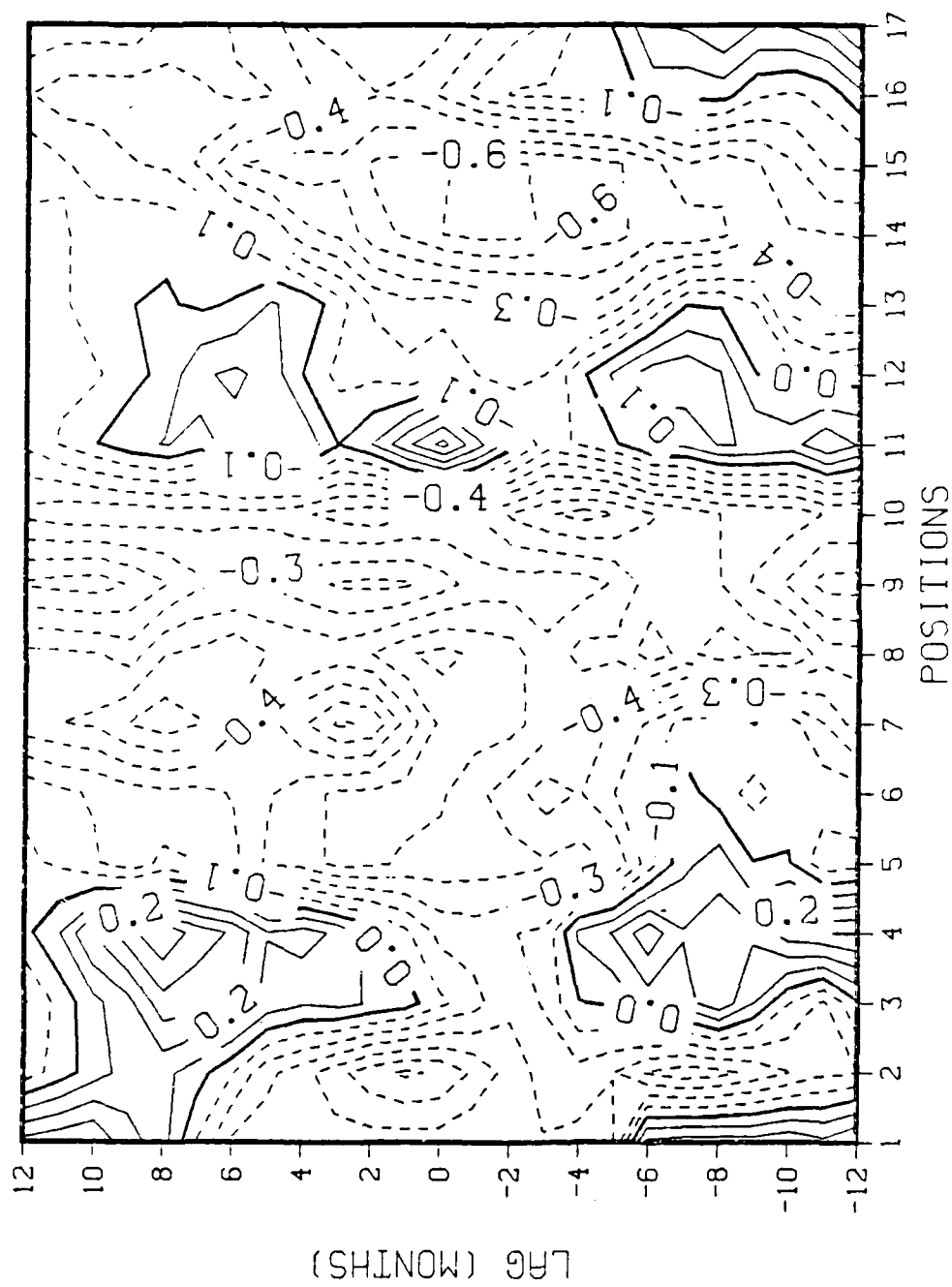


Figure 522 Same as 5.19 except using base month of October.

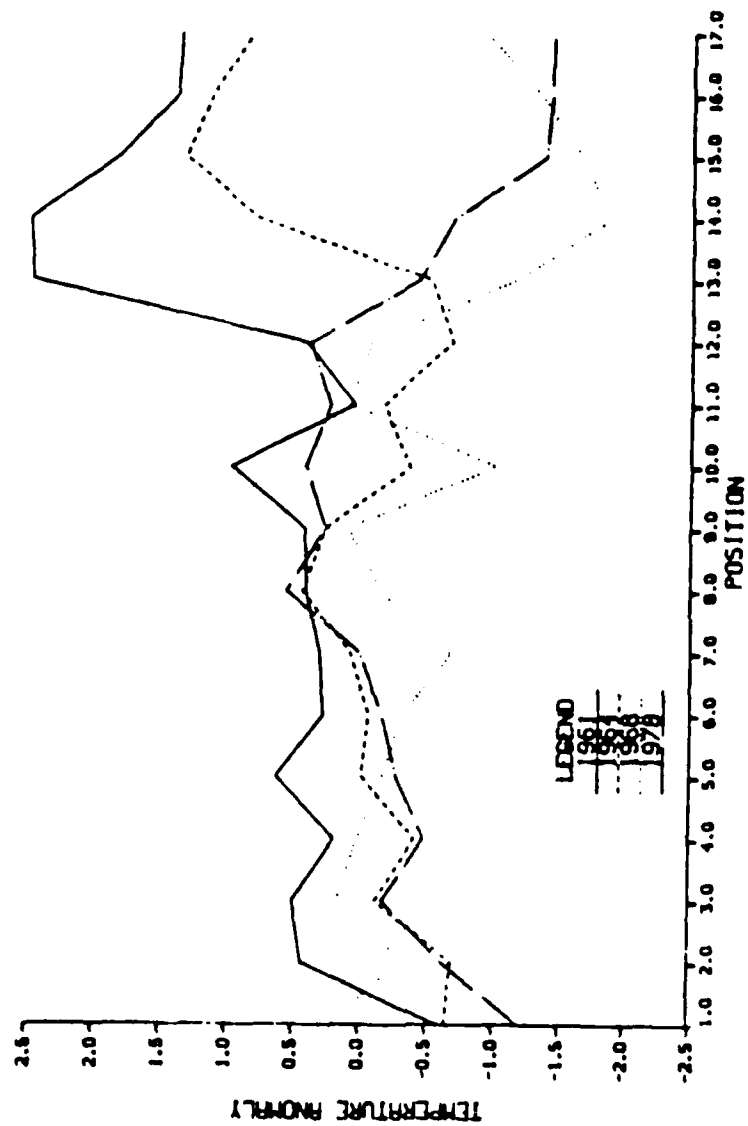


Figure 523 Graph of temperature anomalies for the most influential years for cross-correlation feature A. Anomaly values are for the month of August.

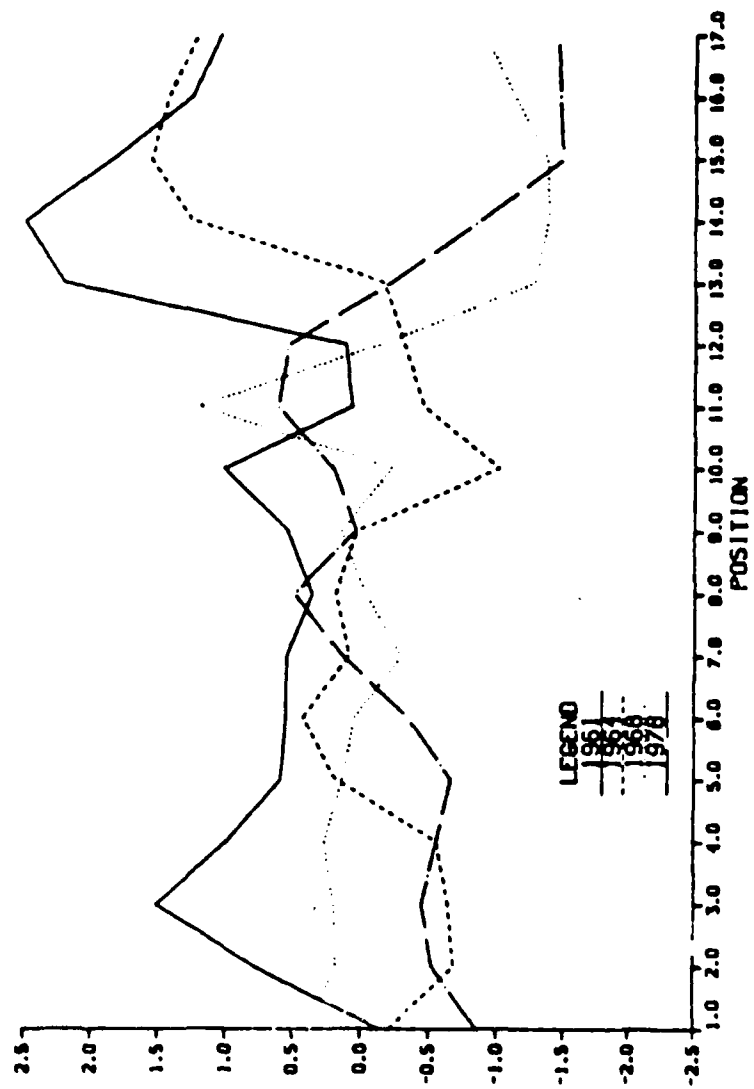
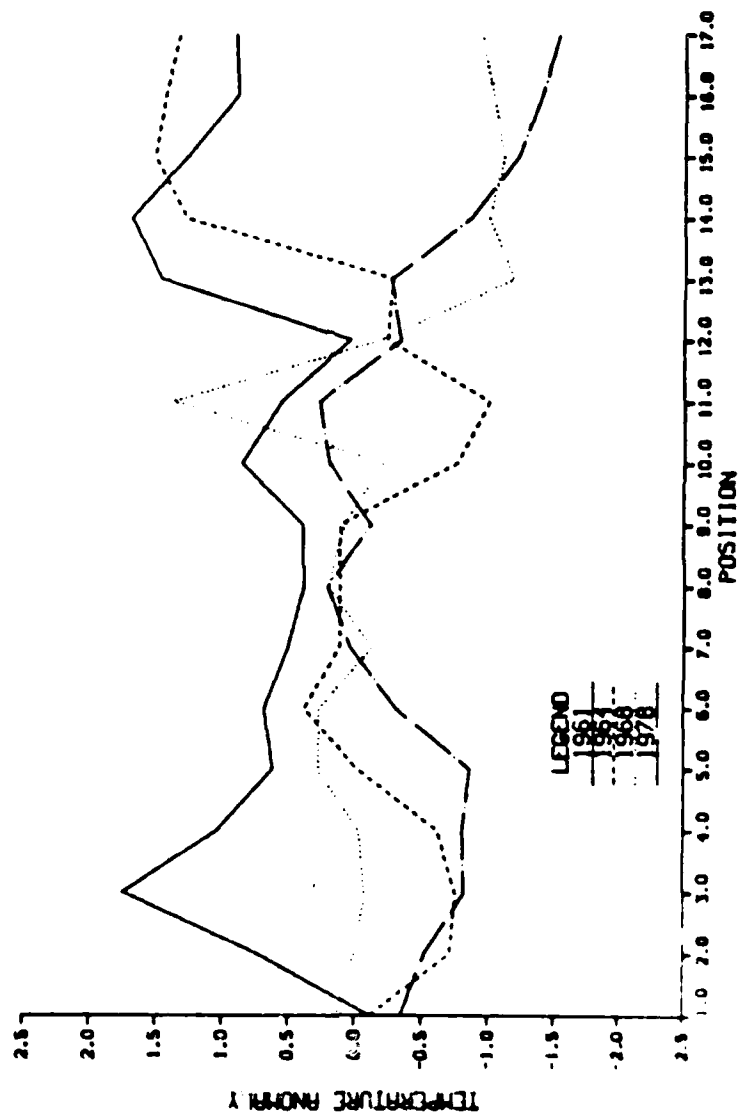


Figure 524 As for 5.23 except anomaly values are for the month of October.



except anomaly values are for the month of November.

AD-A186 621

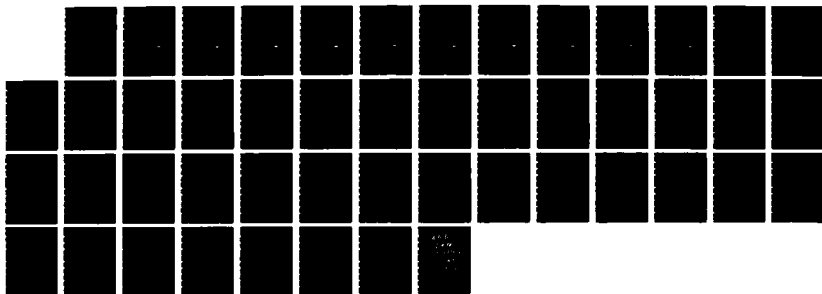
PREDICTABILITY OF ICE ONCENTRATION IN THE  
HIGH-LATITUDE NORTH ATLANTIC F. (U) NAVAL POSTGRADUATE  
SCHOOL MONTEREY CA G H FLEMING SEP 87

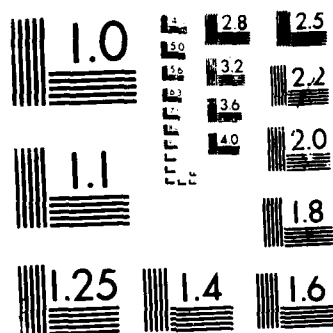
2/2

UNCLASSIFIED

F/G 8/12

NL





MICROGRAPH RESOLUTION TEST CHART  
 NATIONAL BUREAU OF STANDARDS-1963-A

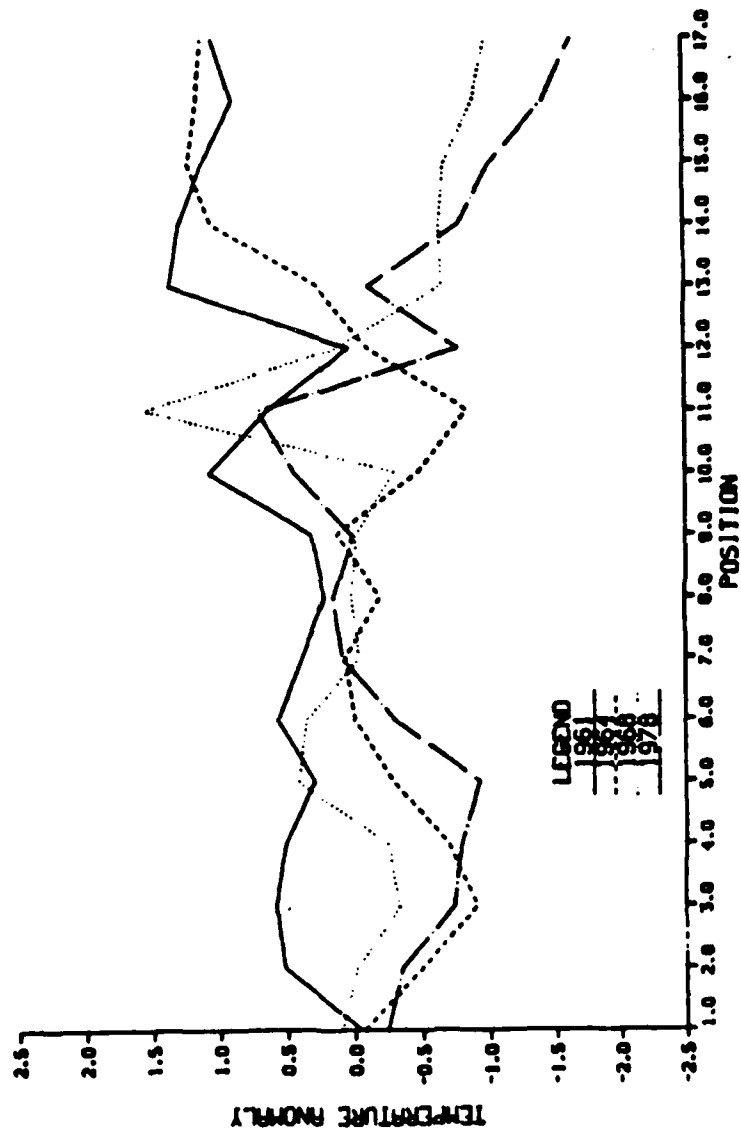


Figure 526 As for 5.23 except anomaly values are for the month of December.

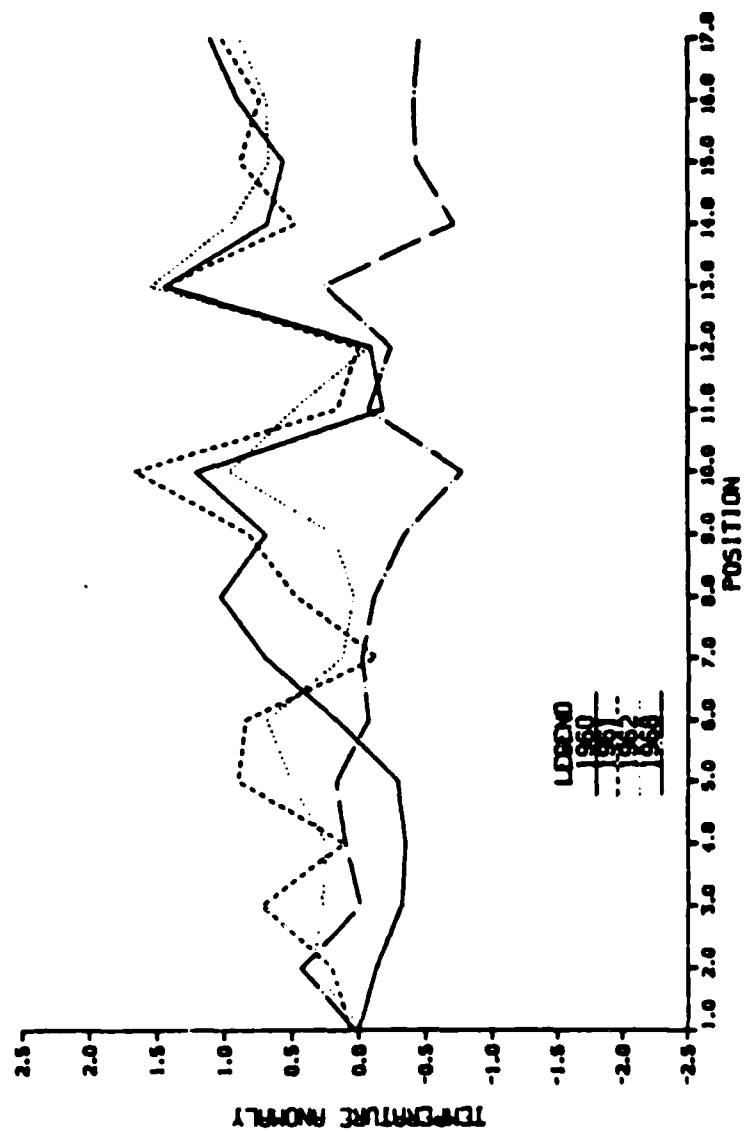


Figure 527 Graph of temperature anomalies for the most influential years for cross-correlation feature B. Anomaly values are for the month of January.

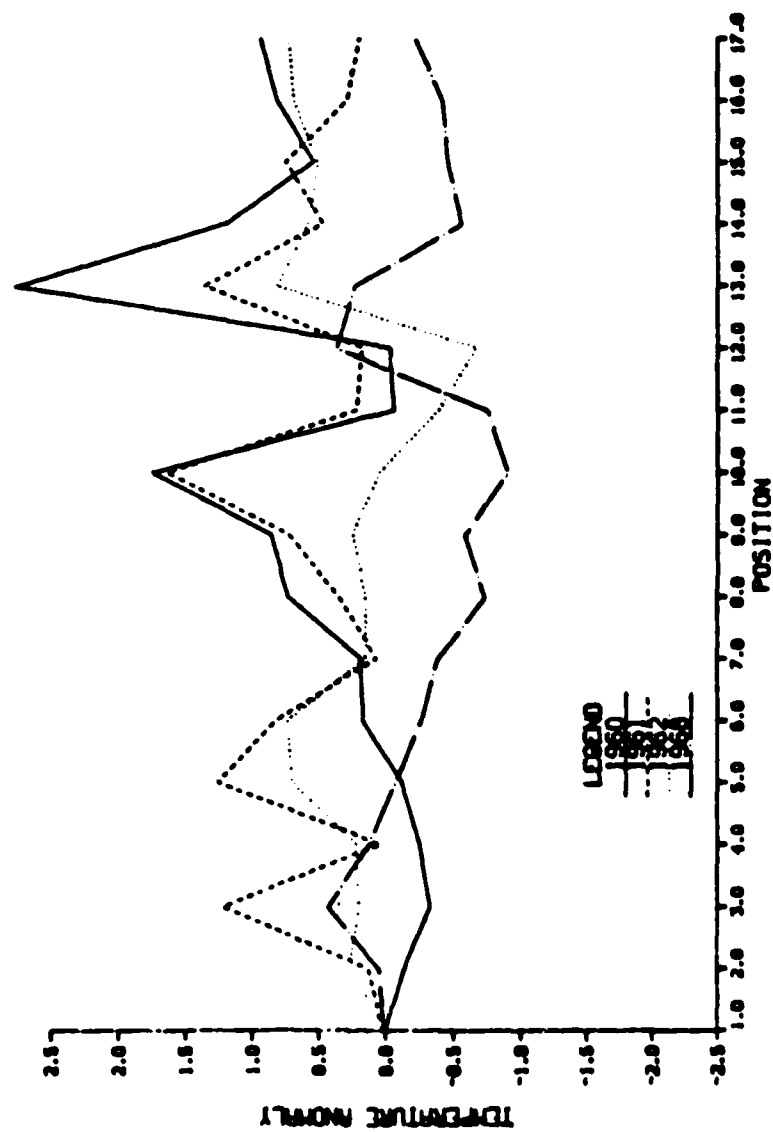


Figure 528 As for 5.27 except anomaly values are for the month of March.

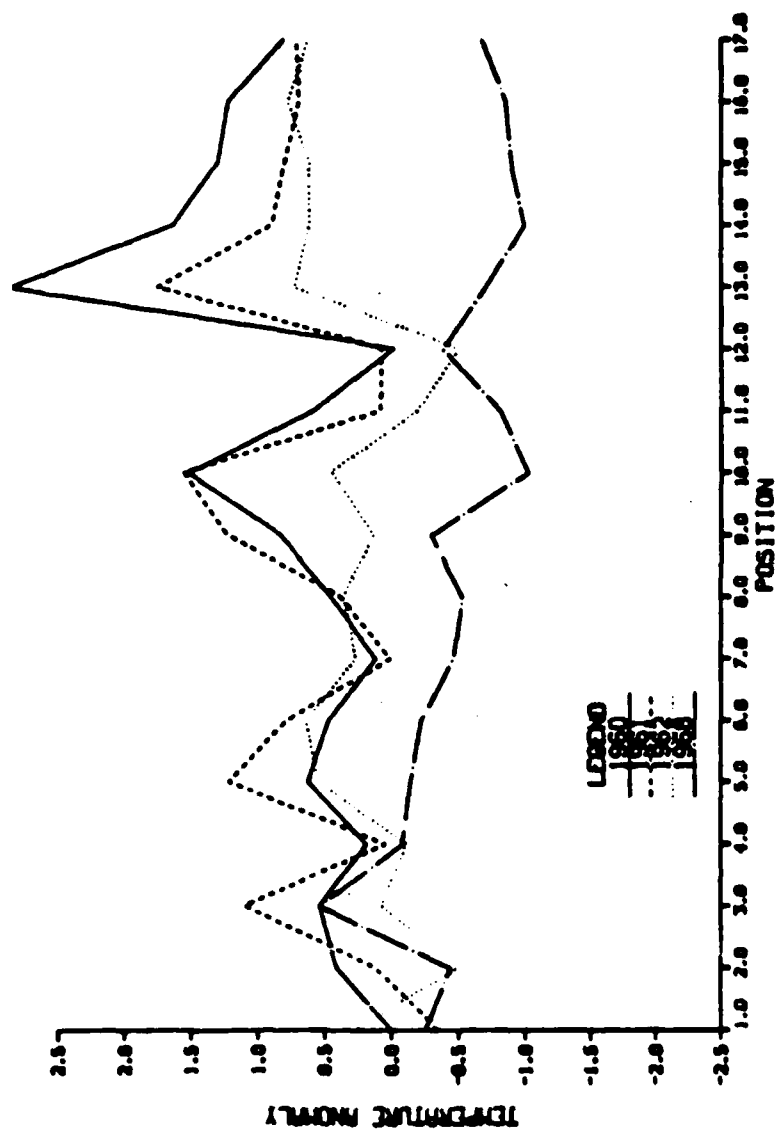


Figure 529 As for 5.27 except anomaly values are for the month of May.

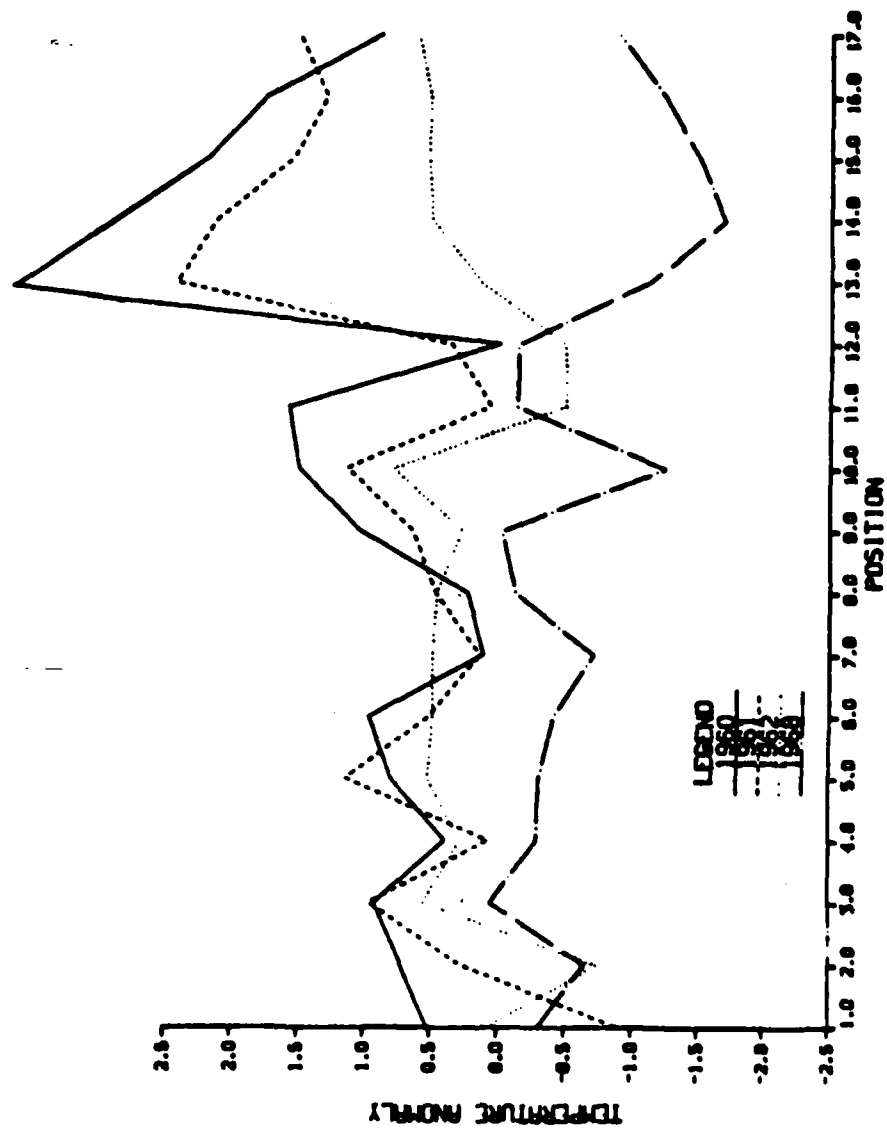


Figure 530 As for 5.27 except anomaly values are for the month of July.

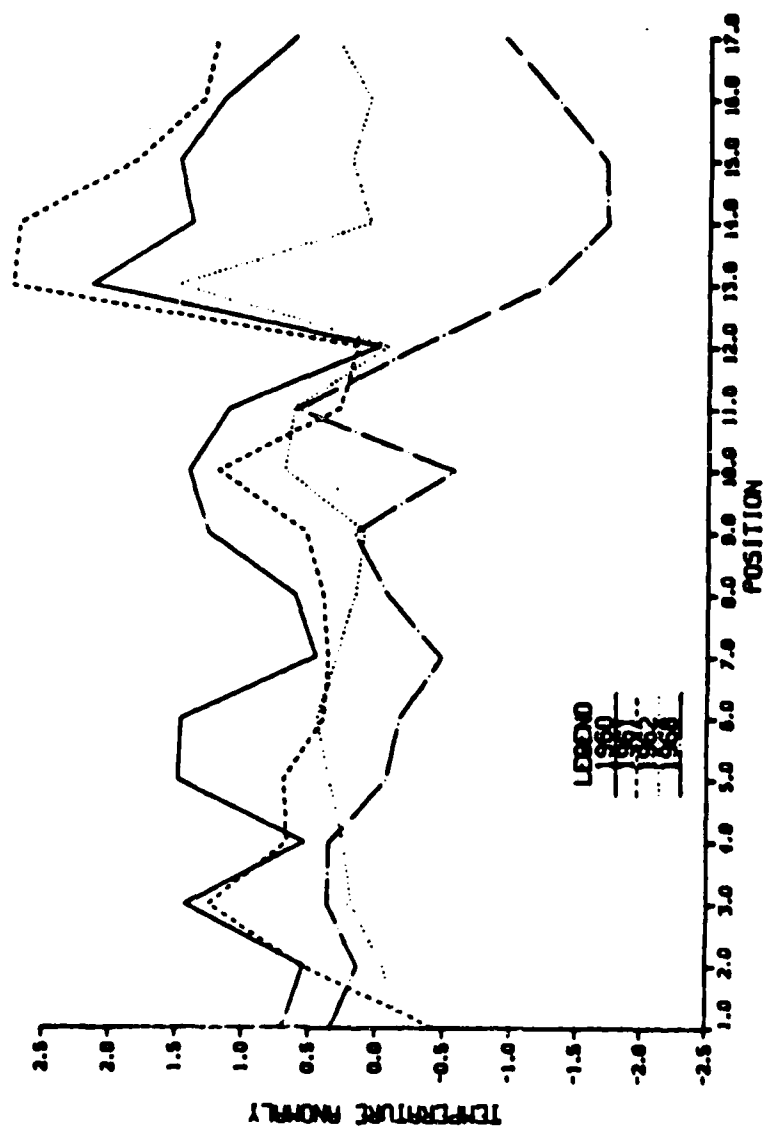


Figure 531 As for 5.27 except anomaly values are for the month of September.

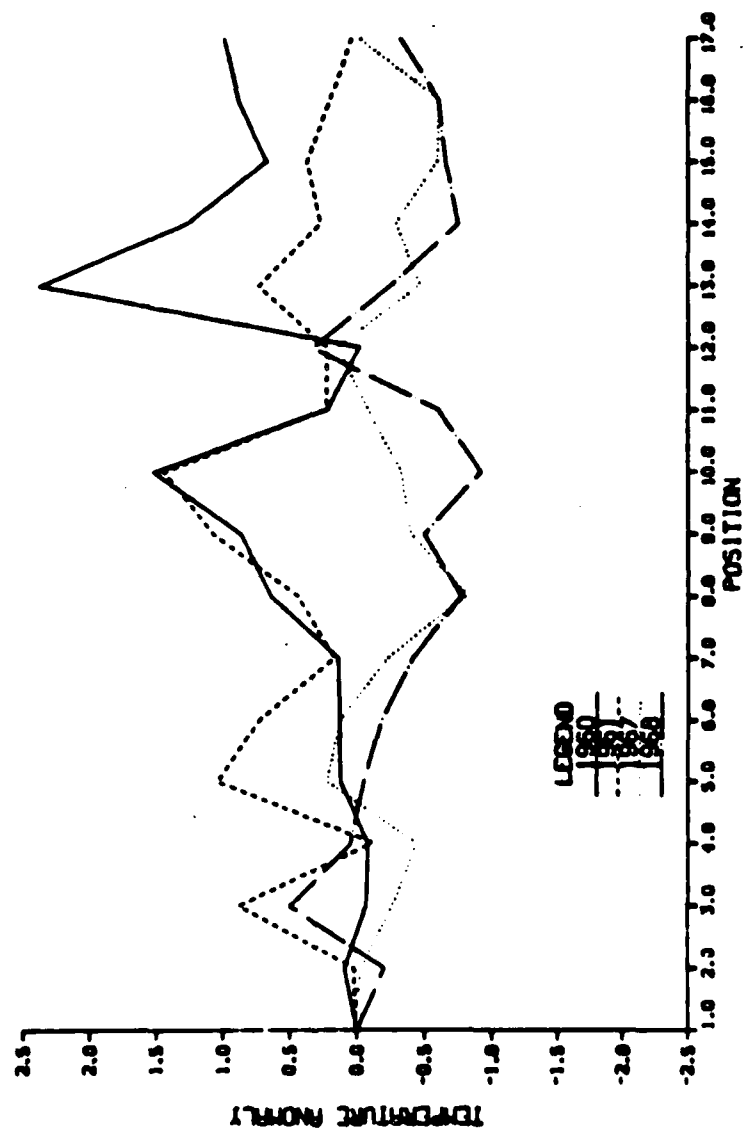


Figure 532 Graph of temperature anomalies for the most influential years for cross-correlation feature C. Anomaly values are for the month of April.

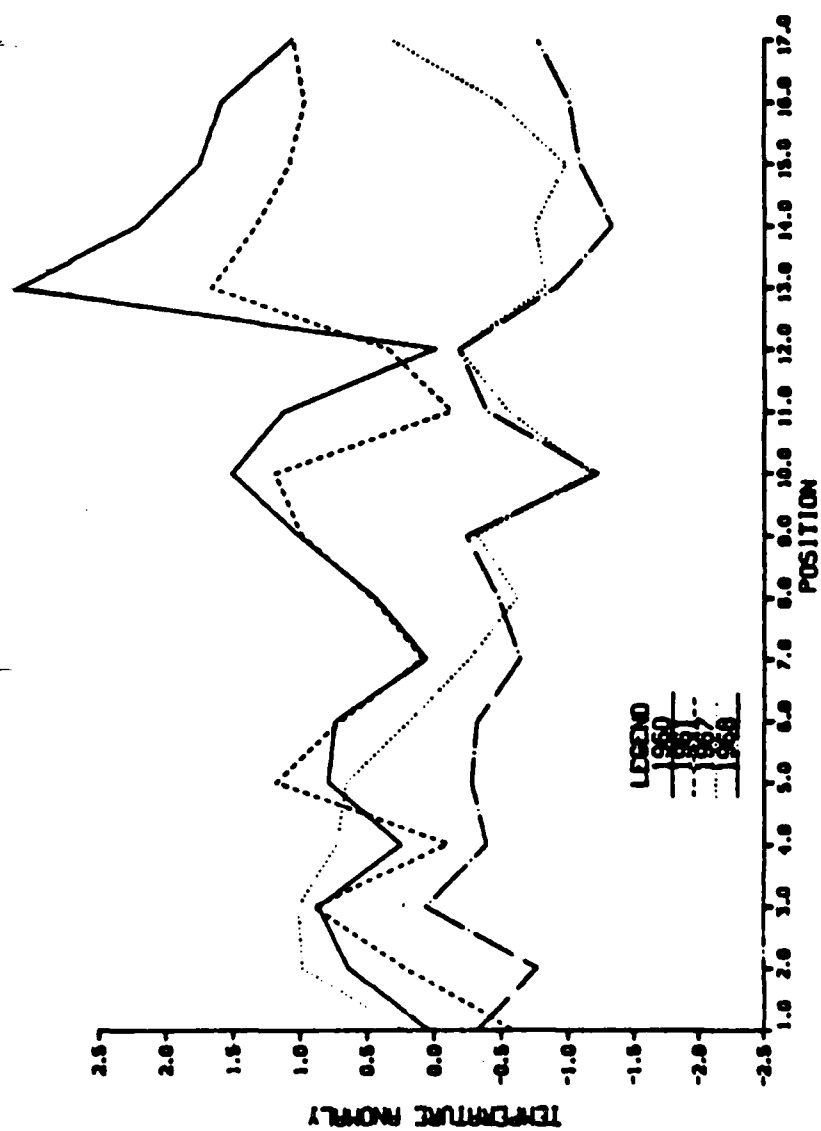


Figure 5.33 As for 5.32 except anomaly values are for the month of June.

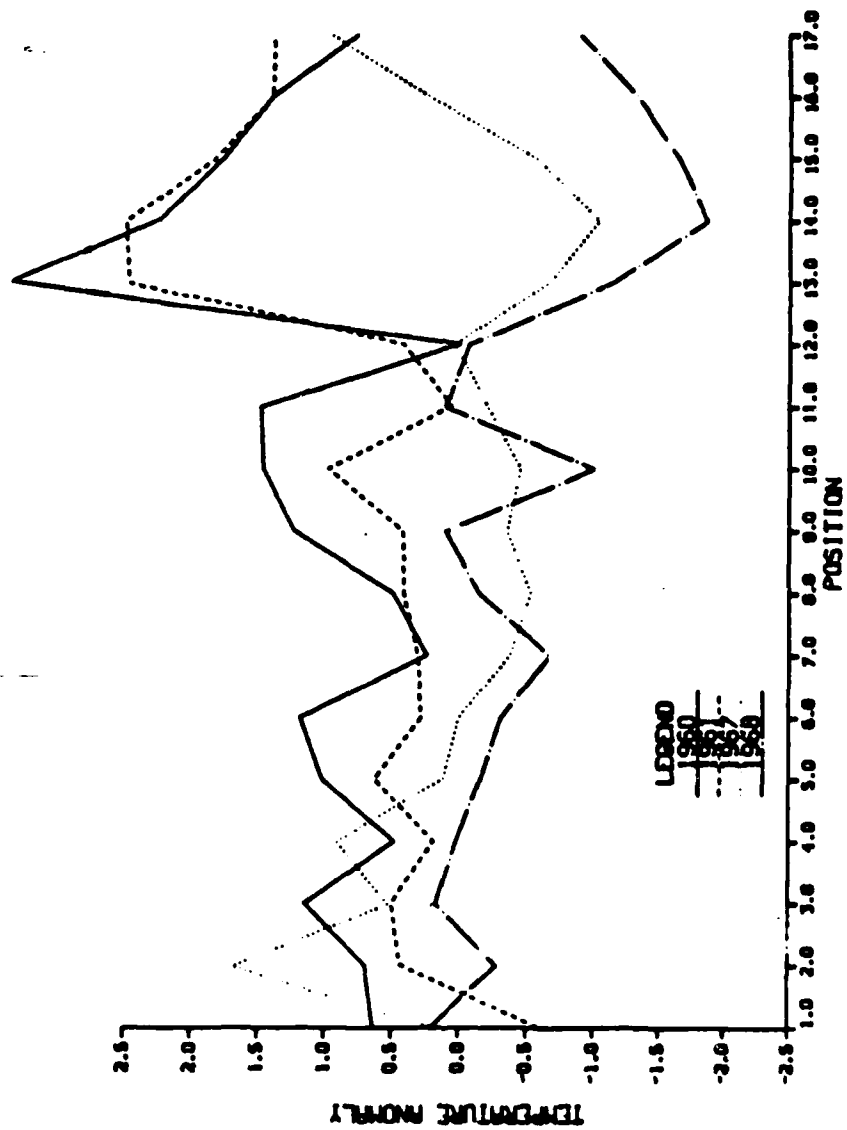


Figure 534 As for 5.32 except anomaly values are for the month of August.

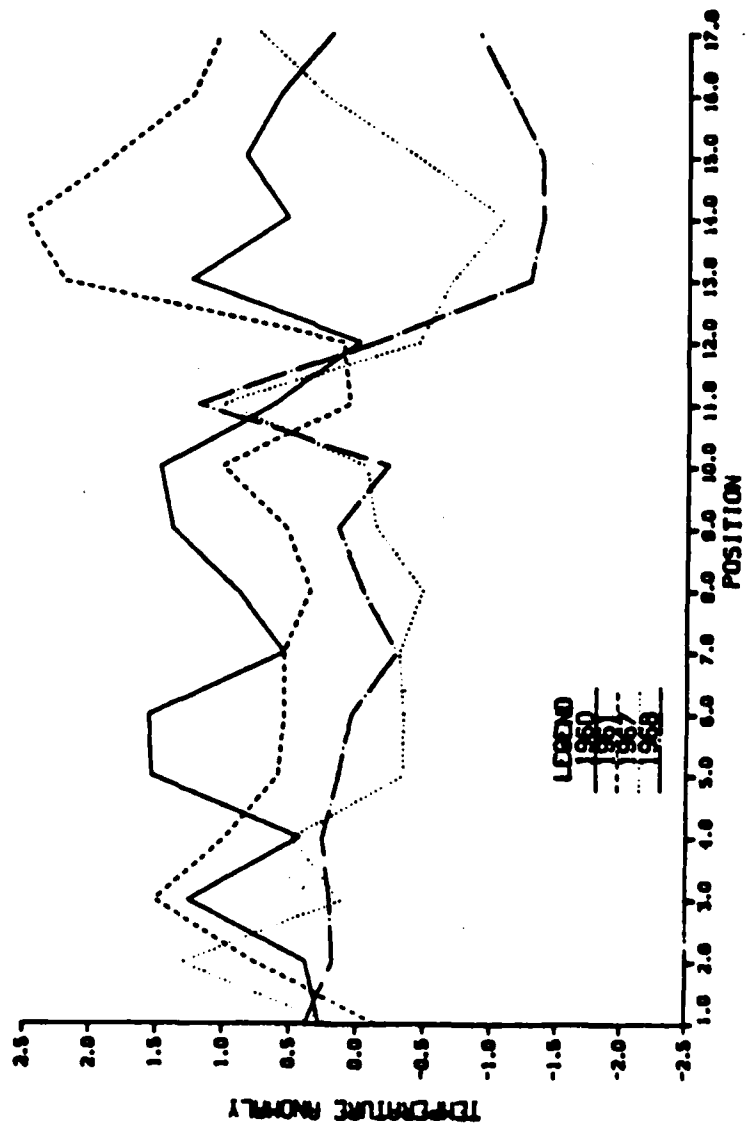


Figure 5.35 As for 5.32 except anomaly values are for the month of October.

## **VI. DISCUSSION**

This discussion is a consolidation (or synthesis) of the results presented in Chapter V. It addresses the considerations and objectives listed in Chapter I. Briefly, these include determination of the anomaly scales, evaluation of the autocorrelations of each variable, and evaluation of SST and ice concentration cross-correlations. Of particular interest is how the results of this work can provide an enhanced framework for sea ice predictability and in some circumstances actually be used to supplement present ice forecasting capabilities.

Discussion of the correlation features and their utility in forecasting ice cover is more meaningful when applied to identifiable oceanic regions. Therefore, the 17 points of interest used in this work were related to specific ocean areas (Table VI). Note that the POIs do not necessarily coincide with the center of each ocean area. The exact geographic position of each POI is listed in Table VI (see also Figure 3.1).

### **A. PERSISTENCE**

Ice anomaly persistence has long been recognized as a useful ice forecast tool. However, Figures 5.7 through 5.10 demonstrate that persistence at lags longer than two months is quite dependent on the region being examined. Several regions were observed to exhibit strong persistence values at significant lags while others were notable for their very low persistence values. Because the data were smoothed

by a five-month centered mean, persistence of anomalies through one season (three months) or less may be a function of data smoothing and is therefore of little practical significance. The following list summarizes the regions of strong and weak ice persistence, and the number of seasons over which significant (greater than 0.4) persistence exists:

1. Labrador Sea—good two-season persistence from fall to spring or winter to summer
2. South Denmark Strait—good persistence in excess of two seasons throughout the year
3. Iceland Sea—strong persistence in excess of three seasons throughout the year
4. Fram Strait—two-season persistence, however this is a data-poor region, therefore suspect
5. Bear Island—good two- to three-season persistence throughout the year
6. Davis Strait—poor persistence, limited to one season in winter
7. North Denmark Strait—poor persistence, limited to slightly greater than one season in winter
8. Greenland Sea—poor persistence, limited to one season in winter

The seasonal dependencies observed in the above list appear physically plausible. Ice anomaly persistence in the Labrador Sea is strongest from the cold months of fall and winter to the warm melting months of spring and summer. The mechanisms which control anomalies of ice concentration during the freezing periods will continue to do so for two or more seasons. However, the reduced persistence values from summer to winter indicate that similar long-term mechanisms do not operate during this time period. Three factors

which may provide an explanation for the reduced summer/fall persistence values are:

1. During the summer, in the region of the annual average MIZ, the ice has usually completely melted away. The differences from monthly means (anomaly values) for grid points here will be near zero. Essentially, there will be no ice concentration anomalies to persist and autocorrelation values will be low.
2. In summer, when the ice is breaking up along the MIZ, atmospheric forcing tends to dissipate the ice. The ice margin will migrate rapidly over long distances. At any given location near the ice edge, the ice concentration will have a high degree of variance, thereby reducing ice persistence to low levels.
3. Sea ice in the Arctic exhibits faster seasonal freezing than seasonal melting (Lemke, 1980) particularly in the Labrador Sea. This type of feature was also noted by Untersteiner, 1983. He observed that, in general, the ice edge and the average  $0^{\circ}\text{C}$  SST isotherm are nearly coincident during the fall-winter ice advance, but are often well removed during the spring-summer melt season. Persistence is enhanced during spring melting because the ice exhibits considerable "thermal inertia." In contrast, the autumn freeze-up appears to be dominated by the shorter-term thermodynamic forcing of the atmosphere and, as a result, the persistence of any ice anomalies is reduced.

Anomalies of autumn ice concentration in the South Denmark Strait persist well over two seasons. The point chosen to represent this region is well within the cold East Greenland Drift Stream. Ice concentration here is influenced by advection of ice from the ice production regions farther north in the northwestern Greenland Sea area. Anomalies originating in the production regions should take a considerable time to dissipate in the relatively cold water of the Denmark Strait (Vowinckel, 1964). This would explain the extended persistence signal noted here.

The Iceland Sea shows strong persistence of three or more seasons throughout the entire year. Figure 6.1 indicates that this is an area of cold water with influenced flow from the EGC, NIC, and EIC. Iceland and the NIC act as barriers preventing any ice dispersion to the south. The result is that ice concentration anomalies, which were probably advected into the region by the EGC from areas farther north, are confined and tend to persist for long periods.

Bear Island and the N. Barents Sea also show strong persistence beyond three or more seasons. According to data presented in Parkinson et al. (1987), this region is north of the front which separates the warm northward-flowing Atlantic water from the cold southward-flowing Arctic water. The front acts as an ice boundary preventing ice movement farther to the south, while Svalbard and the Arctic ice pack provide a boundary to the north. As such, ice anomalies here will not be advected away quickly and the nearly perennial cold water permits the anomalies to persist for long periods.

In summary, there appear to be three common factors which enhance ice concentration persistence. First, the surface waters need to be cold enough that an anomaly can exist for long periods of time. This condition is usually found in regions directly under the influence of the southward flowing cold currents exiting the Arctic Basin. Second, the current, if any, needs to be fairly weak. Third, the area should be bounded in some manner to limit free advection of sea ice. However, boundaries need not be limited to coastlines. Current shear

boundaries, thermal gradient fronts or the pack ice edge may also be effective boundaries for confining the ice.

An explanation for the low persistence values in the Davis Strait, North Denmark Strait, and Greenland Sea is also suggested by Figure 2.3. All three regions are located within dynamic current regimes where strong currents (often with varied water properties) converge, split, and/or interact. The Davis Strait region is influenced by the warm northward-flowing West Greenland Current and the cold southward-flowing Labrador Current. The northern Denmark Strait area experiences the effects of a branch of the warm Irminger Current and the cold East Greenland Current. The ice edge along the east Greenland continental shelf is strongly influenced by the warm Return Atlantic Current and the cold East Greenland Current. Where currents meet, sharp temperature gradients and velocity shears occur, producing instabilities and eddies. These conditions have been observed to cause large changes in ice concentration. The eddies break down the fronts which hold the ice margin in place. This results in lateral advection of the ice cover and rapid melting of the ice which is drawn into warmer water (Wadhams, 1981). The result is very poor persistence.

As noted in Chapter V, the persistence of sea surface temperature anomalies also displays notable longitudinal (geographic) dependence. The temperature anomalies in general show greater persistence values than ice concentration values and the high and low persistence regions are better defined.

With the exception of the data-sparse regions, SST persistence is significant for nearly all regions for periods in excess of one season. The Labrador Sea generally has the lowest SST persistence, especially in the spring. This is most likely a result of rapid divergence of the ice cover during spring breakup and the high insolation rates due to its more southerly latitude. The water is cleared of ice before the months of strongest insolation and can then warm relatively fast.

The Denmark Strait, south to the tip of Greenland, is a large area of strong SST persistence extending to three or more seasons. This is a result of the relatively constant temperatures found in the East Greenland Current.

Bear Island and the N. Barents Sea (POIs 14-16) show significant SST persistence of three or more seasons. The high persistence is a result of two factors. First, as noted earlier, these areas are located north of the warm Norwegian Atlantic Current water. This region is influenced by the cold, relatively constant temperatures of the Bear Island and East Spitzbergen Currents. Second, temperature anomalies covering such a large region would include a large volume of water, especially if the anomaly extended to depths of 50 m or more. Local weather effects could only erode the temperature anomaly slowly due to its large mass and persistence values would remain high.

## **B. TEMPORAL SCALES OF VARIABILITY**

The SST and ice concentration anomaly patterns exhibited no apparent long term trend over the 324-month time series. This is in contrast to the finding of Lemke et al. (1980), who observed a 10-year

trend of decreasing total ice cover in the Arctic for the years 1966 to 1976. They also noted that a large coincident negative trend in ice concentration existed in the eastern Atlantic region and a large positive trend existed in the Davis Strait sector. These trends can be detected in Figures 5.2-5.3 during the months 156-276 which correspond to this 10-year period. However, with respect to the overall 27-year data set, these features are not prevalent, do not repeat, and therefore should probably be regarded as moderate-term sampling fluctuations atypical of the 25-year period as a whole.

The anomaly features shown in Figures 5.1-5.6 exhibit a wide range of time scales; from little more than a month in some cases to over a year in others. The persistence contours contained in Figures 5.7-5.14 are an indication of the prevalent anomaly time scales. For example, in this study significant persistence for ice concentration ( $r = 0.40$  for  $N = 25$  years) was found at lags of approximately  $\pm 5$  months and for SST at lags of approximately  $\pm 8$  months. In contrast, Lemke et al. (1980) obtained significant autocorrelation values of empirical orthogonal functions (EOFs) of Arctic sea ice variability which extended only to approximately three months. It should be noted, however, that their values are not longitude-specific because each EOF assigns at least some weight to fluctuations at all longitudes. Davis (1976) showed three-month smoothed SST anomalies correlating at significant levels extending to lags of  $\pm 6$  months. Again, in contrast to the present study, Davis' use of spatial EOFs did not permit the determination of persistences for specific points. Persistence values

calculated in this work are generally higher because they were not subjected to the extensive spatial averaging inherent in the EOF approach. The longer coherent time scales of this study can also be attributed to the much longer data record and the significantly greater data density used to derive the results.

The difference in time scales between significant persistence levels in SST and ice correlation suggests that SSTs in general display considerably more inertia than ice concentration. The primary reason for this is that sea surface temperature is linked through various mixing processes to a significant amount of water beneath the surface. Factors which influence SST and ice concentration therefore must operate on much larger masses and volumes in the case of the water as compared to ice. Hence, SST anomalies should increase or decrease more slowly than ice concentration anomalies. For example, a strong wind can rapidly clear large areas of heavy ice cover yet the SST will be only minimally affected. Or, in the case of freeze-up, large ocean areas can quickly develop significant ice concentration levels, especially when salinities are low, while the adjacent SSTs do not change dramatically.

Wind, air temperature, and humidity observations display considerably more variance and occur on much shorter time scales than either SST or ice concentration levels. Time series analyses of these atmospheric variables have indicated a very noisy signal characterized by autocorrelations of approximately 0.1 at a one-month lag (Namias and Born, 1970; Davis, 1976). Nevertheless, the atmosphere

undoubtedly plays a major role in the evolution of both SST and ice concentration anomalies. Ice concentration and SST features respond to an integration of, or long-term summation of, atmospheric forcing parameters. Difficulties in formulating the details of this "integral" concept have precluded development of an effective real-time model for long-range ice concentration predictions. Therefore, in the absence of a comprehensive and rigorous framework for diagnosing air-sea-ice interactions, a simple autocorrelation of SST and ice concentration remains a practical source of useful forecasting information.

### C. CROSS-CORRELATIONS

The features of high SST/ice concentration cross-correlation values (A, B, C, and D as defined in Chapter V) correspond to the following geographic areas:

Feature A	POI 14- 16	Bear Island and N. Barents Sea
Feature B	POI 10	Iceland Sea
Feature C	POI 10	Iceland Sea
Feature D	POI 7	Kap Farvel

Possible explanations for the high cross-correlation values in these regions are similar to those proposed during the analysis of the persistence values.

The high negative cross-correlation values obtained for the region of feature A suggests that warm (cold) summer and autumn SST anomalies will result in reduced (increased) ice concentration throughout following ice season (winter and spring). As noted in the previous section, both SST and ice concentration have high

persistence values here. As a result, summer SST anomalies have a long period of time in which to influence ice production. A warm SST anomaly will delay freeze-up and limit ice growth, while a cold SST anomaly would promote early season freezing and heavier ice production. Obviously, the amount of ice eventually produced in winter will also dictate the ice concentration during the spring breakup. In this manner, summer SST anomalies can function as meaningful and reliable precursors for ice concentrations up to three seasons later.

The Iceland Sea is also characterized by little influence of warm water advection. The water remains essentially cold due to cold currents and low air temperatures. Warming can only take place by summer heating (short-lived) or by a pulse of warm water from the westward branch of the Irminger Current. SST and ice concentration persistence here are also significant to over three seasons. The high cross-correlation values indicate that the ice has a sufficiently long time to respond to any SST anomaly that develops. Summer SSTs are good predictors for ice concentration the following fall and winter. In addition, once the winter ice has formed, the ice concentration then becomes a good predictor for SSTs the following autumn, supporting the notion that a local quasi-equilibrium or feedback mechanism develops in this region of weak external forcing.

While the cross-correlation at Kap Farvel is not large spatially, it provides an example of a different type of situation. This region is imbedded in the strong EGC where the current flows westward as it rounds the southern tip of Greenland. A strong, well-defined

cross-correlation signal is observed for this region which suggests that winter ice concentration is a good predictor for SSTs the following autumn. Ice occurs upstream along the east coast of Greenland at all times of the year and will extend as far south as Kap Farvel in seasons of extreme icing. However, the relatively strong current flow and the strong seasonal cycle of insolation do not encourage ice persistence. Therefore, the long-term interaction process between SST and ice cannot take place. An alternative hypothesis for the strong cross-correlation is that the ice at Kap Farvel is associated with SST anomalies which originate upstream probably near the MIZ. In other words, ice concentration at the southern tip of Greenland is influenced by SST anomalies which occur at locations to the north 2-3 seasons worth of travel upstream.

The importance of the SST influence on sea ice variability to the south and east of Greenland as found in this work complements the findings of Soviet researchers on East Greenland ice predictability (Lebedev and Uralov, 1982). While the Soviets utilized an indirect association between SST and sea ice (with the atmosphere presumably serving as a link between SST and ice concentration), the results obtained here can be explained in terms of direct associations: warmer-than-normal surface water is associated with less ice than normal, while colder-than-normal surface water is associated with more ice than normal. SST data from the MIZ (as in this work), as well as from regions farther south (as in the Soviet work), evidently

merits consideration in the design of an optimal statistical system for predicting sea ice coverage south and east of Greenland.

The conclusion that ice concentration may be related to SST anomalies advected downstream with an ocean current, as proposed for the Kap Farvel region, is physically plausible. However, as mentioned earlier, the anomaly contours (Figures 5.1-5.6) and the dominant year graphs (Figures 5.23-5.35) do not provide any indication that large-scale anomaly advection takes place.

An alternative possibility is that advection effects might only be observable in the stronger currents. To examine this, anomalies in the North Atlantic just south of the Norwegian Sea were considered. The strong northern extension of the Gulf Stream should advect SST anomalies into the Norwegian-Barents Sea basin. Anomaly data were extracted from the COADS data set for all  $2^{\circ} \times 2^{\circ}$  grid points in the North Atlantic. The anomalies at each grid point were correlated with subsequent anomalies at all surrounding grid points in the search for a preferred directionality of the largest lagged cross-correlations. Advective control of SST anomalies should produce a spatial asymmetry in the field of lagged cross-correlations with higher correlation values in the direction from which advection is occurring.

Analysis of the anomaly fields in the North Atlantic and in the Norwegian/Barents Seas did not provide evidence of the proposed link. Anomalies in the two regions appeared to develop quite independently. The final conclusion then supports the initial observations, that is, anomaly features are regionally dependent. Advection may

explain anomaly development in small areas but it is not the dominant factor over large areas, i.e., areas encompassing several seas. It should be noted that the data smoothing may affect the results of the advective computations, so further work on SST advection statistics is advisable.

#### **D. ICE FORECAST POTENTIAL**

In the previous section, an analysis of the cross-correlation between SST and ice concentration was discussed. The regions in which cross-correlation values appear strong enough to provide ice forecasting potential have been noted. In order to determine if this potential is useful, the cross-correlation values for these regions must be compared to our "benchmarks." Specifically, are the cross-correlation values larger, and do they therefore represent a larger portion of ice concentration variance than persistence or other established procedures for long-range ice forecasting?

Comparison between SST/ice concentration cross-correlation and ice/ice autocorrelation (persistence) is a straightforward task in this project as both sets of calculations were conducted using the same data base and the same significance levels. Comparison with the Soviet results and previous work by Lemke et al. (1980) is less straightforward due to the aforementioned differences in time and spatial scales and data density. The regions for which considerable ice forecast potential is indicated are the Iceland Sea, Bear Island, and northern Barents Sea.

A review of the Iceland Sea cross-correlation plot (Figure 5.17, point 10) indicates that significant (0.4) SST/ice concentration cross-correlation values exist to a lag of just under nine months. The significant ice autocorrelation values in Figure 5.9 only extend to seven months lag. The autocorrelation values are higher from one to five months lag but the cross-correlation values are approximately 20 percent larger from five to just under nine months. Therefore, summer SSTs in the Iceland Sea have the potential to be better predictors of ice concentration in the following mid-winter and spring than ice persistence. However, summer ice persistence is still the best forecast tool for the fall and early winter.

Comparison of our results to Lemke et al. (1980) is inappropriate for the Iceland Sea region due to the large ( $10^\circ$  longitudinal arc) areal averaging inherent in their approach. The Iceland Sea only fills a small proportion of the  $10^\circ$  arc. The major proportion of this arc contains the EGC. The ice, current and atmospheric conditions in the EGC are significantly different from the Iceland Sea. Consequently, when the EGC areas are averaged with the Iceland Sea, any signal appropriate to the Iceland Sea region alone is masked. It was not possible to make comparisons with the Soviet predictions as a discussion of ice prediction in the Iceland Sea could not be found in the Soviet literature.

Ice persistence and SST/ice concentration cross-correlation values for Bear Island and the N. Barents Sea (POIs 14 to 16) can also be compared using Figures 5.9 and 5.17. The ice persistence plot

indicates significant persistence extending to six months lag in the western part of this region (POI 14) but only to 2-3 months lag elsewhere. The SST/ice concentration cross-correlation values, however, are significant for time periods exceeding a year's lag (for POIs 14 to 16). Ice persistence correlations exceed cross-correlation levels only at lags less than a month. The increase in persistence towards the western part of the region is in qualitative agreement with the results shown by Lemke et al. (1980). POI 14 provides the most direct comparison with their first EOF since it is weighted most heavily in their dominant eigenvectors. Their persistence values, however, are significantly lower than those determined in this work. Interpolation of the Lemke et al. results shows that significant persistence of ice anomalies is limited to approximately five months lag, probably because of the merging of different regions into each eigenvector.

A competing methodology for forecasting the ice cover of the Barents Sea has been described by Soviet researchers (Moskal', 1977). The Soviet procedure is essentially a one-dimensional thermodynamic model of a (variable-depth) mixed layer applied at a network of points 220 km apart in the Barents Sea. The model is based on the set of heat and salinity budget equations developed by Doronin in the 1960s (e.g., Doronin et al., 1970). The treatment of mixing uses constant diffusivities. The model is initialized with temperature, salinity, and ice cover data for late August and is forced by climatological radiative fluxes and station-derived air temperatures, wind speeds, and atmospheric pressures for 10-day periods from late August to late April.

Moskal' (1977) claims that the simulated freeze-up (defined to occur when the mixed-layer temperature drops to the freezing point of the sea water) produces an ice edge which, in 76 percent of the cases, coincided with the actual data within the limits of 1/5 of the amplitude. (The amplitude presumably refers to the envelope containing the interannually variable ice edge at a particular time of year). Since the forecasts extend to the February-April period, the Soviet results imply that thermodynamic considerations alone can provide considerable predictive skill in winter/spring ice coverage in the Barents Sea. This finding supports the validity of the predictability of the Barents Sea ice cover obtained in this study. While the Soviet method of evaluating forecast skill does not permit quantitative comparisons with the results in Chapter V, it should be noted that the Soviet methodology permits only hindcasts (not forecasts) because the simulations require autumn and winter thermal data from the atmosphere. This limitation supports the contention made in Chapter I that long-range forecasting applications of sea ice models will be severely constrained in the absence of skillful atmospheric forecast fields for periods more than 5-10 days in advance.

The conclusion for the Bear Island and N. Barents Sea region is that SST/ice concentration cross-correlations provide significant improvements over ice/ice autocorrelations for use in ice forecasting. In particular, for lags from three months to over a year, cross-correlation techniques outperform persistence techniques by up to 30 percent.

## E. THRESHOLD VALUES

The analysis of SST/ice concentration cross-correlation values indicates that cross-correlation of these two variables can be a more useful predictor for forecasting future ice concentration than ice concentration persistence alone. However, Chapter V showed that strong cross-correlations are usually a result of strong anomalies which occurred in 3 or 4 out of a total of 25 sample years. Had these strong anomaly years not been present, the cross-correlations would probably not have been significant. Therefore, in order for cross-correlation values to be used as an effective predictor for a specified time and location, it would be prudent to determine if the SST anomaly was large enough to be included in the subset of cases that made major contributions to the cross-correlations.

The determination of some "threshold" value of an SST anomaly, above which a corresponding strong ice anomaly could be expected, would be very useful to a forecaster. Graphs of anomaly values for the 25 years of data for Bear Island/N. Barents Sea (feature A) and Iceland Sea (features B and C) are included as Figures 6.2, 6.3, and 6.4, respectively. The plots and the results in Chapter V indicate that a natural dividing line of approximately  $1^{\circ}\text{C}$  exists between major and minor anomalies. It thus appears that  $1^{\circ}\text{C}$  would be a useful threshold number. This means that should the SST near Bear Island or in the N. Barents Sea differ by more than approximately  $1^{\circ}\text{C}$  from the monthly mean, the SST information should be weighted heavily in the preparation of the long range ice forecast. In cases with small ( $<1^{\circ}\text{C}$ )

anomalies of SST, the SST input to the ice forecast should be assigned relatively little weight.

#### **F. DATA LIMITATIONS**

Analysis of the cross-correlations between SST and ice concentration is inevitably subject to uncertainties in the quantity and quality of the data. The impact of the data-sparse regions around POIs 1-4 and 11-12 has already been noted in the results obtained here. Data limitations in these regions are not surprising since these areas are generally inaccessible and surface measurements from these and other remote locations will probably remain infrequent. The very reason data are so limited in these regions (little commercial activity) reduces the requirement to provide accurate forecasts for commercial interests. However, from a military viewpoint, the strategic value of these regions has increased substantially in recent years for both the NATO alliance and the Soviet Union (Conant, 1985; Lindsey, 1977). The future need for additional data and region-specific forecasts may therefore be greater than in the past. The large variability between various regions of the North Atlantic, together with the scarcity of conventional surface observations, implies that remotely sensed data on SST and sea ice concentration (or ice edge location) may merit heavier use in research pertaining to North Atlantic sea ice forecasting.

The data limitations in the COADS data set were found to be most severe during the winter in Hudson Bay, Baffin Bay, and the Svalbard region. The utility of the COADS SST observations in regions

immediately equatorward of the marginal ice zones of the latter region was not explored systematically, primarily because the objective selection of the regions/points of interest was a high priority. Future work may quantify the trade-offs between the gain in observational input and the increase in distance from the MIZ as an SST area is made larger and/or more remote from the climatological ice edge.

The sea ice data may be regarded as homogeneous since the advent in the early 1970s of routine satellite coverage and consistently formatted hemispheric ice charts (U.S. Navy Fleet Weather Facility, 1976). However, prior to the early 1970s, the observational coverage was irregular in space and time. The consolidation of several regional data sources for use in this study undoubtedly introduced inhomogeneities in data quality and quantity. All data identified as "estimated" or "unreliable" in the gridded SEIC data set was used in this study, since the advantage of the longer record length was thought to outweigh the disadvantages of the data inhomogeneities. The correlative results obtained here may thus be regarded as lower bounds on the strength of the signals in the data because the data inhomogeneities serve as an additional source of "noise." Statistical analysis of the later and more data-rich portion of the data sets may indicate a stronger SST-ice coupling in some regions than was found in this work.

TABLE VI

**THE POIS, THEIR GRID AND GEOGRAPHIC POSITIONS,  
AND THE RESPECTIVE OCEANIC AREAS  
WITH WHICH THEY ARE ASSOCIATED**

<b>Point</b>	<b>Grid Point Row-Column</b>	<b>Position</b>	<b>Ocean Area</b>
1	07-48	59.16N 85.10W	HUDSON BAY
2	14-69	50.04N 51.70W	LABRADOR SEA
3	15-59	58.76N 59.81W	LABRADOR SEA
4	15-64	54.77N 54.59W	LABRADOR SEA
5	18-56	62.98N 58.99W	DAVIS STRAIT
6	21-53	67.20N 57.88W	DAVIS STRAIT
7	23-64	58.62N 42.48W	KAP FARVEL
8	27-60	63.75N 37.74W	S. DENMARK STRAIT
9	31-59	65.67N 29.46W	N. DENMARK STRAIT
10	36-57	67.98N 17.40W	ICELAND SEA (South of Jan Mayen)
11	38-51	73.72N 09.38W	GREENLAND SEA (data poor)
12	39-46	78.30N 00.02W	FRAM STRAIT (data poor)
13	42-49	74.35N 06.57E	E. NORWEGIAN SEA
14	45-45	75.86N 25.00E	BEAR ISLAND
15	48-43	74.74N 38.59E	N. BARENTS SEA
16	51-43	72.11N 43.44E	BARENTS SEA
17	54-44	68.98N 44.65E	BARENTS SEA

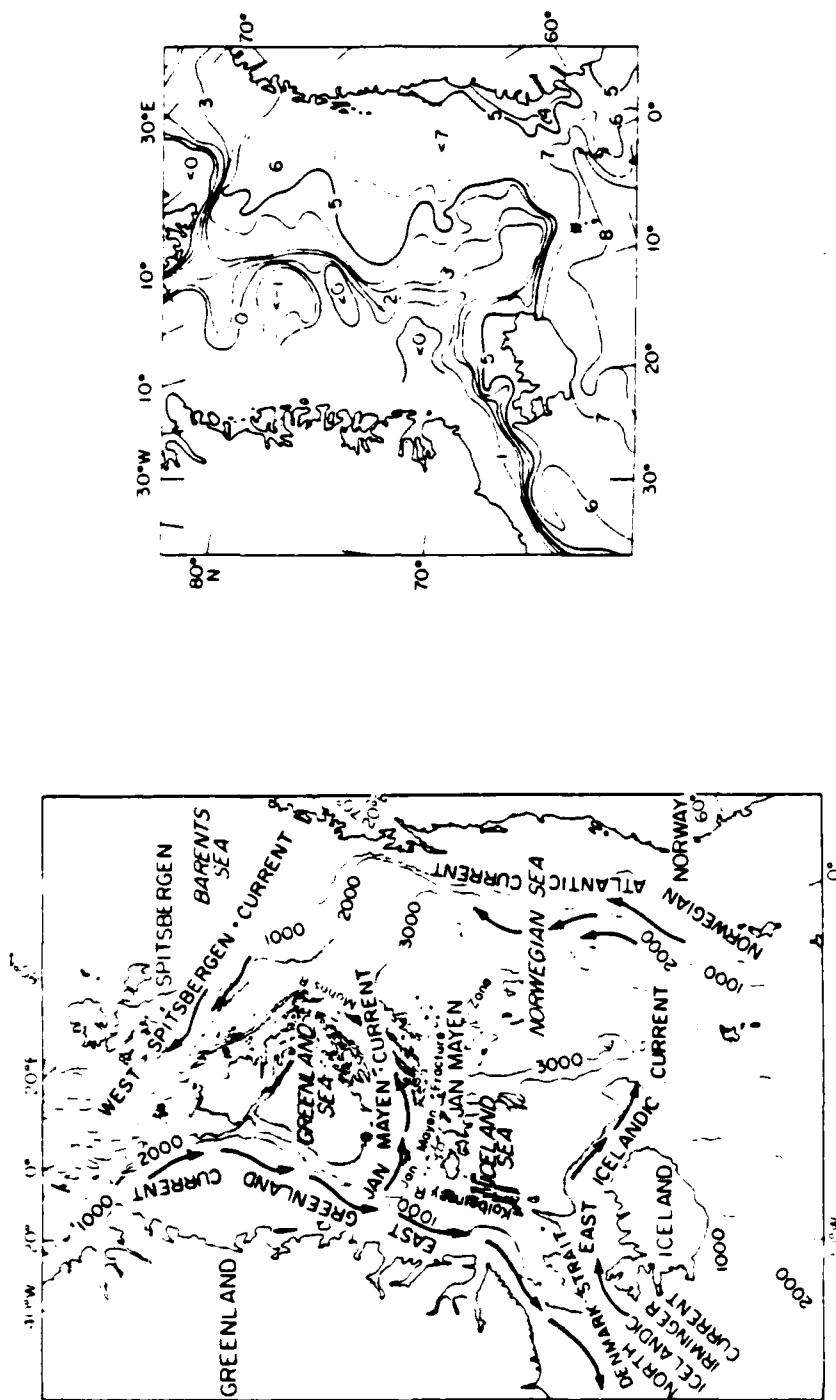


Figure 6.1 Average current and an example of winter temperature distribution in the Iceland Sea. [from Swift and Aagaard 1981)].

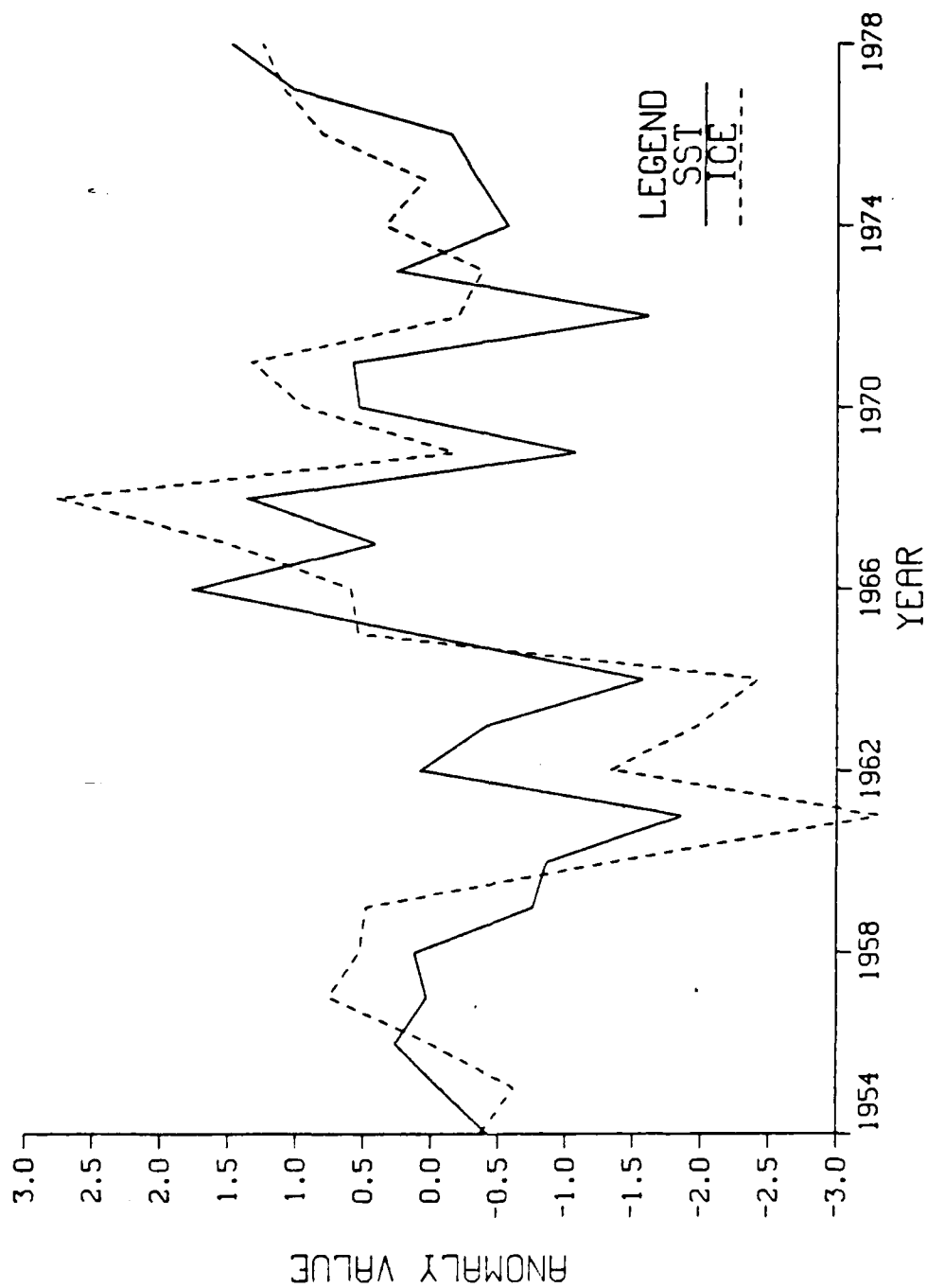


Figure 6.2 SST and ice concentration anomaly values for cross-correlation feature A. SST is plotted in negative scale to emphasize the correlation.

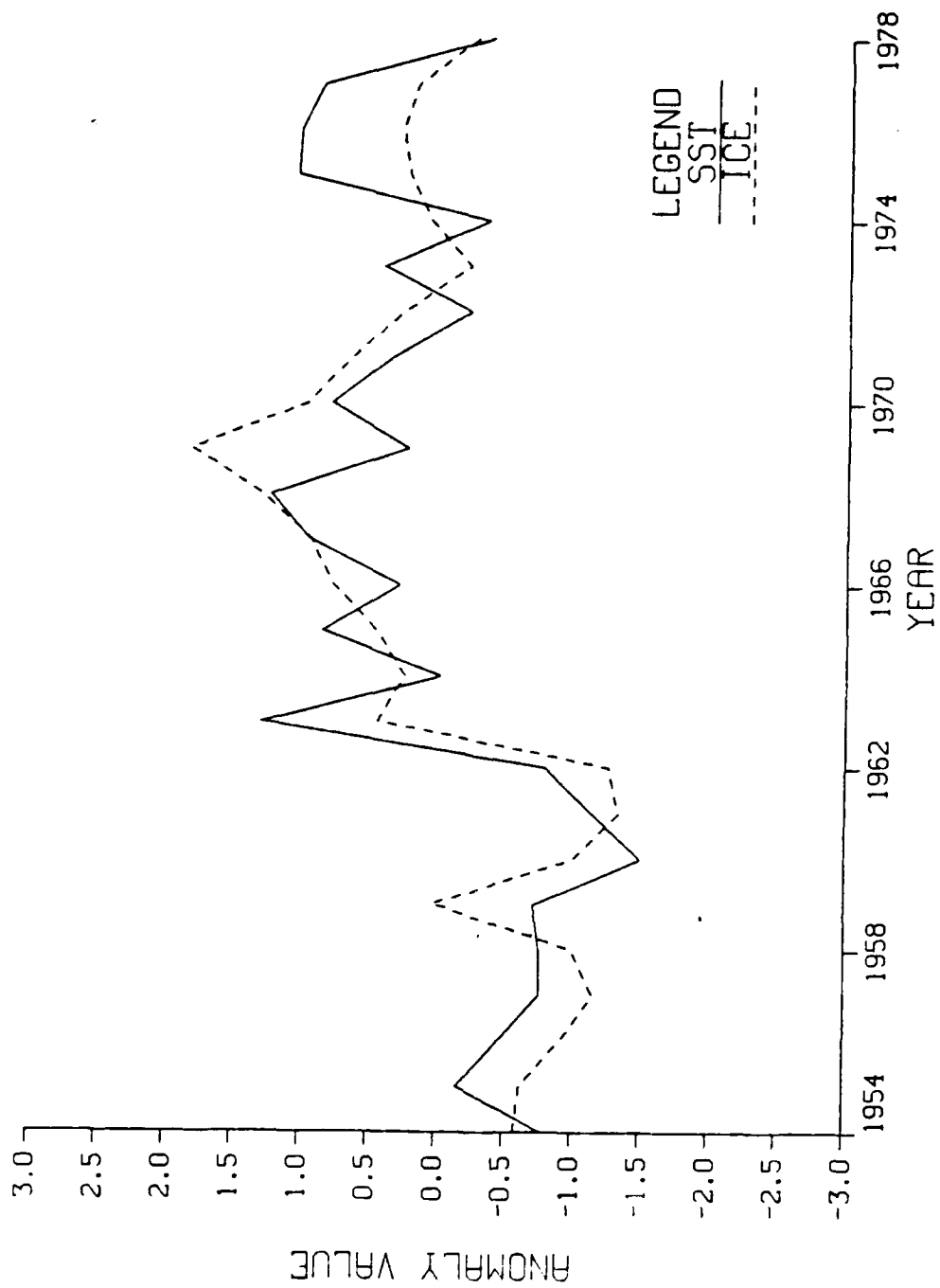


Figure 6.3 Same as 6.2 except for cross-correlation feature B.

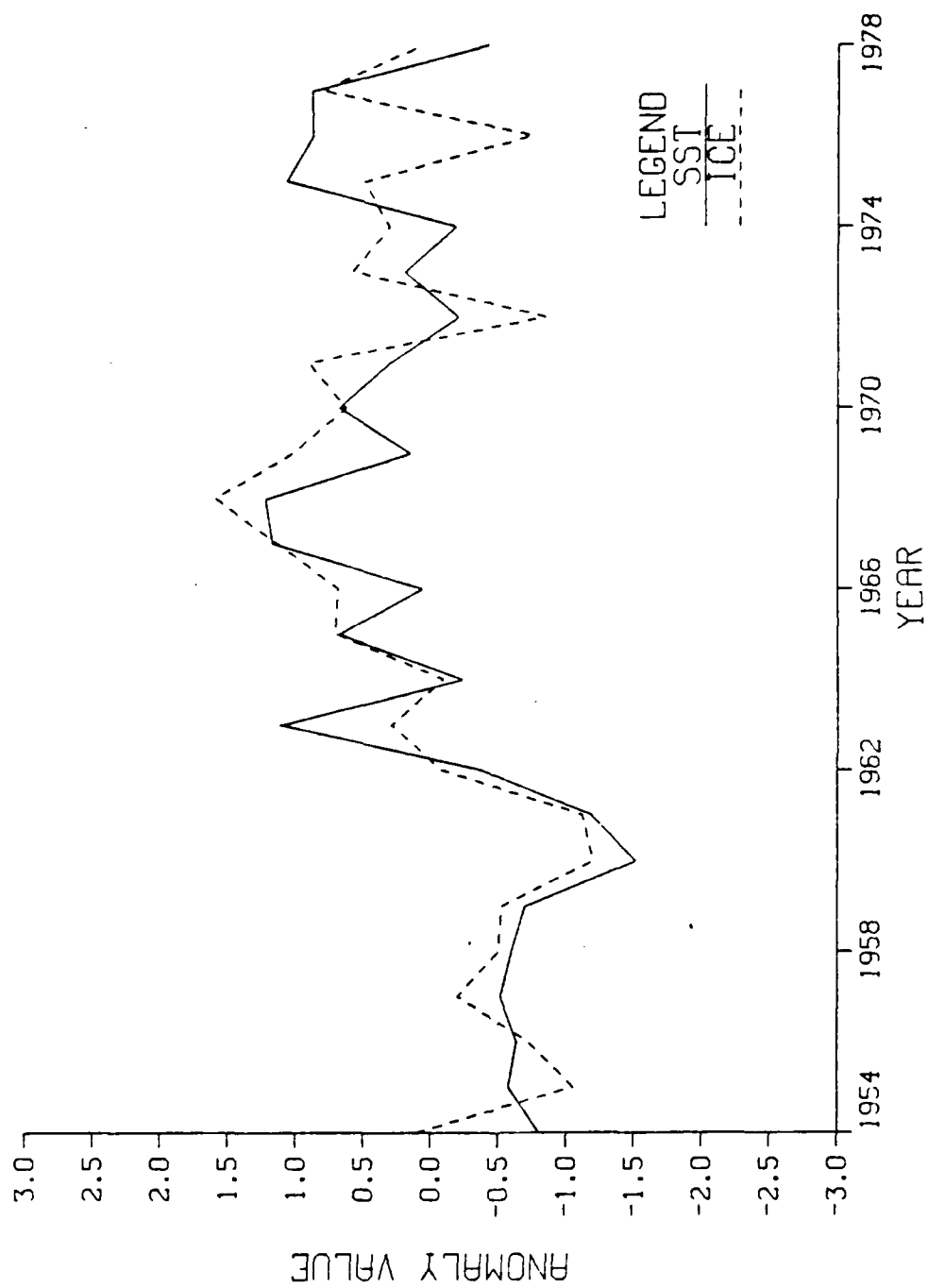


Figure 6.4 Same as 6.2 except for cross-correlation feature C.

## **VII. CONCLUSIONS AND FUTURE WORK**

### **A. CONCLUSIONS**

Previous work by several authors (e.g., Rogers, 1978; Walsh and Sater, 1981) has attempted to correlate the extent and movement of the Arctic ice cover with air pressure fields. While success has been achieved in some regions, other regions like the eastern North Atlantic have not achieved significant correlations.

A statistical analysis of SST and ice concentration anomalies (deviations from the monthly mean) was conducted, using the recently compiled COADS and SEIC data sets, in order to determine whether SST might be an effective and/or useful predictor for the amount of ice cover. In the course of the analysis, a number of interesting observations and conclusions were reached. The following is a brief list of the highlights:

1. SST and ice concentration anomalies occur on spatial scales of 100s and possibly 1000s of kms.
2. SST anomaly time scales are often a year or longer, while ice concentration anomaly time scales average two to three seasons (three months/season). These time scales are based on the periods over which the autocorrelations exceed the 95-percent significance levels.
3. Both variables exhibit strong regional dependence. Anomaly evolution is in general a local event and not strongly associated with anomaly evolution in adjacent or distant regions.
4. Persistence of ice and SST is largest in geographically confined regions of slow and variable surface currents. Persistence of the two variables is smallest in regions of strong currents or areas exhibiting open boundaries.

5. Cross-correlation of SST and ice concentration is highest in regions where the two variables are not subjected to strong dynamical influences such as thermal advection. They may therefore co-exist in an anomalous state for extended periods.
6. Summer SST anomalies appear to be the precursor to winter ice anomalies more frequently than the converse. However, in the Iceland Sea region, a feedback mechanism was present whereby SSTs influenced the winter ice concentration, which in turn influenced the SST pattern of the following summer.
7. SST was found to be a stronger predictor of ice concentration than was ice concentration persistence in the Iceland Sea region and around Bear Island and the N. Barents Sea. Specifically, the SST/ice concentration cross-correlation had higher values in these regions than the ice/ice autocorrelations.
8. The larger and more comprehensive data sets used for this work resulted in larger correlation values than in most previous studies. A possible exception was the Soviet predictions for the Greenland Sea. However, when the Soviet statistical models were tested using COADS and SEIC data, the skill of these models was less than claimed by the Soviets.
9. Current thermodynamic and dynamic models, limited by boundary conditions and initial field inaccuracies, cannot as yet produce sufficiently accurate ice forecasts beyond several days. In the absence of major breakthroughs in the long-range prediction of the major forcing variables, statistical approaches probably hold the most promise for effective ice concentration forecasting in the near future.
10. The COADS and SEIC data sets, although limited by inhomogeneities in the raw data input, can still permit useful statistical analyses for some regions of the high-latitude North Atlantic.

## **B. FUTURE WORK**

The SEIC and COADS data sets provide the potential to conduct a wide array of statistical analyses on Arctic environmental variables. Results from this work indicate that interesting and useful information can be obtained. More extensive studies incorporating additional

regions and variables would undoubtedly produce further worthwhile results. In particular, the following topics merit special attention:

1. The spatial coverage of the data should be increased. The computer programs written for this work can be used to calculate persistence and cross-correlations for any point on the 58 x 80 grid. This includes regions in the North Pacific, Bering Strait, Beaufort Sea, etc. The current work demonstrates the regional dependence or the local nature of ice and SST anomalies. Prudent selection and examination of many more POIs would refine the estimates of the anomaly fields. More specifically, the selection of POIs on the basis of SST and ice data availability rather than the ice edge climatology might enhance the correlation signal.
2. A close examination of strong current regions should be conducted. The present work indicated that advection influenced the ice conditions at Kap Farvel in the EGC. The possibility exists that similar influences occur in other regions dominated by strong currents. Some quantitative measure of these influences would be useful.
3. The current work has indicated that SST and ice concentration anomalies occur on spatial scales much smaller than those for which much previous work has been conducted (e.g., Rogers and van Loon, 1979). Correlation of SST and ice concentration with other environmental variables such as mean pressure and temperature fields should be re-examined at these smaller scales. The logical extension to this would be to conduct a multiple regression analysis of the predictors and develop a high-resolution statistical ice forecast model for the Arctic Seas. The sensitivity of such models to the scale of the ice predictions should be systematically explored.
4. The apparent feedback mechanisms found in areas such as the Iceland Sea should be explored in more detail in order to unravel the causes and effects, which may well extend to "external" forcing such as the atmospheric circulation and air temperature (e.g., Lamb and Morth, 1978).
5. The sensitivity of operational models to initial SST fields needs to be examined in order to determine whether ice model forecasts can achieve skill in the absence of accurate long-range atmospheric forecasts.

### LIST OF REFERENCES

- Aagaard, K., J. H. Swift, and E. C. Carmack, 1985: Thermohaline circulation in the Arctic Mediterranean seas. J. Geophys. Res., 90, 4833-4846.
- Aagaard, K., and L. K. Coachman, 1968 a: The East Greenland Current north of Denmark Strait: Part I. Arctic 21 (3), 181-200.
- Aagaard, K., and L. K. Coachman, 1968 b: The East Greenland Current north of Denmark Strait: Part II. Arctic 21, (4), 267-290.
- Bourke, R. H., and R. P. Garrett, 1987: Sea ice thickness distribution in the Arctic Ocean. Cold Regions Science and Technology, 13, 259-280.
- Broccoli, A. J., and R. P. Harnack, 1981: Predictability of monthly North Pacific sea level pressure from monthly sea surface temperature for the period 1933-1976. Monthly Weather Rev., 109, 2107-2117.
- CIA, 1978: Polar Regions Atlas, National Foreign Assessment Center, CIA, 66 pp.
- Coachman, L. K., and K. Aagaard, 1974: Physical oceanography of Arctic and Subarctic Seas. In: Marine Geology and Oceanography of the Arctic Seas (Y. Herman, Ed.), Springer-Verlag, New York, 1-72.
- Coachman and Barnes, 1961: The contribution of Bering Sea water to the Arctic Ocean. Arctic, 14(3), 146-161.
- Conant, M. A., 1985: Polar strategic concerns. Oceanus, 28, 62-66.
- Davis, R. E., 1976: Predictability of sea surface temperature and sea level pressure anomalies over the North Pacific Ocean. J. Phys. Oceanogr., 6, 249-266.
- Doronin, Y. P., A. V. Smetannikova and A. S. Grushkina, 1970: Use of a numerical computation method for predicting autumn-winter ice conditions in Arctic Seas. Trudy AANII, 292, 87-105.
- Elsberry, R. L., and S. D. Raney, 1978: Sea surface temperature response to variations in atmospheric wind forcing. J. Phys. Oceanogr., 8, 881-887.

Gross, C. E., 1986: Joint Ice Center global sea ice digital data. Snow Watch '85, Glaciological Data GD-18, World Data Center for Glaciology, Boulder, Co, 125.

Haupt, I., and V. Kant, 1976: Satellite ice surveillance studies in the Arctic in relationship to the general circulation. In: Proceedings of the Symposium on Meteorological Observations from Space: Their Contribution to the First GARP Global Experiment, International Council of Scientific Unions, Paris, 179-187.

Haworth, C., 1978: Some relationships between sea surface temperature anomalies and surface pressure anomalies. Quart. J. Roy. Meteor. Soc. 104, 131-146.

Hibler, W. D. III, and K. Bryan, 1987: A diagnostic ice-ocean model. J. Phys. Oceanogr., 17, in press.

Kelly, P. M., 1979: A basis for forecasting the Arctic sea ice over a few months to many years. Annual Report No. 1, ONR Contract N00014-77-G-0074, 18 pp.

Kirillov, A. A., 1977: Ice forecasts for the Arctic seas and their practical application. Soviet Meteorology and Hydrology, No. 4, 59-65.

Kirillov, A. A., and M. S. Khromtsova, 1971: Long-term variability of the ice cover of the Greenland Sea and the method of forecasting it. Trudy AANII, 320, 47-64.

Kogan, B. A., and N. F. Orlov, 1981: New methods of ice forecasting for the Northwestern Atlantic. Soviet Meteorology and Hydrology, No. 11, 21-26.

Krauss, W., 1986: The North Atlantic Current. J. Geophys. Res., 91, 5061-5074.

Lamb, H. H., and H. T. Morth, 1978: Arctic ice, atmospheric circulation and world climate. Geographical Journal, 144 (1), 1-22.

Lebedev, A. A., and N. S. Uralov, 1976: Features of the thermal state of the North Atlantic and of the atmospheric circulation in association with the formation of anomalous ice cover in the Greenland Sea. Trudy AANII, 320, 47-64.

Lebedev, A. A., and N. S. Uralov, 1982: Forecasting of ice cover of the Greenland Sea in relation to the thermal state of the North Atlantic Ocean and atmospheric circulation. Problemy Arktiki i Antarktiki, 50

(1977), 36-39; English translation published by Amerind Publishing Co. Pvt. Ltd., New Delhi, 36-41.

Lemke, P., E. W. Trinkl and K. Hasselmann, 1980: Stochastic dynamic analysis of polar sea ice variability. J. Phys. Oceanogr., 10, 2100-2120.

Lindsey, G. R., 1977: Strategic Aspects of the Polar Regions. Canadian Institute of International Affairs, Toronto, 1977.

Moskal', T. N., 1977: Results of application of numerical method for computing ice regime elements in Barents Sea during autumn-winter. Leningrad Trudy Ordena Lenina Arkticheskogo i Antarkticheskogo Nauchno-Issledovatel'skogo Institute: Metodika Ledovykh Prognozov i Raschetov Dlya Arkticheskikh Morey, Vol. 346, 45-54.

Namias, J., 1976: Negative ocean-air feedback systems over the North Pacific in the transition from warm to cold seasons. Mon. Weather Rev., 104, 1107-1121.

Namias, J., and R. M. Born, 1970: Temporal coherence in North Pacific sea-surface temperature patterns. J. Geophys. Res., 75, 5952-5955.

Nikol'skaya, N. A., V. L. Senyukov and B. A. Kogan, 1977: Relationship between integral indices of the thermal state of the ocean and atmospheric circulation and ice cover of the Danish Strait. In: Problems of the Arctic and Antarctic, 52, 44-53. Editor-in-Chief A. F. Treshnikov.

NOAA, 1987: Climate Diagnostics Bulletin 87/5. Climate Analysis Center/NMC. U. S. National Weather Service/NOAA. 25 pp.

Orlov, N. F., 1977: Space-time variability of the ice cover and location of the ice edge in the northwestern North Atlantic. Problems of the Arctic and Antarctic, 52, 64-71.

Parkinson, C. L., C. C. Josefino, H. J. Zwally, D. J. Cavalier, P. Gloerson and W. J. Campbell, 1987: Arctic Sea Ice 1973-1976: Satellite Passive Microwave Observations 296 pp.

Preller, R. H., 1985: The NORDA/FNOC Polar Ice Prediction System (PIPS)-Arctic: A technical description. NORDA Report 108, NSTL, MS, 61 pp.

Ramage, C. S., 1984: Can shipboard measurements reveal secular changes in tropical air-sea heat flux? J. Climate Appl. Meteor., 23, 187-193.

Ratcliffe, R. A. S., and R. Murray, 1970: New lag associations between North Atlantic sea temperatures and European pressure, applied to long-range weather forecasting. Quart. J. Roy. Meteor. Soc., 96, 226-246.

Rogers, J. C., 1978: Meteorological factors affecting the interannual variability of summertime ice extent in the Beaufort Sea. Mon. Weather Rev., 106, 890-897.

Rogers, J. C., and H. van Loon, 1979: The seesaw in winter temperatures between Greenland and northern Europe. Part III: Some oceanic and atmospheric effects in middle and high latitudes. Mon. Weather Rev., 107, 509-519.

Rowntree, P. R., 1976: Response of the atmosphere to a tropical Atlantic ocean temperature anomaly. Quart. J. Roy. Meteor. Soc., 102, 607-625.

Sater, J. E., A. G. Ronhovde and L. C. van Allen, 1971: Arctic Environment and Resources. Arctic Institute of North America, Washington, DC, 309 pp.

Schell, I. I., 1970: Arctic ice and sea temperature anomalies in the northeastern North Atlantic and their significance for seasonal forecasting locally and to the eastward. Mon. Weather Rev., 98, 833-850.

Semtner, A. J., Jr., 1987: A numerical study of sea ice and ocean circulation in the Arctic. J. Phys. Oceanogr., 17, in press.

Slutz, R. J., S. J. Lubken, J. D. Hiscox, S. D. Woodruff, R. L. Jenne, D. H. Joseph, P. M. Steurer and J.D. Elms, 1985: Comprehensive Ocean-Atmosphere Data Set Release 1, 39 pp.

Stringer, W. J., D. G. Barnett and R. H. Godin, 1984: Handbook for Sea Ice Analysis and Forecasting. Naval Env. Res. and Pred. Facility, Monterey, CA, 324 pp.

Swift, J. H., and K. Aagaard, 1981: Seasonal transitions and water mass formation in the Iceland and Greenland Seas. Deep-Sea Res 28A, 1107-1129.

U.S. Navy Fleet Weather Facility, 1976: Arctic Sea Ice Analyses, 1972-1975 (Eastern and Western). Suitland, MD, 204 pp.

Untersteiner, N., 1983: Air-Sea-Ice Research Program for the 1980's. Applied Physics Laboratory, APL-UW-8306, Univ. of Washington, Seattle, 83 pp.

Vowinckel, E., 1964: Ice transport in the East Greenland Current and its causes. Arctic, 17, 111-119.

Wadhams, P., 1981: The ice cover in the Greenland and Norwegian Seas. Reviews of Geophys. and Space Phys., 19 (3), 345-393.

Walsh, J. E., and C. M. Johnson, 1979: An analysis of arctic sea ice fluctuations, 1953-1977. J. Phys. Oceanogr., 9, 580-591.

Walsh, J. E., and J. E. Sater, 1981: Monthly and seasonal variability in the ocean-ice-atmosphere systems of the North Pacific and the North Atlantic. J. Geophys. Res., 86, 7425-7445.

Walsh, J. E., 1982: Continental snow cover and association with 700 mb height: 1966-1980. Proceeding of 7th annual climate diagnostic workshop (NOAA) pub. Washington, D.C., 189-195.

Weeks, W. F., 1978: Sea ice conditions in the Arctic. In: Arctic Sea Ice, Glaciological Data, GD-2, World Data Center A for Glaciology, Boulder, CO, 1-20.

Weigel, A. M., 1987: Mesoscale variability in the West Spitsbergen Current and adjacent waters in Fram Strait. Masters Thesis, Naval Postgraduate School, Monterey, CA.

## INITIAL DISTRIBUTION LIST

	<u>No. Copies</u>
1. Defense Technical Information Center Cameron Station Alexandria, VA 22304-6145	2
2. Library, Code 0142 Naval Postgraduate School Monterey, CA 93943-5002	2
3. Chairman (Code 68Mr) Department of Oceanography Naval Postgraduate School Monterey, CA 93943	1
4. Chairman (Code 63Rd) Department of Meteorology Naval Postgraduate School Monterey, CA 93943	1
5. Dr. R. H. Bourke (Code 68Bf) Naval Postgraduate School Monterey, CA 93943	1
6. LCDR Gordon H. Fleming Department of Oceanography Naval Postgraduate School Monterey, CA 93943	1
7. Director Naval Oceanography Division Naval Observatory 34th and Massachusetts Avenue NW Washington, DC 20390	1
8. Commander Naval Oceanography Command NSTL Station Bay St. Louis, MS 39522	1

- |     |   |   |
|-----|---|---|
| 9.  | Commanding Officer<br>Naval Oceanographic Office<br>NSTL Station<br>Bay St. Louis, MS 39522   | 1 |
| 10. | Commanding Officer<br>Fleet Numerical Oceanography Center<br>Monterey, CA 93940   | 1 |
| 11. | Commanding Officer<br>Naval Ocean Research and Development<br>Activity<br>NSTL Station<br>Bay St. Louis, MS 39522   | 1 |
| 12. | Commanding Officer<br>Naval Environmental Prediction<br>Research Facility<br>Monterey, CA 93940   | 1 |
| 13. | Chairman, Oceanography Department<br>U. S. Naval Academy<br>Annapolis, MD 21402   | 1 |
| 14. | Chief of Naval Research<br>800 N. Quincy Street<br>Arlington, VA 22217  | 1 |
| 15. | Office of Naval Research (Code 420)<br>Naval Ocean Research and Development<br>Activity<br>Attn: Dr. T. Curtin<br>Dr. L. Johnson<br>800 N. Quincy Street<br>Arlington, VA 22217 | 3 |
| 16. | Scientific Liason Office<br>Office of Naval Research<br>Scripps Institution of Oceanography<br>La Jolla, CA 92037   | 1 |
| 17. | Library<br>Scripps Institution of Oceanography<br>P. O. Box 2367<br>La Jolla, CA 92037  | 1 |

- |     |  |   |
|-----|--|---|
| 18. | Library<br>Department of Oceanography<br>University of Washington<br>Seattle, WA 98105   | 1 |
| 19. | Library<br>CICESE<br>P. O. Box 4803<br>San Ysidro, CA 92073  | 1 |
| 20. | Library<br>School of Oceanography<br>Oregon State University<br>Corvallis, OR 97331  | 1 |
| 21. | Commander<br>Oceanographic Systems Pacific<br>Box 1390<br>Pearl Harbor, HI 96860   | 1 |
| 22. | Chief, Ocean Services Division<br>National Oceanic and Atmospheric<br>Administration<br>8060 Thirteenth Street<br>Silver Springs, MD 20910 | 1 |
| 23. | Naval Postgraduate School<br>Attn: Dr. E. Weinberg<br>Monterey, CA 93943   | 1 |
| 24. | Department of Oceanography<br>University of British Columbia<br>Vancouver, B. C., Canada<br>V6T 1W5  | 1 |
| 25. | Library<br>Bedford Institute of Oceanography<br>P. O. Box 1006<br>Dartmouth, N. S., Canada<br>B2Y 4A2                                      | 1 |
| 26. | Department of Oceanography<br>Dalhousie University<br>Halifax, N. S., Canada<br>B3H 4J1  | 1 |

- |     |  |   |
|-----|--|---|
| 27. | Dean of Science<br>Royal Roads Military College<br>F.M.O. Victoria, B. C., Canada<br>V0S 1B0                         | 1 |
| 28. | Institute of Ocean Sciences, Pat Bay<br>P. O. Box 6000<br>9860 West Saanich Road<br>Sidney, B. C., Canada<br>V8L 4B2 | 1 |
| 29. | Library<br>Defence Research Establishment Pacific<br>F.M.O. Victoria, B. C., Canada<br>V0S 1B0                       | 1 |
| 30. | Library<br>Defence Research Establishment Atlantic<br>F.M.O. Halifax, N. S., Canada<br>B3K 2X0                       | 1 |
| 31. | Weapons Division<br>Canadian Forces Fleet School Halifax<br>F.M.O. Halifax, N. S., Canada<br>B3K 2X0                 | 1 |
| 32. | Naval Polar Oceanography Center<br>Attn: LCDR H. Rosner<br>4301 - Suitland Road<br>Washington, DC 20390              | 1 |
| 33. | USA CRREL<br>Attn: Stephen Ackley<br>72 Lyme Road<br>Hanover, NH 03755   | 1 |
| 34. | Swedish Meteorological and Hydrological<br>Institute<br>Attn: Dr. Anders Omstedt<br>S-60176 Norrkoping, Sweden       | 1 |
| 35. | University of Illinois<br>Attn: Dr. J. E. Walsh<br>1101 West Springfield Avenue<br>Urbana, IL 61801                  | 3 |

36. DPED 1  
National Defence Headquarters  
Ottawa, Ont., Canada  
K1A 0K2
37. Canadian Forces Maritime Warfare School 1  
Attn: SSO Environment  
F.M.O. Halifax, N. S., Canada  
B3K 2X0
38. Department of Meteorology 1  
McGill University  
Attn: Dr. L. Mysak  
805 Sherbrooke St. W  
Montreal, P. Q., Canada  
H3A 2K6

END

DATE

FILMED

JAN

1988